UNIVERSITÉ DU QUÉBEC À MONTRÉAL

OPTIMISATION DE L'APPROCHE DE LA RÉDUCTION D'ÉCHELLE MULTIPLE POUR RÉALISER UNE PROJECTION CLIMATIQUE DE LA PRÉCIPITATION MIXTE À HAUTE RÉSOLUTION

THÈSE

PRÉSENTÉE

COMME EXIGENCE PARTIELLE

DU DOCTORAT EN SCIENCES DE LA TERRE ET DE L'ATMOSPHÈRE

PAR

DOMINIC MATTE

JANVIER 2018

UNIVERSITY OF QUÉBEC AT MONTRÉAL

OPTIMIZATION OF THE MULTIPLE NESTING APPROACH TO REALIZE A CLIMATE PROJECTION OF MIXTE PRECIPITATION AT HIGH RESOLUTION

THESIS

PRESENT

AS PARTIAL REQUIREMENT OF THE DOCTORATE

IN EARTH AND ATMOSPHERIC SCIENCES

BY

DOMINIC MATTE

JANUARY 2018

À Luce, tu sais...aussi

REMERCIEMENTS

De par les grandes difficultés techniques, professionnelles et relationnelles qu'un parcours doctoral peut comporter, il est assez peu probable d'y arriver sans aide. Cette thèse n'en fait pas exception et doit son accomplissement grâce à l'aide de plusieurs personnes.

Mes premiers remerciements vont à mon directeur de thèse René Laprise qui a été pour moi non seulement une grande source d'information, mais aussi d'inspiration. Je le remercie pour ses muliples conseils (autant scientifiques que personnels), sa très grande rigueur, son support et la grande liberté qu'il m'a laissée. Bien que la fin d'un tel projet me procure une grande joie, elle m'attriste tout autant, car elle met fin à une relation directeur-étudiant que je chérissais.

Mes seconds remerciements vont à ma codirectrice de thèse, Julie M. Thériault. Je la remercie pour sa grande rigueur, son enthousiasme, ses conseils et sa patience. Ses conseils scientifiques m'ont permis d'atteindre une qualité exceptionnelle dans les divers travaux que nous avons réalisés ensemble.

Un grand merci à Mélissa Cholette pour son support et ses conseils toujours d'une grande pertinence. Merci à Katja Winger pour ses conseils, sa patience sans limites et son enthousiasme; à Bernard Dugas pour ses précieux conseils sur le MRCC5; à Oleksandr (Sasha) Huziy pour ses conseils techniques. Merci aussi à Guillaume Dueymes, Frédéric Chosson, Emmanuel Poan pour leur support, leurs conseils et leur amitié.

Je remercie également la faculté des sciences de l'UQAM pour m'avoir décerné le prix 2017 de la meilleure publication scientifique étudiante.

Je remercie aussi ma conjointe Luce; merci sans toi rien de ceci ne serait possible! Finalement, un dernier remerciement à ma défunte mère, mon père, mes frères et mes ami(e)s pour tout le plaisir que vous me procurez.

TABLE DES MATIÈRES

LISTE DES FIGURES

LISTE DES ABRÉVIATIONS, SIGLES ET ACRONYMES

AR5	the Fifth Assessment Report
BB	Big-Brother simulation
BBE	Big-Brother Experiment
CF	Conditions aux frontières
CGCM	Coupled Global Climate Model
CLASS	Canadian Land Surface Scheme
CMC	Canadian Meteorological Centre
C_{MCG}	Coût de calcul d'un MCG
C_{MRC}	Coût de calcul d'un MRC
CORDEX	COordinated Regional climate Downscaling Experiment
CRCM5	Fifth-generation Canadian Regional Climate Model
DCT	Discrete Cosine Transform
ERA-I	Era-Interim reanalysis
GCM	Coupled Global Climate Model
GEM	Global Environnement Multiscale model
GF	Simulation du grand frère
IC	Initial Conditions
IPCC	Intergovernmental Panel on Climate Change
J	Jump of resolution between the driving data and the nested model
LB	Little-Brother simulations
LBC	Lateral Boundary Conditions
LE	Long-duration event
MCG	Modèle de circulation générale
MetUM	Met Office United Model
MP	Mixed precipitation
MRC	Modèle régional du climat
MRCC5	Cinquième génération du Modèle Régional Canadien du Climat

PF	Simulations du petit frère
RCM	Regional Climate Model
RCP	Representative Concentration Pathway
SB	Step Brother simulation
SE	Short-duration event
SLRV	St. Lawrence River Valley
SN	Spectral Nudging
SS	Small Scales
WRF	Weather Research and Forecasting Model

RÉSUMÉ

La précipitation verglaçante peut avoir des impacts néfastes sur la société, tels que causer des pannes de courant majeures, ainsi que produire de sérieux problèmes dans les réseaux de transport. Malgré les conséquences catastrophiques associées à ce type de précipitation, elle est encore peu étudiée dans un contexte de changement climatique. Pour représenter ce type de précipitation dans les modèles du climat, il est important de correctement simuler les écoulements atmosphériques près de la surface. Les simulations climatiques à haute résolution sont, donc, nécessaires pour représenter adéquatement la topographie, mais ces dernières exigent des ressources informatiques considérables, surtout lorsqu'on utilise des modèles de circulation générale. Or, les modèles régionaux du climat (MRC) sont des modèles à aire limitée qui permettent la simulation du climat à fine échelle à un moindre coût de calcul. Ces derniers utilisent les solutions des modèles de circulation générale à leurs frontières pour développer leurs propres solutions. Cependant, lorsqu'ils sont utilisés à très haute résolution, le nombre de calculs requis peut être hors de la portée des ressources informatiques disponibles. L'utilisation en cascade d'un modèle régional du climat pourrait être une alternative pratique pour garder le coût de calcul raisonnable. L'objectif principal de cette thèse est d'étudier et optimiser l'utilisation de la réduction d'échelle dynamique multiple comme une approche appropriée pour réaliser une étude du climat de la précipitation verglaçante à faible coût de calcul. Cette thèse est divisée en trois sections.

La première partie étudie l'approche de la cascade pour réaliser des simulations climatiques à haute résolution. Dans cette étude, des résultats de simulations obtenues avec une approche de réduction d'échelle simple et double sont comparés selon le protocole expérimental "idéalisé" du grand frère. Une première simulation, nommée la simulation du grand frère, est réalisée sur un grand domaine à la résolution désirée. Cette simulation sert de référence. La solution du grand frère est ensuite traitée par un filtre passe-bas permettant de garder seulement les grandes échelles qui serviront de conditions aux frontières (CF) à des simulations tests appelées les simulations du petit frère. Pour la réduction d'échelle simple, les simulations tests sont directement pilotées par la solution de la simulation de référence filtrée, alors que pour la réduction d'échelle double un substitut d'une simulation de résolution intermédiaire est utilisé. L'étude de la composante stationnaire montre très peu de différences entre les deux approches, alors que la composante de la variabilité transitoire montre de grandes différences. L'approche de la réduction d'échelle double dégrade légèrement les grandes échelles, mais permet une importante réduction de la grandeur de domaine requise pour développer adéquatement les caractéristiques de fines échelles. Ceci a un impact considérable sur le coût de calcul.

La seconde partie porte sur la distance nécessaire à partir de la frontière latérale pour que circulation entrante développe ses caractéristiques de fine échelle permises par la résolution plus fine du MRC. Pour étudier cette question, les solutions de simulations réalisées par un MRC piloté par des CF de différentes résolutions sont étudiées selon le protocole du grand frère. Plusieurs expériences ont été réalisées pour évaluer la largeur de la région du "spin-up" requise pour un développement adéquat des fines échelles en fonction de la résolution du MRC, des conditions aux frontières ainsi que du saut de résolution. Cette distance se trouve à être seulement fonction de la résolution des conditions aux frontières, indépendamment de la résolution du MRC. Lorsque la résolution du MRC varie pour un même saut de résolution, la distance "spin-up" peut être convertie, selon la résolution du MRC, en nombre de points de grille. Ces résultats peuvent être utilisés pour choisir le domaine et la configuration du MRC pour un développement optimal des fines échelles permises par la résolution.

La troisième partie de cette thèse est une application des deux précédentes études pour étudier l'impact des changements climatiques sur la précipitation verglaçante au sud du Québec avec un MRC utilisé en cascade pour atteindre un maillage de 0.11° selon le scénario d'émission RCP 8.5. La précipitation verglaçante est diagnostiquée selon cinq méthodes empiriques (Cantin & Bachand, Bourgouin, Ramer, Czys et, Baldwin). Les précipitations diagnostiquées sont étudiées pour le passé récent (1980-2009) et comparées avec le scénario climatique futur (2070-2099). En premier lieu, la climatologie passée se compare aux observations. Les projections futures suggère une diminution des occurrences de précipitation verglaçantes pour le sud du Québec d'octobre à avril, principalement due à une diminution des évènements de longues durées (>6h). Les résultats montrent une plus grande diminution de décembre à février. En général, cette étude contribue à une meilleure compréhension de la distribution de la précipitation verglaçante sous un climat plus chaud et permet de mettre en lumière l'importance des conditions atmosphériques pour ce type de précipitation.

Mots-clés: Simulation climatique à haute résolution, L'expérience du grand frère, Réduction d'échelle dynamique multiple, Développement des petites échelles, Modélisation régionale du climat, Saut de résolution, Changement climatique, Diagnostique du type de précipitation, Pluie verglaçante, Grésil

ABSTRACT

Freezing precipitation events can have major impacts on the society by causing power outages and disruptions to the transportation networks. Despite the catastrophic consequences associated with these precipitation types, very few studies have investigated how the occurrences will evolve under warmer climate scenarios. To correctly simulate freezing precipitations, the topographic flow has to be correctly simulated. Climate simulations at high resolution are necessary to improve the representation of the topography in models, but these could be very expensive to run with General Circulation Model. To overcome these issues, Regional Climate Models (RCM) are widely used to reach higher spatial resolution at a reduced computational cost. However, at really high resolution RCM's computational costs can become again an issue to which multiple nesting might offer a solution. The focus of this thesis is to investigate multiple nesting as a conceivable approach to realize a climate study of freezing precipitation at a reasonable computational cost. The work presented in this thesis is divided in three parts.

The first part studies the multiple nesting approach to reach high resolution while keeping reasonable computational costs. In this study the results obtained with single and double nesting are compared within the idealized "perfect model" framework of the Big-Brother Experiment. This method consists in first realizing a simulation, nicknamed the Big-Brother simulation, on a relatively large domain at the desired resolution, to serve as a reference dataset. The Big-Brother results are then processed by a low-pass filter to emulate a coarse-resolution dataset to be used as lateral boundary conditions (LBC) to drive further test simulations, nicknamed the Little-Brother simulations, using an identical model configuration and resolution as the Big-Brother simulation. For the single nesting, the Little-Brother simulations are directly simulated, while for the double nesting a surrogate intermediate-resolution simulation is used. The study of the stationary component shows that little difference is noted between the two approaches. Transient-eddy components, however, shows important differences. The double nesting approach weakly degrades the large scales but allows a significant reduction of the required domain size to allow adequate spin-up of fine-scale features. This results in an important reduction of the computational cost.

The second part focuses on the distance needed from the lateral inflow boundary, within a limited-area regional climate model, to allow the full development of the small-scale features permitted by the finest resolution. To address this issue, RCM simulations using various resolutions driving data are compared following the Big-Brother protocol. Several experiments were carried out to evaluate the width of the spin-up region (i.e. the distance between the lateral inflow boundary and the domain of interest required

for the full development of small-scale transient eddies) as a function of the RCM and LBC resolutions, as well as the resolution jump. The spin-up distance turns out to be a function of the LBC resolution only, independent of the RCM resolution. When varying the RCM resolution for a given resolution jump, it is found that the spin-up distance corresponds to a fixed number of RCM grid points that is a function of resolution jump only. These findings can serve a useful purpose to guide the choice of the domain and RCM configuration for an optimal development of the small scales allowed by the increased resolution of the nested model.

The third part of this thesis is a application of the finding of the two previous chapters to investigate the variation of mixed precipitation over southern Québec with climate change using high-resolution regional climate simulations. This study used the fifth-generation Canadian RCM with climate scenario RCP 8.5 at 0.11° grid mesh. The precipitation types such as freezing rain, ice pellets or their combination are diagnosed with 5 methods (Cantin & Bachand, Bourgouin, Ramer, Czys and Baldwin). The analysis of the diagnosed precipitation is studied during past climate (1980-2009) and compared with future climate scenarios (2070-2099). First, the past climatology is similar to the observations. The future projections suggested a decrease in the occurrences of mixed precipitation over southern Qubec from October to April, mainly because of a decrease in long-duration events (>6h). However, the results show a more pronounced decreased from December to February. Overall, this study contributes to better understand how the distribution of precipitation types will change in a warmer climate and highlight the importance of the atmospheric conditions to the type of precipitation reaching the surface.

Keywords: High-resolution climate simulations, Big-Brother Experiment, Multiple dynamical downscaling, Spatial spin-up, Regional climate modelling, Nested model, Jump of resolution, Climate change, Precipitation type algorithms, Freezing Rain, Ice pellet, Precipitation-type algorithm

CONTRIBUTIONS À LA SCIENCE

L'utilisation des modèles régionaux du climat est de plus en plus commune dans la plupart des centres de recherche se concentrant sur l'étude de l'évolution du climat. Cependant, bien que très prometteur, leur emploi soulève encore plusieurs questions. Il est très important de connaître l'impact de cette approche sur les simulations.

Une importante contrainte de la modélisation régionale est le "spin-up" spatial. Dans la dernière décennie, la résolution des modèles de circulation générale à peu évoluée alors que la résolution des modèles régionaux ne cesse d'augmenter. Cette différence grandissante exacerbe le "spin-up" spatial et peut devenir particulièrement contraignante pour les utilisateurs des modèles régionaux du climat. Cependant, il existe une alternative à cette dernière contrainte: l'approche de la réduction d'échelle multiple. L'objectif principal de cette thèse est d'étudier cette approche pour réaliser une étude climatique de la précipitation verglaçante. Les principales conclusions sont:

- En plus de posséder les mêmes avantages que la réduction d'échelle simple, l'appro che de la réduction d'échelle dynamique double permet de diminuer le coût de calcul par un facteur de cinq.
- Le "spin-up" spatial est défini par le saut de résolution entre le MRC et le pilote ainsi que de la circulation atmosphérique moyenne.

Une meilleure description du "spin-up" spatial permet de choisir correctement la location des domaines pour l'approche de la réduction d'échelle double et ainsi réaliser de façon optimale une simulation de haute résolution. L'utilisation de cette approche a permis de réaliser une étude climatique de la précipitation verglaçante pour le sud du Québec et d'apporter plusieurs points nouveaux et innovateurs à la littérature existante sur ce type de précipitation tels que:

- Une étude climatique de la précipitation verglaçante à haute résolution spatiale ($\leq$0.11°) en utilisant un MRC.
- L'utilisation de cinq algorithmes diagnostiques pour déterminer le type de précipitation.
- L'étude des événements de courtes (<6h) et de longue durée ($\geq$6h).
- L'étude du changement climatique dans la vallée du Saint-Laurent de la précipitation verglaçante.

Mon projet de recherche permettra d'édifier une ligne de conduite quant au "spin-up" spatial et ainsi améliorer la configuration de simulations à haute résolution à travers des protocoles expérimentaux stricts tels que CORDEX où la grandeur et la localisation du domaine sont imposées. De plus, dans la quête d'atteindre une plus haute résolution, ce projet apportera des informations importantes pour réaliser la réduction d'échelle multiple. Cette dernière méthode permettra d'étudier le climat des phénomènes météorologiques exigeant une grande résolution spatiale telle que la précipitation verglaçante à un coût de calcul raisonnable.

CONTRIBUTIONS PERSONNELLES

L'objectif de cette section n'est pas de faire de l'ombre à l'immense travail que mes superviseurs de thèse René Laprise et Julie M. Thériault ont accompli pour mon projet de doctorat, mais bien de mettre en contexte ma propre contribution. Ce projet a été premièrement formulé par le professeur René Laprise et portait principalement sur la possibilité de réaliser des simulations à haute résolution en respectant certaines contraintes méthodologiques qui restaient à définir telle que le "spin-up" spatial. Certaines recherches antérieures réalisées sous sa direction ont été essentielles à la forme que cette thèse a prise (par ex. Leduc and Laprise, 2009; Leduc et al., 2011; Cholette et al., 2015). La proposition de départ était inspirée d'une étude que Mélissa Cholette avait réalisée dans le cadre de sa maîtrise. Cette étude avait, en autre, permis de démontrer la faisabilité de la cascade pour réaliser une simulation avec un maillage de ≈1 km à un coût de calcul raisonnable avec le MRCC5. L'idée générale était donc de faire un pas de plus et d'évaluer l'impact que la cascade pouvait avoir sur la simulation.

Ce fut dans ce contexte que la première étude a débutée. Cette dernière m'a permis de parfaire mes connaissances avec le MRCC5, l'expérience du grand frère et les contraintes méthodologiques reliées à la régionalisation telles que le "spin-up" spatial. Grâce à ces premiers pas, il a été plus aisé de poursuivre mon projet de thèse de façon un peu plus naturelle. Suite à cette étude, il devenait clair qu'une meilleure compréhension du "spin-up" spatial devenait essentielle pour réaliser une cascade optimale. L'intérêt était de mieux comprendre le "spin-up" spatial en tant que distance et non seulement en termes de grandeur de domaine. Une telle compréhension permettrait de correctement configurer l'approche de la cascade. Encore une fois, le protocole du grand frère était l'approche idéale pour répondre à mes questions. Bien que ce travail fut réalisé étroitement avec la collaboration de mes superviseurs de thèse, l'aisance que j'avais acquise avec la méthode et le modèle m'ont permis de prendre certaines libertés qui m'ont apparues bénéfiques à l'étude.

Les précédents résultats permettaient enfin de mettre en pratique l'approche de la cascade pour des simulations climatiques à faible coût de calcul. L'application d'une telle cascade devenait la suite logique de ce projet et devait être appliquée pour faire l'étude d'un phénomène qui bénéficierait d'une plus haute résolution spatiale. Dès le départ, il avait été discuté que la précipitation verglaçante serait le banc d'essai parfait d'une telle approche. Donc un protocole expérimental fut défini pour réaliser une projection climatique de la précipitation verglaçante pour le sud du Québec avec l'approche de la cascade avec le MRCC5. Une fois les simulations réalisées, les algorithmes diagnostiques pour déterminer les types de précipitation ont été écrits, testés et utilisés pour produire la projection climatique de la précipitation verglaçante. Bien que j'ai encore bénéficié d'une grande liberté pour la production et l'analyse des résultats de cette étude, la collaboration avec mes superviseurs a permis de produire une étude d'une grande qualité.

INTRODUCTION

Bien qu'il y ait un fort consensus au sein de la communauté scientifique sur le réchauffement du climat, son impact sur les phénomènes météorologiques et conséquemment sur la société est encore au coeur de plusieurs secteurs de la recherche environnementale. Dans les dernières décennies, les modèles du climat sont devenus des outils indispensables permettant de simuler les composantes qui influencent notre climat telles que les processus atmosphériques, océaniques et de surfaces. En effet, ils permettent de mieux comprendre l'évolution du climat afin d'anticiper l'impacts qu'auront les changements climatiques sur la société. Ces derniers pourraient mener à une augmentation d'évènements météorologiques qui pourraient être catastrophiques. Ces phénomènes peuvent se définir par des évènements extrêmes (Field et al., 2013) tels que des vagues de chaleur (Meehl and Tebaldi, 2004; Sillmann et al., 2013), des sècheresses (Sillmann et al., 2013), des précipitations intenses et soutenues (Sillmann et al., 2013), des ouragans (Zappa et al., 2013) et des épisodes de précipitation verglaçante (Cheng et al., 2007, 2011; Klima and Morgan, 2015; Lambert and Hansen, 2011). Pour bien simuler ces évènements, il est essentiel de mieux simuler les différentes composantes du système terre-atmosphère-océan et leurs interactions.

Or, puisque la simulation du climat est intrinsèquement liée aux ressources informatiques, la résolution et l'archivage des données sont d'importantes limitations qui doivent être abordées dès les premières étapes du protocole expérimental. De façon générale, plus la résolution du modèle augmente, plus la représentation de phénomènes locaux s'améliore (Lucas-Picher et al., 2016). Par contre, en augmentant la résolution, le coût de calcul devient de plus en plus contraignant. Pour les modèles de circulation générale (MCG), ce coût dépend de plusieurs facteurs tels que la résolution horizontale, la résolution verticale, du matériel informatique, ainsi que de la configuration et la complexité du modèle. De plus, puisque la simulation doit être réalisée sur tout le globe, le coût de calcul pour une simulation est élevé, même à basse résolution. Ce coût augmente selon l'inverse de la troisième puissance de la taille du maillage. Pour une plus grande résolution, l'utilisation de modèles régional du climat (MRC) devient plus appropriée. Ceux-ci sont des modèles à aire limitée qui utilisent la solution des MCG ou des réanalyses à leurs frontières pour produire leur propre solution à plus haute résolution. Il devient alors possible d'avoir une information à plus haute résolution sur une section du globe tout en ayant un coût de calcul plus raisonnable. Leur coût de calcul dépend donc sensiblement des mêmes facteurs que les MCG à la différence que la grandeur du domaine de calcul des MRC peut être choisie. En diminuant le domaine de calcul d'un MRC, le coût de calcul associé est grandement réduit et n'augmente qu'avec la première puissance du maillage (en fixant le nombre de points de grille). Pour une même résolution, lorsqu'on compare le coût d'un MCG et d'un MRC pour une même résolution, le coût de calcul est réduit selon le ratio entre le nombre de points de grille fixé par le MCG et ceux choisis par le MRC. Par exemple, pour le domaine CORDEX nord-américain le coût de calcul est réduit par un facteur d'environ 16.

Bien que les MRCs permettent de réduire considérablement le coût de calcul, leur utilisation soulève certaines problématiques importantes telles que l'effet sur la simulation de la grandeur du domaine et du saut de résolution entre les conditions aux frontières et de la résolution du MRC. Si la grandeur du domaine n'est pas imposée par le protocole expérimental, elle l'est par certaines contraintes méthodologiques. Par exemple, Jones et al. (1995) ont montré que pour le choix de la taille du domaine soit optimal, ce dernier devrait être assez grand pour permettre aux fines échelles de se développer et assez petit pour que les conditions aux frontières maintiennent un contrôle adéquat sur la simulation. En utilisant l'expérience du grand frère, Leduc and Laprise (2009) ont montré qu'une distance minimale est requise à partir de la frontière de la circulation entrant pour le développement adéquat des petites échelles. Ce "spin-up" spatial étant particulièrement large pour la saison d'hiver dans les régions de moyennes latitudes qui sont caractérisées par une forte circulation provenant de l'ouest. Cette dernière notion impose une contrainte non négligeable sur la grandeur du domaine affectant donc le coût de calcul. Bien que la grandeur du domaine et le "spin-up" spatial aient été étudiés, il est généralement accepté qu'un grand saut de résolution accentue le "spin-up" spatial, mais la notion est encore floue (Denis et al., 2003; Leduc and Laprise, 2009; Leduc et al., 2011).

Cette problématique s'accentue à mesure que le saut de résolution entre les MCG et les MRC augmente. Or, la résolution spatiale des MCG a très peu changé au cours de la dernière décennie (en moyenne un maillage de 321 km dans les projections climatiques du 21e siècle du 5^e rapport du groupe d'experts intergouvernemental sur l'évolution du climat (GIEC)). Par contre le maillage des MRC est passé de 45-60 km à 10-15 km dans la dernière décennie (p.ex. EURO-CORDEX, Vautard et al., 2013; Jacob et al., 2014), et il a récemment atteint la valeur où la convection n'est plus paramétrisée de

2.5-4 km (p.ex. Pan et al., 2011; Rasmussen et al., 2014; Fosser et al., 2014; Ban et al., 2015) faisant considérablement augmenter le saut de résolution d'un facteur de ≈7, ≈30 et ≈80, respectivement. Pour un grand saut de résolution, le "spin-up" spatial doit être considéré lorsque l'on choisit la grandeur de domaine du MRC pour s'assurer un développement adéquat des petites échelles à l'intérieur du domaine simulé. A priori, cela signifierait que l'on doit utiliser un plus grand domaine, puisque le "spin-up" spatial associé augmente. Par conséquent, il devient important de mieux comprendre cette notion de "spin-up" en fonction du saut de résolution. Une fois cette notion précisée, si le saut de résolution est grand, l'approche de la réduction d'échelle dynamique multiple (aussi appelé l'approche en cascade) peut être envisagée comme solution au grand saut de résolution. Cette approche consiste à imbriquer une dans l'autre plusieurs simulations d'un MRC tout en diminuant la taille du domaine et en augmentant sa résolution de façon progressive.

Cholette et al. (2015) ont montré que non seulement l'utilisation en cascade du MRCC5 était techniquement faisable pour réaliser des simulations à haute résolution à un coût de calcul raisonnable, permettant de mieux représenter la topographie lorsqu'on diminuait le maillage (de $\Delta x \approx 81$ km à $\Delta x \approx 1$ km). Par exemple, la canalisation du vent dans la vallée du Saint-Laurent, particulièrement lorsque $\Delta x \leq 9$ km, était mieux représentée par le modèle, également démontré par Lucas-Picher et al. (2016). Ce dernier phénomène peut avoir un effet non négligeable sur certains phénomènes météorologiques tels que la précipitation verglaçante.

La pluie verglaçante se forme généralement dans les régions de moyennes latitudes lors du passage d'un front chaud (Cortinas, 2000). Ce mouvement de masse d'air peut cré une couche d'air chaude ($T > 0°C$) en altitude et couche d'air froid ($T < 0°C$) près de la surface. Lorsque la précipitation tombe dans un tel profil de température, elle est sujette à de multiples changements de phase. Il existe deux façons de représenter ce type de précipitation dans les modèles atmosphériques. La première nécessite de résoudre explicitement certains processus tels que la fonte, la coalescence, la condensation, la nucléation et la collection. Bien que cette méthode soit considérée comme plus réaliste, son très grand coût de calcul la rend inabordable pour des études climatiques. La seconde méthode est de type diagnostique et consiste à calculer le type de précipitation à partir de l'état de l'atmosphère simulé en utilisant des variables telles que la température, l'humidité et la pression. Cette approche est moins coûteuse et donc plus appropriée pour des études climatiques.

Plusieurs études ont souligné l'importance des caractéristiques topographiques sur la formation de la précipitation verglaçante pour l'Amérique du Nord (Laflamme and Périard, 1998; Stuart and Isaac, 1999; Cortinas, 2000; Changnon and Karl, 2003; Cortinas Jr et al., 2004; Groisman et al., 2016), ainsi que pour la Norvège et la Russie (Groisman et al., 2016). Changnon and Karl (2003) ont étudié les occurrences de pluie verglaçante aux États-Unis et ont montré qu'il y avait un maximum d'occurrence sur le versant est des Appalaches produit par un phénomène de blocage d'air froid (Xu, 1990). Bernstein (2000), Cortinas Jr et al. (2004) et Roebber and Gyakum (2003) suggèrent qu'en plus de la trajectoire des tempêtes et la proximité de masse d'eau, les caractéristiques de la topographie sont importantes pour la formation de ce type de précipitation. Il est donc nécessaire que la résolution de la simulation soit suffisamment élevée, impliquant un coût de calcul non négligeable. C'est alors que l'approche de la cascade peut être envisagée. Même si l'on sait que l'approche est prometteuse pour atteindre la haute résolution (Cholette et al., 2015), son impact sur la simulation est encore inconnu.

0.1 Objectifs et Approche

Depuis les dernières années, la cascade est de plus en plus utilisée pour les études du climat (Hohenegger et al., 2008; Chan et al., 2012; Lauwaet et al., 2013; Ban et al., 2015; Prein et al., 2015; Trapp et al., 2007; Pavlik et al., 2012; Kendon et al., 2014), cependant très peu d'études ont étudié l'effet d'une telle approche (Cholette et al., 2015; Brisson et al., 2015). À ce jour, l'impact de la cascade sur la simulation est encore inconnu. L'objectif principal de cette thèse est d'étudier la cascade comme une approche concevable pour réaliser une étude du climat de la précipitation verglaçante à haute résolution à un coût de calcul raisonnable. Cet objectif principal est divisé en 3 sous-objectifs:

1. L'évaluation de l'impact de la cascade sur la simulation dans un cas où il y a un grand saut de résolution entre les conditions aux frontières et le maillage du modèle régional du climat.

2. La caractérisation de l'impact du saut de résolution sur le développement des champs atmosphériques à petites échelles dans les simulations de modèle régional du climat.

3. L'utilisation de la configuration optimale de la cascade pour réaliser une simulation

à haute résolution à faible coût de calcul appliqué à l'évolution de la précipitation mixte (pluie verglaçante et grésil) sur le sud du Québec.

Pour répondre à ces sous-objectifs, la recherche a été menée en trois étapes formant les trois chapitres de cette thèse. Dans le premier chapitre, on compare une simulation produite par l'approche de réduction d'échelle simple à une simulation produite par double réduction d'échelle dans le cadre du protocole expérimental idéalisé du grand frère. Dans le deuxième chapitre, on analyse le développement spatial des petites échelles, toujours dans le cadre de l'expérience du grand frère, en fonction de la distance de la frontière du domaine, plutôt que d'étudier selon la grandeur du domaine comme dans les études précédentes. Finalement, dans le troisième chapitre, une approche optimale selon les résultats obtenus précédemment est utilisée pour réaliser une étude climatique de la précipitation mixte. Cette étude se penche sur l'occurrence de précipitation verglaçante future en utilisant plusieurs méthodes diagnostiques pour déterminer le type de précipitation selon une simulation réalisée à haute résolution. Les résultats sont présentés sous forme d'articles scientifiques publiés/soumis à la revue Climate Dynamics.

CHAPITRE I

COMPARISON BETWEEN HIGH-RESOLUTION CLIMATE SIMULATIONS USING SINGLE AND DOUBLE NESTING APPROACHES WITHIN THE BIG-BROTHER EXPERIMENTAL PROTOCOL

This chapter is presented in the format of a scientific article published in the journal *Climate Dynamics*. The detailed reference is:

Matte, D.; Laprise, R. & Thériault, J. M., 2016: Comparison between high-resolution climate simulations using single- and double-nesting approaches within the Big-Brother experimental protocol. https://doi.org/10.1007/s00382-016-3031-9, Clim. Dyn., 1-14, doi: 10.1007/s00382-016-3031-9

Abstract

Regional climate models (RCM) are widely used to downscale global climate models' (GCMs) simulations. As the resolution of RCM increases faster than that of GCM used for climate-change projections till the end of this century, the resolution jump will become an issue. Cascade with multiple nesting offers an approach to reach high resolution while keeping reasonable computational cost. Few studies have addressed whether the best results are obtained with the single or multiple nesting approaches. In this study the results obtained with single and double nesting are compared within the idealised "perfect model" framework of the Big-Brother Experiment. This method consists in first realizing a simulation, nicknamed the Big-Brother (BB) simulation, on a relatively large domain at the desired resolution, to serve as reference dataset. The BB results are then processed by a low-pass filter to emulate a coarse-resolution dataset to be used as lateral boundary conditions (LBC) to drive further simulations, nicknamed the Little-Brother (LB) simulations, using an identical model formulation and resolution as the BB simulation. For the single nesting, the LB simulations are directly simulated, while for the double nesting a surrogate intermediate-resolution simulation is used.

The study of the time-mean (stationary) component shows that little difference is noted between the single- and double-nesting approaches. The time-deviation (transient-eddy) component, however, shows important differences. The double nesting approach weakly degrades the large scales but allows a significant reduction of the required domain size to allow adequate spin-up of fine-scale features. This results in an important saving in the computational cost.

Key words: High-resolution climate simulation, Big-Brother experiment, Multiple dynamical downscaling, Spatial spin-up

1.1 Introduction

General Circulation Models (GCMs) are widely used for climate-projection studies; their heavy computational cost rapidly becomes an issue if one attempts increasing their resolution. The use of nested limited-area Regional Climate Models (RCMs) to dynamically downscale GCM output allows drastically reducing the computational cost while benefiting from the added value related to the increased resolution. With very fine grid meshes, however, the computational cost of an RCM also becomes an issue. Over the recent years, several groups have embarked upon the production of very high spatial resolution, and even convection-permitting climate simulations (e.g. Hohenegger et al. 2008; Chan et al. 2012; Lauwaet et al. 2013; Ban et al. 2015; Prein et al. 2015) and climate-change projections (e.g. Trapp et al. 2007; Pavlik et al. 2012; Kendon et al. 2014) using multiple grid nesting. Such simulations indicate great perspectives for added value of high-resolution climate simulations. For example, de Vries et al. (2014) used a mesh of 12 km to study changes of mean snowfall and seasonal extremes. Jacob et al. (2014) presented the first high-resolution (12.5 km grid mesh) future climate projections of EURO-CORDEX. They highlighted a clear change of pattern of heavy precipitation events compared to coarser simulations. Kendon et al. (2012) pointed out that 12 km grid mesh is still too coarse to give a realistic spatial and temporal structure of heavy rain, suggesting convection-permitting 1.5 km grid-mesh simulation for improvement.

Cholette et al. (2015) have shown that with grid meshes of 1 to 3 km, the fifth-generation Canadian Regional Climate Model (CRCM5) showed a clear improvement in the simulation of wind channelling effect in the St. Lawrence River Valley located in Québec, Canada. The study of Wang et al. (2013) revealed that high resolution improves local features such as sea breezes and funnelling winds in the Met Office United Model (MetUM) RCM. In the case of simulations over complex topography with the Weather Research and Forecasting (WRF) RCM version 3.0, Rasmussen et al. (2011) have shown that spatial snowfall distribution is much more representative of observations with 2 km than 36 km grid-mesh simulations; they attributed this result to a more realistic vertical motion at higher resolution.

Recently, Kjellström et al. (2014) had put forward that international cooperation is important to reinforce our knowledge about very high-resolution regional climate modelling. Two of the central issues of dynamical downscaling are the regional domain size and the resolution jump between the driving lateral boundary conditions (LBCs) and the nested RCM grid mesh, both issues being interrelated. For example, Jones et al. (1995) have shown that the domain size should be large enough to allow the full development of fine scales but small enough to maintain suitable control by the LBC on the regional simulation. Using the Big-Brother Experiment (BBE) protocol, Leduc and Laprise (2009) and Leduc et al. (2011) have shown that a minimum distance from the lateral inflow boundary is required for the suitable development of small-scale transient-eddy permitted by the fine mesh of a RCM. This spatial spin-up distance is particularly large for mid-latitude winter conditions characterized by strong westerly flow. The spatial spin-up imposes a non-negligible constraint on the domain size, which has repercussions on the computational cost. While domain size and spatial spin-up have been studied in several studies, its relation to resolution jump is poorly known; practitioners of dynamical downscaling, however, are fully aware that larger jumps exacerbate the spin-up issue. Recently, Di Luca et al. (2015) have discussed some of the important factors influencing the added value brought by RCM using multiple dynamical downscaling. They raised the point that even if the grid mesh could be reduced substantially, errors from the nesting may limit its application. In order to keep the computational cost low, Brisson et al. (2015) have investigated different nesting approaches to perform convection-permitting climate simulations on a 0.025° mesh. They compared simulations performed with single nesting (0.025°-mesh simulation performed using directly ERA-Interim as initial conditions (IC) and LBCs), double nesting (an intermediate-resolution on a 0.22° mesh between ERA-Interim and the 0.025°-mesh simulation) or triple nesting (two intermediate-resolution on a 0.22° and 0.0625° mesh simulations between ERA-Interim and the 0.025°-mesh simulation). Their results suggested that the intermediate-resolution 0.0625°-mesh simulation does not make a significant impact and that this nest could therefore be removed. They also mentioned that single nesting increased model deficiencies. However, it remains unclear what is the impact of a multiple dynamical downscaling approach. Hitherto, it is not well understood how a multiple nesting approach affects high-resolution climate simulations. To the best of the authors' knowledge, no study has yet addressed this issue.

This paper investigates dynamical downscaling in situations of large resolution jump between the driving LBC and the RCM grid mesh, by comparing the performance of single and double nesting approaches, using the BBE protocol. It is constructed as follows. A brief description of the regional model is presented in Section 2. Sections 3 and 4 discuss experimental design and the analysis tools used to analyze the simulations. The results are presented in Section 5. Finally, Section 6 presents the summary and discussions.

1.2 Model description

The experiments have been performed with the fifth-generation Canadian RCM (CRCM5; Hernández-Díaz et al. 2013; Martynov et al. 2013; Šeparović et al. 2013). CRCM5 is based, in large part, on the Global Environmental Multiscale model (GEM; Côté et al. (1998a,b)) developed by Environment Canada for use in numerical weather prediction (NWP). The dynamical core uses a two-time-level quasi-implicit semi-Lagrangian marching scheme, and the horizontal discretization is based on an Arakawa staggered C-grid. The model has a fully elastic non-hydrostatic option (Yeh et al., 2002), in which case the vertical coordinate is the terrain-following hydrostatic pressure (Laprise, 1992). In CRCM5, a sponge zone (Davies, 1976) of ten grid points is applied around the perimeter of the regional domain where the inner solution is gradually blended with the outer solution imposed as LBCs.

The model configuration uses Kain-Fritsch deep convection parameterization (Kain and Fritsch, 1990), Kuo-transient shallow convection (Kuo, 1965; Bélair et al., 2005), Sundqvist resolved-scale condensation (Sundqvist et al., 1989), correlated-K terrestrial and solar radiation schemes (Li and Barker, 2005), subgrid-scale orographic effects are parameterized following the McFarlane mountain gravity-wave drag (McFarlane, 1987) and the low-level orographic blocking scheme of (Zadra et al., 2003), and turbulent kinetic energy closure planetary boundary layer and vertical diffusion (Benoit et al., 1989; Delage and Girard, 1992; Delage, 1997). Unlike the NWP version of GEM, however, CRCM5 uses the most recent version of the Canadian Land Surface Scheme (CLASS 3.5; Verseghy 2000, 2008) that allows for a detailed representation of vegetation, land-surface types, organic soil and a flexible number of layers.

1.3 Experimental design

Regional climate model simulations resulting from single and double nesting approaches are compared using the Big-Brother Experiment (BBE) protocol as devised originally by Denis et al. (2002b). This experiment is a perfect prognosis approach that isolates the nesting errors from other modelling errors, thus emphasizing the influence of nesting on the RCM solution

In the BBE, a first simulation using the desired grid mesh is realized on a very large domain. This simulation, named the Big Brother (BB), serves two purposes: (1) it is used as reference to evaluate the test simulations nicknamed the Little-Brother

(LB) simulations, and (2) it provides, after filtering manipulations described below, IC and LBC to LB simulations. In our case, we used as Big Brother a CRCM5 simulation on a 0.15° mesh covering a 760 x 760 grid-point domain centred on Montréal, Québec, Canada, with 56 levels in the vertical. The Big-Brother simulations were driven by ERA-Interim reanalysis for four two-month periods starting November first of the years 1997, 1998, 1999 and 2000 (see Fig.1.1 for experimental design and Fig.1.2 for domains location and size). These Big-Brother simulations will be noted BB.15.

In an attempt to mimic the case when a low-resolution GCM simulation provides initial conditions (IC) and LBC for dynamical downscaling, the BB-simulated data is processes by a low-pass filter that retains only the large scales; the resulting dataset is termed "filtered BB" (BB.15_Fr), with "r" the equivalent mesh size resolution. These BB.15_Fr fields are in some sense perfect as far as the large-scale fields are concerned, because they do not suffer from simulation errors that would occur in coarse-mesh model simulations. Diaconescu et al. (2007) mentioned that those are due to the inability to represent fine-scale topography and the eddy processes, the imperfection in capturing internal variability and difficulty in parameterizing subgrid-scale processes. BB.15_Fr fields are devoid, however, of small scales, as do coarse-mesh GCM simulations. The BB.15_Fr dataset is used as IC and LBC for LB simulations that are performed using the same model formulation and resolution as the BB.15, but driven by BB.15_Fr data over smaller domains. These LB simulations are evaluated by comparing with the reference BB simulation. The differences between the LB and BB.15 can be unambiguously attributed to nesting errors because of such perfect-prognosis protocol.

The low-pass filter is based on the discrete cosine transform (Denis et al., 2002a), with a gradual response function that attempts to mimic the spectrum of an equivalent 1.8°-mesh simulation. The lower and upper wavelength limits for the BB.15_F1.8 are chosen to be 396 km and 1386 km, corresponding respectively to the Nyquist length scale 2 Δx and to the smallest adequately resolved scales 7 Δx, as shown by Skamarock (2004) and Cholette et al. (2015); a cosine-squared function response is used between these two limits (as shown by the red line in Fig.1.3).

Two dynamical downscaling approaches will be compared using the BBE protocol: the single and double nesting, as shown on Fig.1.1.

1.3.1 Single nesting approach

The LB simulations using the single nesting follow the usual BBE protocol as in (Denis et al., 2002b). In our case, the LB simulations were performed for four 1.5-month periods starting on November 15 (thus leaving out the initial 15 days as spin-up of the BB.15 simulations), for the years 1997 to 2000, using the BBF dataset as IC and LBC at 6 h intervals. The LB simulations were performed over five different domain sizes: 460 x 460, 260 x 260, 160 x 160, 110 x 110 and 60 x 60 grid points, respectively (Fig.1.2). The climate statistics of the LB were compared to those of the BB for the four months of December (thus leaving out the initial 15 days as spin-up of the LB simulations) over a common area of 44 x 44 grid points indicated by the dashed black square in Fig.1.2.

1.3.2 Double nesting approach

While the single nesting follows the standard BBE procedure, the design of the double-nesting experiment deserves special attention. The challenge is to maintain the perfect-prognosis attribute of the BBE while designing a double-nesting strategy that normally involves the use of an intermediate-resolution simulation. After considering several alternatives, the following procedure was adopted. A surrogate to an intermediate-resolution simulation on a 0.45° mesh has been generated using a 0.15°-mesh simulation performed over a moderately large domain, and then using specific filters to replicate the spectral characteristics and behaviour of a 0.45°-mesh simulation over an optimal domain size. The resulting simulation data will be referred to as Step Brother (SB.45). The Appendix details the procedure followed to determine the optimal conditions so that the SB.45 dataset represents a good proxy to an idealized 0.45°-mesh simulation while maintaining the perfect-prognosis approach using 0.15°-mesh LB simulations.

The SB.45 dataset corresponds to the first stage of the double nesting procedure in Fig.1.1. In turn, this SB.45 dataset serves to drive a 0.15°-mesh LB simulations for the second stage of double nesting. Several 0.15°-mesh LB simulations were performed on various domain sizes (260 x 260, 160 x 160, 110 x 110 and 60 x 60 grid points, respectively), using a nesting interval of 1 h.

1.4 Analysis tools

A proper evaluation of high-resolution nested RCM simulations requires separating the large scales that are present in the driving LBC from the smaller scales that are only resolved by the finer mesh of the RCM. The black line in Fig.1.3 shows the response of the analysis filter used to isolate the large-scale component: wavelengths longer than 400 km are retained entirely and those smaller than 300 km are removed, with a gradual cosine-squared function transition in between. The small-scale component is obtained by subtracting the large-scale component from the original fields. In particular, large scales refer to those scales present in the driving data and small scales correspond to those absent in the driving data. It is important to note that the analysis filter has been applied on a common area for all simulations, irrespective of the simulation domains.

Temporal decomposition of each variables Ψ is applied before analysis. Any variable ($\Psi(\vec{x},t)$) function of space $\vec{x}$ and time t will be split to analyze their time mean (also called stationary component) and time deviation (also called transient-eddy component), as follows

$$\Psi(\vec{x},t) = \overline{\Psi}(\vec{x}) + \Psi'(\vec{x},t) \tag{1.1}$$

where $\overline{\bullet}$ is the temporal mean and ' the time deviation. The transient-eddy variance is obtained as

$$\sigma'^2(\vec{x}) = \overline{\Psi'^2}(\vec{x}) \tag{1.2}$$

The LB and BB statistics will be compared in terms of the ratio of their transient-eddy standard deviation

$$\Gamma' = \frac{\sigma'_{LB}(\vec{x})}{\sigma'_{BB}(\vec{x})}, \tag{1.3}$$

the transient-eddy correlation

$$\rho'(\vec{x}) = \frac{\overline{\left(\Psi'_{BB}(\vec{x},t) * \Psi'_{LB}(\vec{x},t)\right)}}{\sigma'_{BB}(\vec{x})\sigma'_{LB}(\vec{x})}, \tag{1.4}$$

and the transient-eddy root mean square (RMS) difference

$$RMS'(\vec{x}) = \sqrt{\overline{\left(\Psi'_{LB}(\vec{x},t) - \Psi'_{BB}(\vec{x},t)\right)^2}}. \tag{1.5}$$

Likewise, statistics from spatial structure will be obtained as follows

$$\overline{\Psi}(\vec{x}) = \langle\overline{\Psi}(\vec{x})\rangle + \Psi^{*}(\vec{x}), \tag{1.6}$$

where $\langle\rangle$ and * refer, respectively, to the spatial average and the spatial deviation of the field; the spatial-eddy variance is defined as

$$\sigma^{*2} = \langle\Psi^{*2}(\vec{x})\rangle. \tag{1.7}$$

The LB and BB statistics can be compared in terms of the ratio of spatial standard deviation as

$$\Gamma^{*} = \frac{\sigma^{*}_{LB}}{\sigma^{*}_{BB}}, \tag{1.8}$$

the spatial correlation as

$$\rho^{*} = \frac{\langle\Psi^{*}_{BB}(\vec{x})\Psi^{*}_{LB}(\vec{x})\rangle}{\sigma^{*}_{BB}\sigma^{*}_{LB}}, \tag{1.9}$$

and the RMS difference of spatial deviation as

$$RMS^{*} = \sqrt{\left\langle\left(\Psi^{*}_{LB}(\vec{x}) - \Psi^{*}_{BB}(\vec{x})\right)^{2}\right\rangle}. \tag{1.10}$$

The Taylor diagrams (Taylor, 2001) are useful to summarise succinctly the spatial and temporal behaviours of the LBs compared to the BB.15_F1.8. On the presented diagrams, the RMS are normalized by the standard deviation of the BB.

1.5 Results

In this section, selected variables are presented to give a representative picture of the general behaviour of the spatial and temporal properties.

1.5.1 Stationary component

The large-scale stationary component of the simulations has been investigated. Figure 1.4 shows the Taylor diagrams for the large-scale stationary component of both the single- and double-nesting LB simulations over various domain sizes. They were compared to the reference BB.15, for the mean sea level pressure (Fig.1.4a) and the 850-hPa relative humidity (Fig.1.4b) fields.

These two variables have their spatial structure dominated by large-scale stationary component. Given that the large scales are driven by the LBC, all LB simulations showed a rather high skill level, except for the largest domain sizes that show weaker spatial correlations and larger amplitude errors, which confirmed earlier results about the influence of RCM domain sizes. The mean sea level pressure field is particularly well reproduced, as also noted by Leduc and Laprise (2009), except for the largest domain with both approaches. A glance at 2-D large-scale map (not shown) confirmed that, for all cases, there are quite similar, and small differences are not physically meaningful. There is overall little difference between the single- and double-nesting results, although we noted that over the smallest domains the best correlation with the double nesting is slightly lower than that with the single nesting.

The amplitude of the small-scale stationary component is negligible compared to that of the large scales, and hence results are not shown.

1.5.2 Transient-eddy component

In this section, the transient-eddy component is examined. The transient-eddy component represents the day-to-day meteorological fluctuations. Figure 1.5 presents the spatial mean of the large-scale transient-eddy statistics for 300-hPa meridional wind component (Fig.1.5a) and 850-hPa relative humidity (Fig.1.5b). These results illustrate that large-scale transient-eddy amplitudes are well represented, independently of domain size and the use of single or double nesting. The time correlation, however, decreases with increasing domain size, reflecting the weaker control exerted by LBC with larger domains, and this is somewhat more pronounced with double nesting.

Figure 1.6 presents the small-scale transient-eddy component of 700-hPa relative vorticity (Fig.1.6a) and 850-hPa relative humidity (Fig.1.6b). These variables have been selected because the spectral slope of their variance spectra is much flatter, reflecting the fact that their spatial structure contains substantial small-scale features. As mentioned by Leduc and Laprise (2009), small-scale features are fluctuations, absent from the LBC, causes by the interaction from large flow with local fine-scale forcing (such as topography, the land-surface heterogeneities and other subgrid-scale parameterized physical processes). The most notable feature shown in Fig.1.6 is that the time correlation is very weak, which is to be expected given that LBC do not contain small-scale informations. The remaining, non-vanishing time correlation is probably due a second-order effect of preconditioning of small-scale features by the time-fluctuating large-scale flow interacting with fine-scale surface forcing. For large domains the amplitude of small-scale transient-eddy converges to the correct value (a value of one in relative terms). For single-nesting simulations over smaller domains, however, the small-scale transient eddies are amplitude-deficient, reflecting the fact that the complete spin-up of small scales did not have enough room to occur. This effect is not as clear in Fig.1.6b mainly because at 850-hPa surface forcing effect is still noticeable which promotes the development of small-scale features. This has also been noted, in a more pronounced way, over the Canadian Rocky Mountains (Antic et al., 2004). Double-nesting simulations, on the other hand, hardly suffer from such spin-up problem because of the smaller resolution jump afforded by the use of the first step in the cascade with the surrogate intermediate-resolution SB.45. Therefore, only the simulation performed on the smallest 60 x 60 grid-point domain shows some amplitude deficiency.

These results highlight important differences between the single- and double-nesting results. As the domain size is reduced, the results from single nesting showed a clear underestimation of the small-scale transient-eddy amplitude, which was referred to by Leduc and Laprise (2009) as the spatial spin-up issue. This occurs when a domain is too small to allow the full development of the small scales for a given resolution jump between the driving LBC and the RCM grid mesh. Double nesting clearly leads to a reduction of the spatial spin-up issue due to the use of the intermediate-resolution simulation (SB.45). For this case, the double nesting allows to halve the domain size of the high-resolution simulation, which implies a clear reduction in computational cost.

1.5.3 Single nesting VS Double nesting

The previous results can succinctly be summarised by looking at Fig.1.7, which shows the 700-hPa relative humidity field statistics as a function of the horizontal domain dimension in abscissa. The choice of introducing another variable that has not been shown yet in this study was made to show that the general behaviour is common to many variables. Fig.1.7a shows the time correlation of large-scale transient eddies and Fig.1.7b the relative small-scale transient-eddy standard deviation. The black and blue lines correspond to the statistics of the single- and the double-nesting simulations, respectively. An increase of the large-scale transient-eddy time correlation is noted as the domain size decreases, asymptoting to unity for single-nesting approach and to about 0.8 for double-nesting approach. The somewhat less than unity asymptotic value for double nesting arises from the use of a surrogate intermediate-resolution simulation, which introduced an upper bound to the skill of the ensuing LB in the second step with the double-nesting approach (see Appendix).

The small-scale transient-eddy standard deviation (Fig.1.7b) clearly shows the effect of spatial spin-up. The single nesting shows a marked decrease of the standard deviation for a smaller lateral domain dimension of 260 grid points ($\approx$ 4300 km). Whereas with double nesting the domain dimension can be reduced to as small as 110 grid points ($\approx$ 1800 km) before a marked amplitude deficiency occurs. The sensitivity of the small scales is much reduced with the double-nesting approach, because the smaller resolution jump between each step in the cascade results in a reduced spatial spin-up requirement. The main conclusion from the single-nesting results is that with domains larger than about 2600 km the control exerted by the LBC is too weak and that domains smaller than about 4300 km do not allow sufficient spin-up space.

As also noted in Fig.1.7a, the double-nesting results, however, showed that the large scales suffer from some lack of time correlation, even for small domain sizes. This is due to some loss of correlation in the first step (i.e. SB.45, see Appendix) in the double-nesting approach. The issue of the less than unity time correlation of large scales with double nesting can be addressed through the application of large-scale spectral nudging (e.g. von Storch et al. 2000) in generating the LB. Figure 1.8 shows results that are equivalent to those previously shown in Fig.1.7, but obtained with spectral nudging activated in generating the surrogate intermediate-resolution simulation needed in the double-nesting approach. Figure 1.8a shows that double-nesting results with spectral nudging become rather similar to those of single nesting. Indeed, it shows little sensitivity of large-scale transient-eddy time correlation with domain size, and the asymptotic value for double-nesting strategy approaches unity for small domains. Small-scale transient-eddy statistics (Fig.1.8b) show hardly any sensitivity to the application of spectral nudging, for both single- and double-nesting approaches, which makes sense given that spectral nudging by definition only affects the large scales.

1.6 Summary and Discussions

The resolution jump between a nested RCM and its driving data is an important parameter in dynamical downscaling applications. For large jumps, spatial spin-up must be taken in consideration when choosing an RCM domain size to allow an adequate development of small scales within the limited-area domain. Multiple dynamical downscaling might offer beneficial perspectives to achieve high-resolution regional climate simulations, although its use may have an impact on the simulations quality. The objective of this work was to investigate the impact of multiple dynamical downscaling by comparing single- and double-nesting approaches for climate simulations within the Big-Brother Experimental protocol.

A Big-Brother simulation was performed with CRCM5 on a 0.15° mesh over a very large domain for four periods of two winter months. This BB.15 simulation was then filtered to an equivalent 1.8°-mesh typical of operational global climate models. The resulting dataset (noted BB.15_F1.8) was used to drive a series of 0.15°-mesh Little Brother (LB) simulations in the single-nesting case. In the double-nesting case, an additional simulation (nicknamed Step Brother, SB.45) was introduced as a surrogate to an intermediate-resolution (0.45° mesh) model to drive the LB (as described in Appendix).

The study of the time-averaged (stationary) component, which is dominated by large scales, has not shown much difference between the two approaches. In both cases, the use of excessively large domains (greater than 260 x 260 grid points in our application) resulted in a lack of control exerted by the LBC.

Transient-eddy component shows more sensitivity to varying domain size. The double-nesting approach exhibits a small but systematic reduction in time correlation compared to the single nesting approach. The culprit is the intermediary simulation that introduces a weakening of control by the LBC. From a climate-simulation point of view (i.e. by analyzing usual climate statistics), temporal correlation is generally not of paramount importance. If, however, a specific application required improved temporal correlation, such as for case studies, then large-scale spectral nudging could be used advantageously.

The largest sensitivity to domain size was noted in the small-scale transient eddies. With single nesting, small domain sizes (smaller than 260 x 260 grid points in our application) resulted in amplitude-deficient small-scale transient eddies due to insufficient spatial spin-up. This effect is greatly reduced with double nesting, and adequate amplitudes are recovered with much smaller domains (as small as 110 x 110 grid points in our application). These results were traced back to the use of the intermediate-resolution simulation in the double nesting approach, which reduces the effective resolution jump, drastically decreases the effect of spatial spin-up, and allows a reduction of the optimal domain size of the high-resolution simulation, resulting in important computational savings.

In summary, the results obtained within the BBE protocol indicated that a minimum lateral domain dimension of about 4300 km was required when driving a 0.15°-mesh RCM with 1.8°-mesh LBC to ensure an adequate development of the small-scale features with single nesting, while with double nesting, this minimum lateral domain size is reduced to about 1800 km. This reduction of the minimum required domain size leads to reduce the computational cost (including the small computational cost of the intermediate-resolution simulation) by nearly a factor of 5. This represents an important gain in term of computing resources required to perform high-resolution climate simulations.

Acknowledgements: This research was supported by the Natural Sciences and Engineering Research Council (NSERC) of Canada. Computations were made on the supercomputer guillimin, managed by *Calcul Québec* and Compute Canada. The operation of this supercomputer is funded by the Canada Foundation for Innovation (CFI), the *Fonds de recherche du Québec - Nature et technologies* (FRQ-NT), NanoQuébec, and the *Réseau de médecine génétique appliquée* (RMGA). The authors are greatly indebted to Dr. Bernard Dugas and Ms. Katja Winger for their essential help with the use of CRCM5, and to Mr. Georges Huard and Ms. Nadjet Labassi for maintaining user-friendly local computing facilities.

1.7 Appendix

The double-nesting approach requires the introduction of an intermediate-resolution simulation between the 1.8° coarse-mesh driving LBC and the final 0.15° fine-mesh RCM simulations (Fig.1.1: double nesting). This additional simulation (named Step Brother, SB.45) needs to be carefully designed to satisfy two criteria: (1) to generate a dataset with characteristics similar to those of a 0.45°-mesh simulation, but (2) to use the same 0.15°-mesh RCM to maintain the perfect-prognosis nature of the BBE protocol. To satisfy these requirements, a surrogate to an intermediate-resolution (0.45° mesh) simulation was generated using a 0.15°-mesh RCM simulation performed and massaged under specific conditions as shown in Fig.1.9 and described below into three steps. The first step (step A) aims at finding the optimal domain size for the intermediate-resolution and highlighting its statistics needed for the next step. The second step (step B) is important for finding the optimal spectral nudging configuration for a 0.15°-mesh simulation that will fit better the statistics of the optimal domain size found in step A. Finally, step C has been designed to find the appropriate filter that fits the variance spectrum of a 0.45°-mesh simulation.

1.8 Appendix [Step A]: The optimum domain for the intermediate-resolution simulation

We address these requirements by performing another set of BBE with a 0.45°-mesh RCM with single nesting. In this case, the BB.45 simulation covers a large, 260 x 260 grid-point domain (not shown) centred on Montréal, Québec, Canada, with a 0.45° mesh. As before the BB.45 simulations were driven by Era-Interim reanalysis for four two-month periods starting on November first of the years 1997, 1998, 1999 and 2000. The same low-pass filter as described in section 1.3 is applied on BB.45 (reproduced for convenience as the red line in Fig.1.10) to serve as IC and LBC for subsequent LB simulations (LB.45). The LB.45 simulations were performed for four 1.5-month periods starting on November 15th for years 1997, 1998, 1999 and 2000, using BB.45_F1.8 at 6 h intervals. Five simulations were performed over different domain sizes of 180 x 180, 120 x 120, 90 x 90, 70 x 70 and 50 x 50 grid points, respectively (domains not shown). The climate statistics were computed on a common area of 38 x 38 grid points centred over Montréal, Québec, Canada, for the four months of December. For analysis the large and small scales are separated using a low-pass filter shown by the black line in Fig 1.10.

Only a small sample of the results obtained from this BBE will be discussed to identify the optimum domain size. Figure 1.11a shows the Taylor diagram of the time-averaged, stationary component of the relative humidity field at 850 hPa. The smaller domain simulations (90 x 90, 70 x 70 and 50 x 50 grid points) exhibit excellent spatial correlation and amplitude, while the larger domains (180 x 180 and 120 x 120 grid points) exhibit weaker spatial correlations, indicating a weaker control exerted by the LBC. Figure 1.11b shows the Taylor diagram of the small-scale transient-eddy component of the relative humidity field at 700 hPa. It shows a gradual decrease of time correlation as the domain size increases, indicative of the lesser control exerted by the LBC, but a small deficit of amplitude as the domain is reduced, reflecting the aforementioned spatial spin-up issue. Overall, the 90 x 90 grid-point domain appears to offer the best compromise, being large enough to allow the full development of the small scales permitted by the grid mesh, but not too large so as to maintain suitable control by the LBC driving data. For these reasons this domain size has been chosen as the optimal domain size.

This 0.45°-mesh simulation however cannot be used as the first step of the double nesting because it would contravene the perfect-prognosis nature of the BBE approach.

To avoid this pitfall, a 0.15°-mesh RCM must be used that emulates the characteristics of a 0.45°-mesh simulation. This 0.45°-mesh simulation over the optimal domain will be used as reference to: (1) find the optimal spectral nudging configuration that one must apply on a 0.15°-mesh RCM simulation to correctly reproduce the large-scale of a 0.45°-mesh simulation (as detailed in step B), and to (2) find the optimal filter that one must apply on a 0.15°-mesh RCM simulation to correctly reproduce the small scales of a 0.45°-mesh simulation (as detailed in step C).

1.9 Appendix [Step B]: The optimum large-scale spectral nudging

The BB.45_F1.8 dataset was used to drive a 460 x 460 grid-point simulation (Fig.1.2 same as the burgundy domain) on a 0.15° mesh with spectral nudging (SN) activated (Fig.1.9: CRCM5.15 with SN). A large domain was used to ensure the full development of the small scales and spectral nudging was applied to control the large scales. The nudging parameters were tuned to reproduce the large-scale statistics of the LB.45. After several tests it has been found that nudging the horizontal wind for wavelengths larger than 1000 km, with strength set to zero below the 600-hPa level and increasing linearly with height until the top model level, with a maximum strength of 1.4% applied at each time step. This configuration is used as optimal spectral nudging configuration in step C.

1.10 Appendix [Step C]: Optimal filter to reproduce the variance spectrum of a 0.45°-mesh simulation

Another simulation of the 0.15°-mesh simulation over a 460 x 460 grid-point domain (Fig.1.9: CRCM5.15 with optimal SN), driven by the original BB.15_F1.8 data (same as section 1.3) was performed with the optimal SN parameters found in step B. The corresponding dataset (Fig.1.9: SB.15) has then a large-scale behaviour of LB.45 over the optimal domain, but an incorrect small-scale behaviour. To adjust that, a specific low-pass filter was then designed in such a way that the variance spectrum of this 0.15°-mesh simulation best approximates the reference 0.45°-mesh simulation. Figure 1.12 shows the energy spectrum for the 700-200 hPa atmospheric layer of the reference 0.45°-mesh simulation driven by BB.45_F1.8 (LB.45; red line), 0.15°-mesh simulation with optimal SN parameters driven by BB.15_F1.8 (SB.15; black line), and the resulting optimally filtered version of the latter (SB.45; blue line). To correctly simulate a 0.15°-mesh simulation that has properties of a 0.45°-mesh simulation, a filter should have been used that cuts the tail of SB.45 represented by the dashed blue line in Fig 1.12. But for the experiment shown, this was not done; a parallel experiment has shown that it has almost no influence on the results presented in this study. This dataset will be used as driving data for the second step of the double-nesting simulations.

In summary, the SB.45 dataset represents in some sense perfect LBC as required by the BBE protocol, in the sense that it is produced by the same model at the same resolution and, compared to an equivalent 0.45°-mesh simulation, it has a similar skill as discussed in step B above and similar variance spectrum as discussed in step C above.

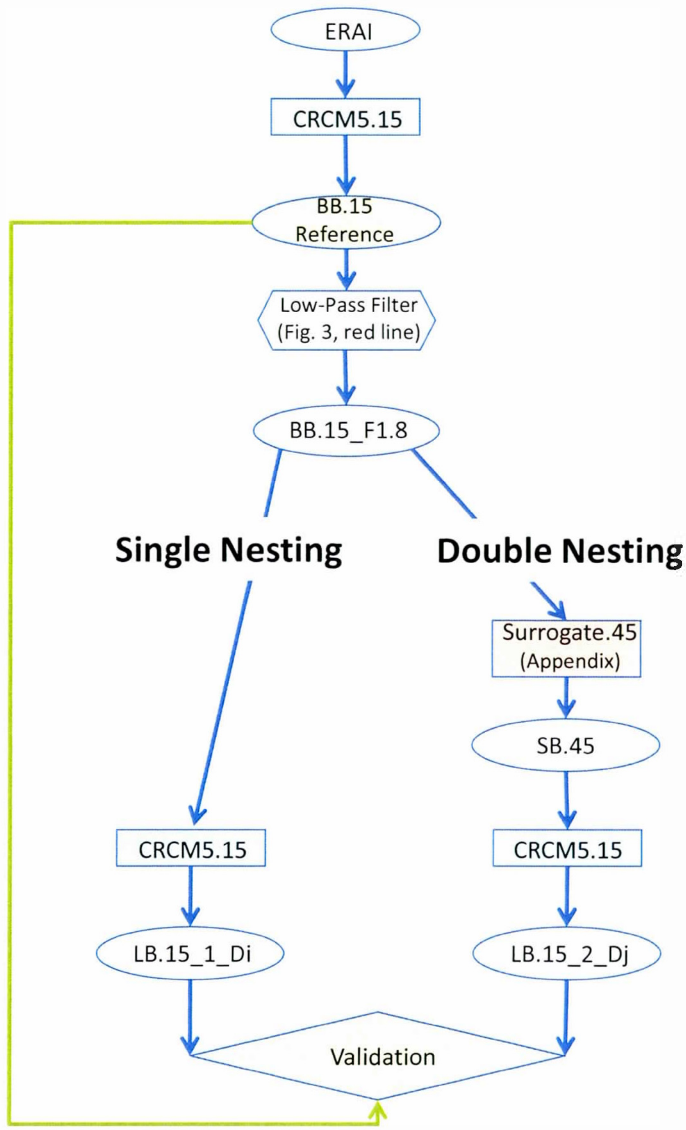

Figure 1.1 The experimental flowchart. Era-interim (ERAI) is used to drive the CRCM5 on a 0.15° mesh (RCM.15), the result is the Big-Brother simulation (BB.15). This simulation is used as reference to validate the Little-Brother (LB) simulation and also processed by a low-pass filter creating BB.15_F1.8, which is used as driving data for the two approaches. For the single nesting, the BB.15_F1.8 dataset is used to drive the CRCM5 on a 0.15° mesh (CRCM5.15) on multiple domain size (Di) with the same configuration used to simulate BB.15. The resulting datasets (LB.15_1_Di: Little-Brother simulations for the i domain sizes of the single nesting (see Fig.1.2)) are compared to BB.15. For the double nesting, the BB.15_F1.8 dataset is used to create the surrogate intermediate simulation (Surrogate.45: see Appendix) that provides the SB.45 dataset used to drive the CRCM5 on a 0.15° mesh (CRCM5.15) on multiple domain size (Dj) with the same configuration used to simulate BB.15 (LB.15_2_Dj: Little-Brother simulations for the j domain sizes of the double nesting (see Fig.1.2)) are compared to BB.15 and LB.15_1_Di.

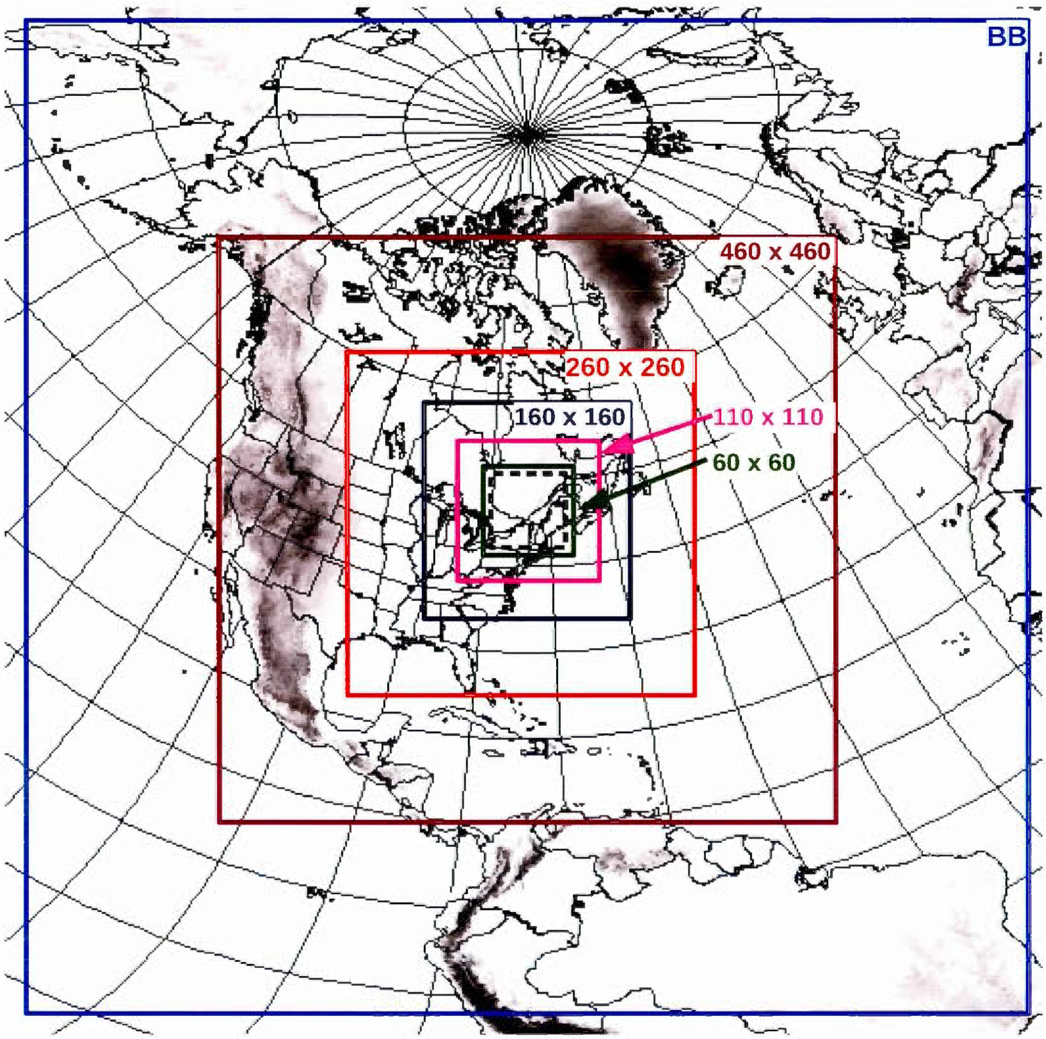

Figure 1.2 The simulation domains for the BB.15 (760 x 760 grid points), the LBs with domain size of 460 x 460, 260 x 260, 160 x 160, 110 x 110 and 60 x 60 grid points for the single nesting (Fig.1.1: LB.15_1_Di) and 260 x 260, 160 x 160, 110 x 110 and 60 x 60 grid points for the double nesting (Fig.1.1: LB.15_2_Dj). Climate statistics were computed in the black dashed square area of 44 x 44 grid points.

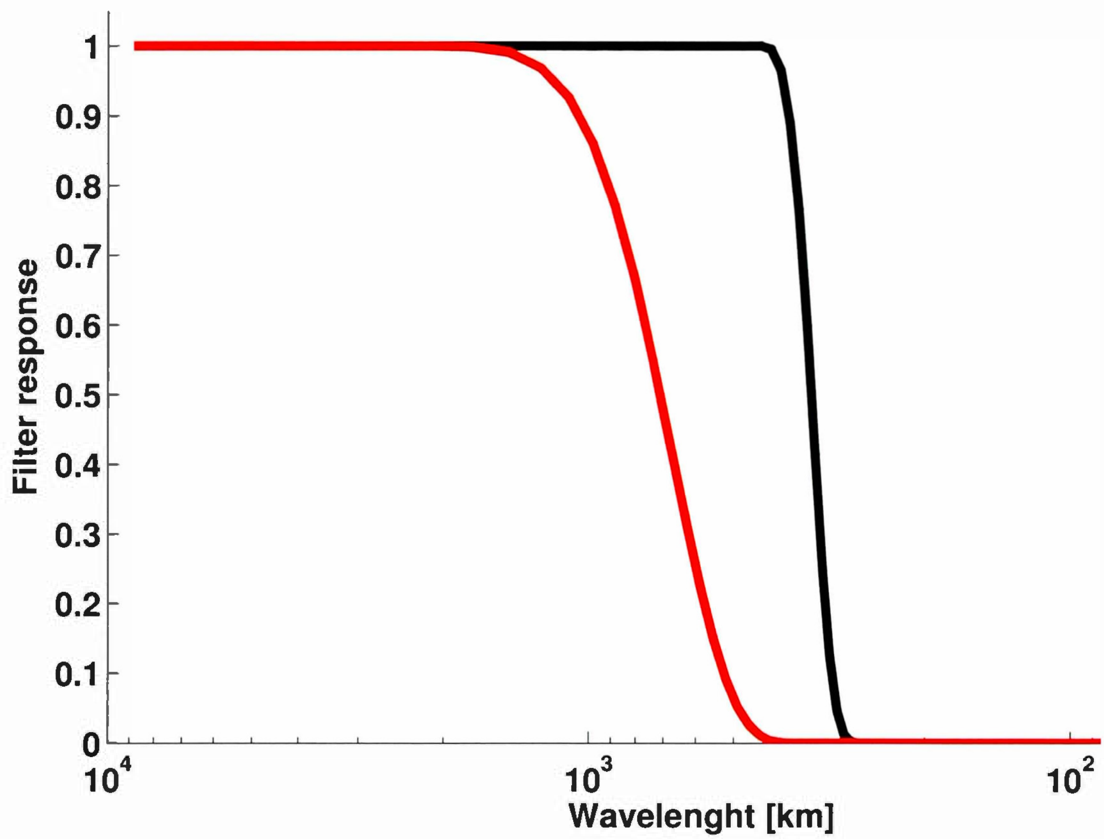

Figure 1.3 Filter response for the BB filter (red line) and the analysis filter (black line).

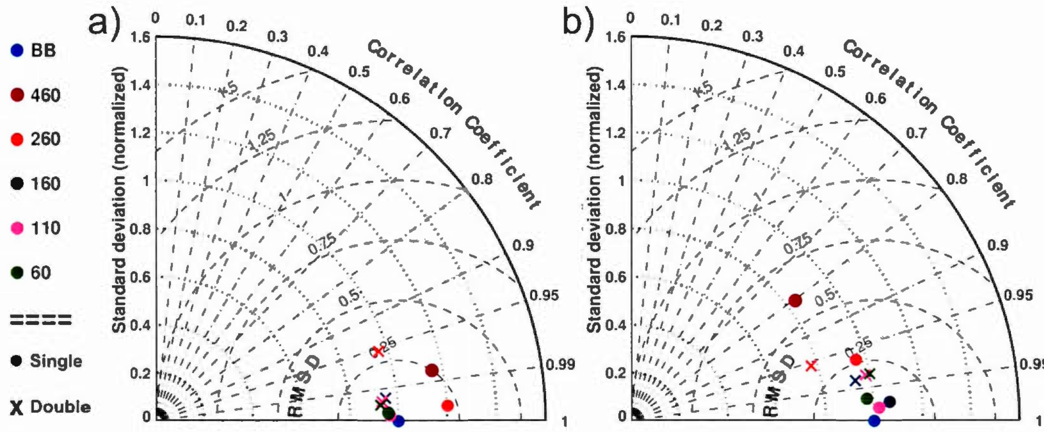

Figure 1.4 Large-scale stationary component of the mean sea level pressure (a) and 850-hPa relative humidity (b) fields. The dots correspond to the single-nesting results and the crosses to the double-nesting results. The colours correspond to the various domain sizes of the LB. The blue dot corresponds to the reference BB.15 simulation.

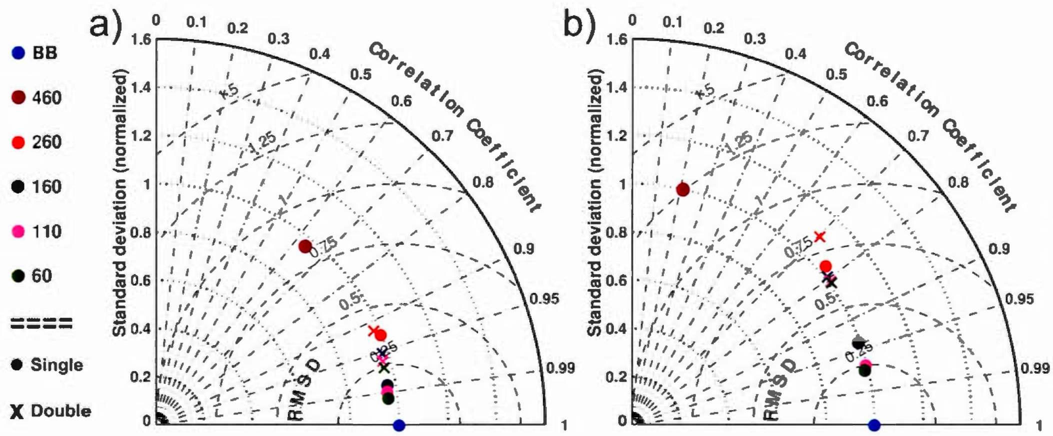

Figure 1.5 Spatial mean of the large-scale transient-eddy component of 300-hPa meridional wind (a) and 850-hPa relative humidity (b).

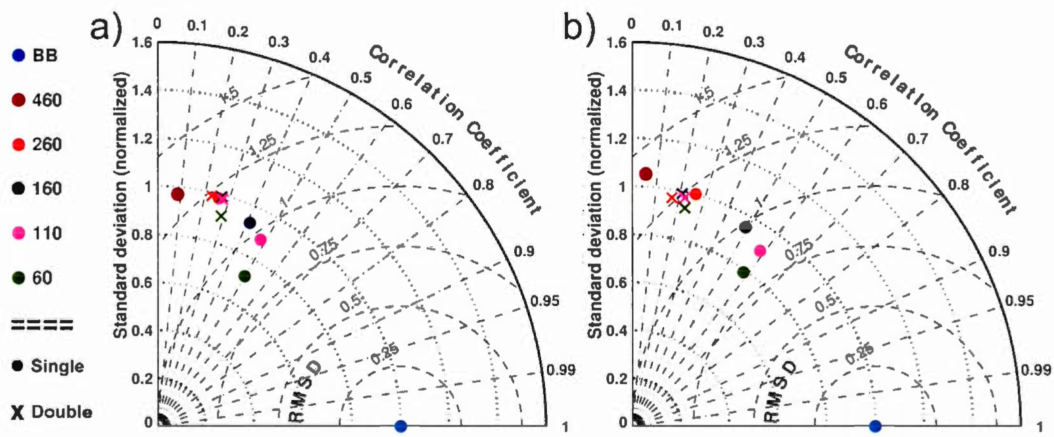

Figure 1.6 Small-scale transient-eddy component of 700-hPa relative vorticity (a) and 850-hPa relative humidity (b).

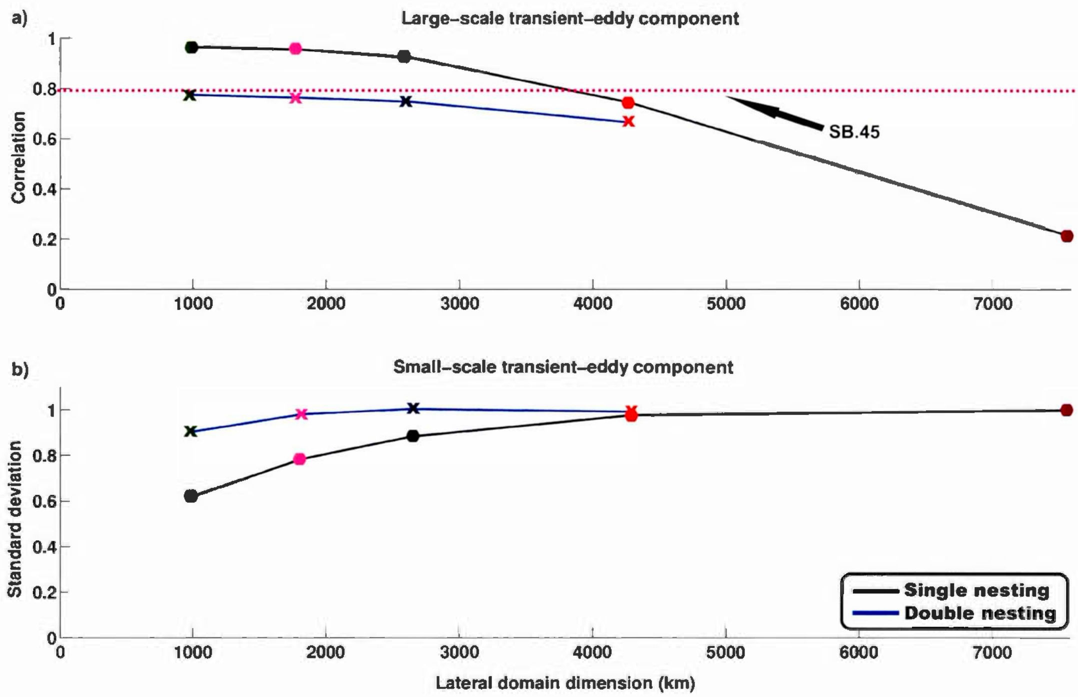

Figure 1.7 Transient-eddy statistics for the single nesting (solid black line) and the double nesting (solid blue line). The first figure (a) represents the large-scale transient-eddy correlation and the second figure (b) the small-scale transient-eddy standard deviation for the relative humidity at 700 hPa by the lateral domain dimension (km). The magenta dashed line represents the large-scale transient-eddy correlation of the SB.45 simulation.

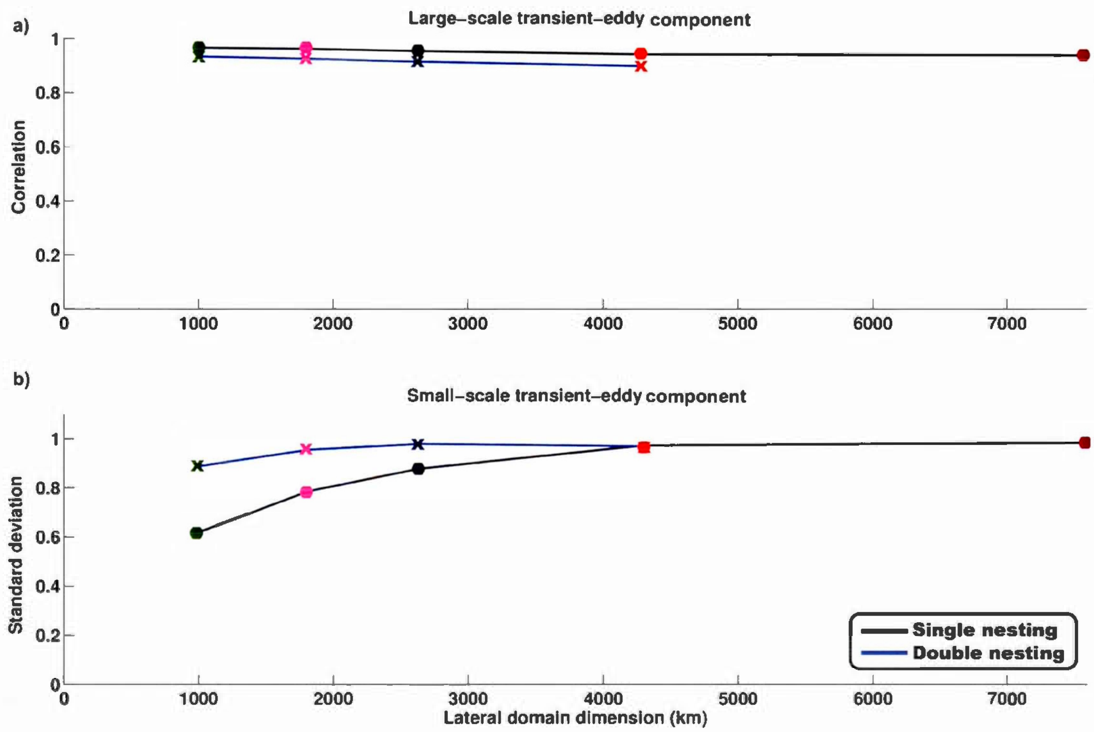

Figure 1.8 Same as Fig.1.7 but with large-scale spectral nudging activated in generating the LBs. The SN was applied to horizontal wind components with horizontal length scales larger than 1000 km, with a recall strength set to zero below the 850-hPa level, then increasing linearly to its maximum value at 500 hPa, and remaining constant to the model top level. The spectral nudging maximum strength is 1.3% applied at each time step.

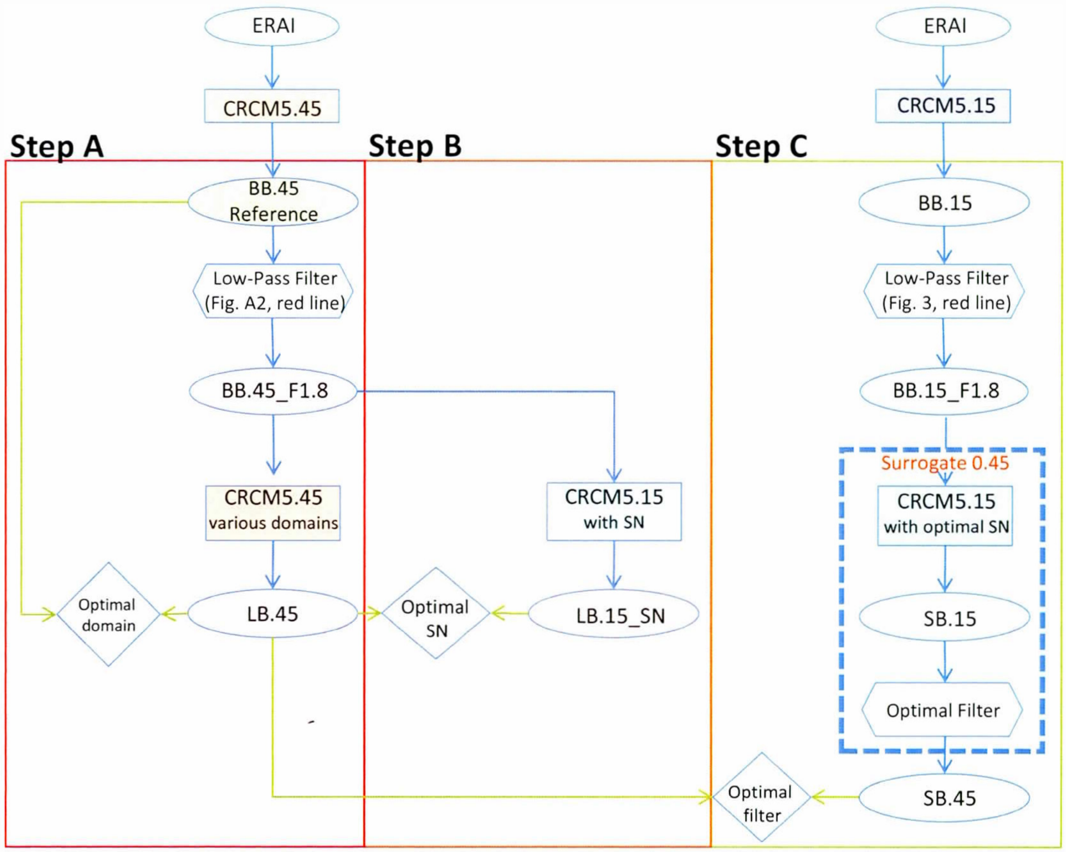

Figure 1.9 Flowchart of the protocol for the surrogate simulation. For the step A, Era-Interim (ERAI) is used to drive the CRCM5 at 0.45° mesh (CRCM5.45), the result is the Big-Brother simulation (BB.45). This simulation is used as reference to validate the Little-Brother (LB.45) simulation and also processed by a low-pass filter creating BB.45_F1.8 that is used as driving data for the CRCM5 (CRCM5.45; various domains) on various domain sizes with the same configuration used to simulate BB.45. The resulting datasets (LB.45) are compared to BB.45 to highlight the optimal domain size. For the step B, BB.45_F1.8 is used to drive the CRCM5 (CRCM5.45; with SN) on a unique domain size with different spectral nudging configurations. The large scales of the resulting datasets (LB.15_SN) are compared with optimal domain size simulation from the previous step. For the step C, Era-Interim (ERAI) is used to drive the CRCM5 at 0.15°-mesh (CRCM5.15), the result is the Big-Brother simulation (BB.15: same as in section 3). This simulation is processed by a low-pass filter creating BB.15_F1.8 (same as in section 3) which is used as driving data for the CRCM5 at 0.15°-mesh with the optimal spectral nudging configuration highlights in step B (CRCM5.15; with optimal SN). The resulting dataset (SB.15) has been processed by several spectral filters and results compared to the variance spectrum of LB.45 in order to find the optimal spectral filter. The results dataset is the surrogate simulation (SB.45) as presented in Fig.1.1.

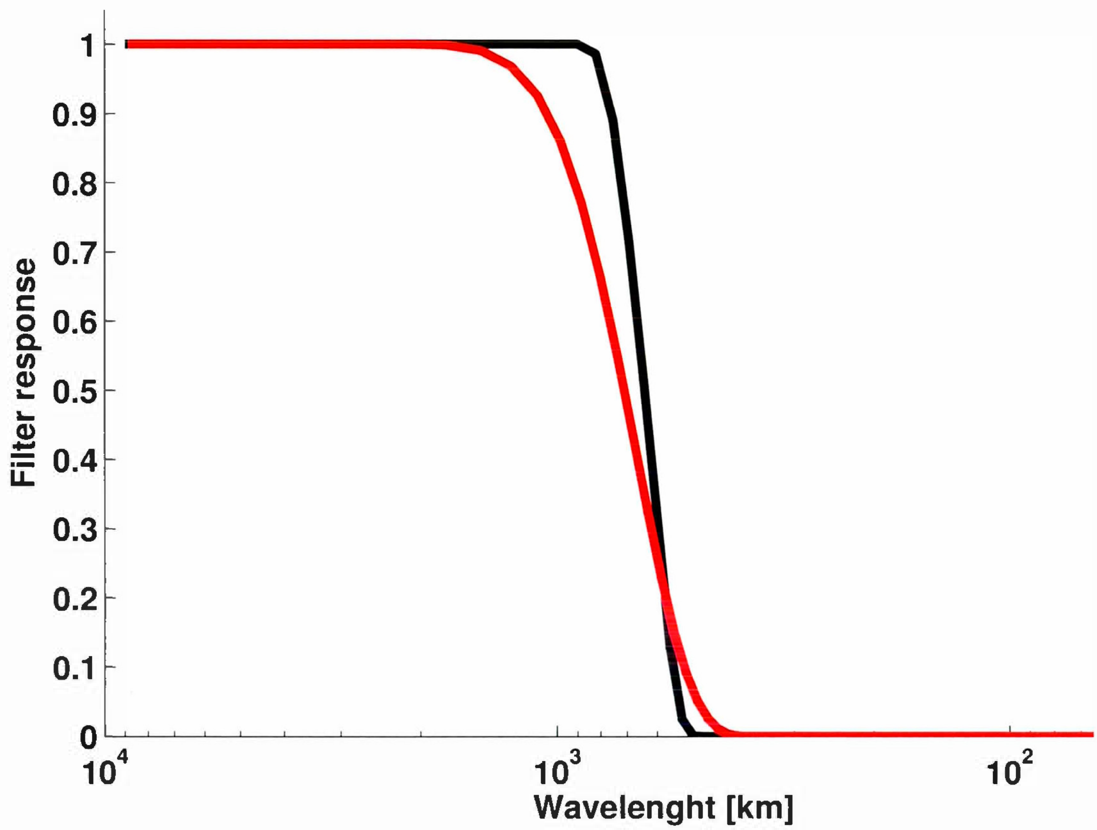

Figure 1.10 Filter response for the BB filter (red line) and the analysis filter (black line).

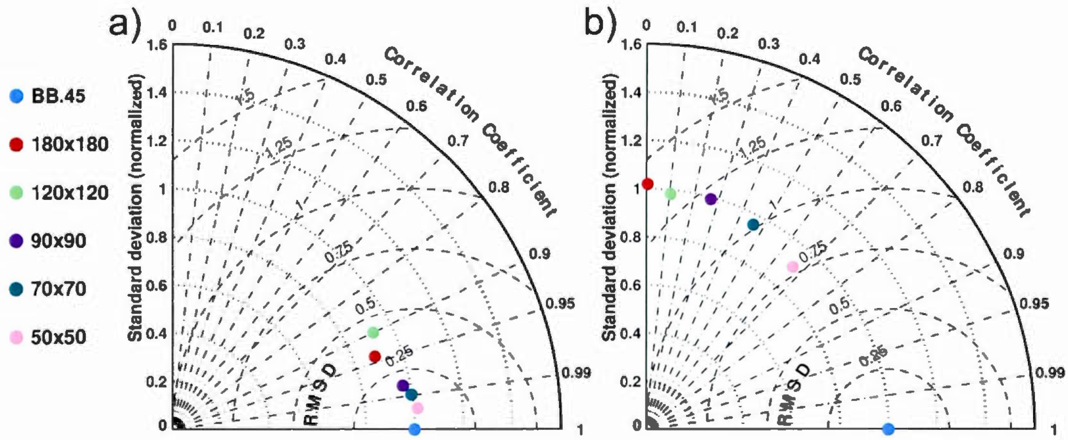

Figure 1.11 Relative humidity statistics from the Big-Brother experiment realized at 0.45° mesh for the stationary component of the original fields at 850 hPa (a) and the transient-eddy component of the small-scale field at 700 hPa (b).

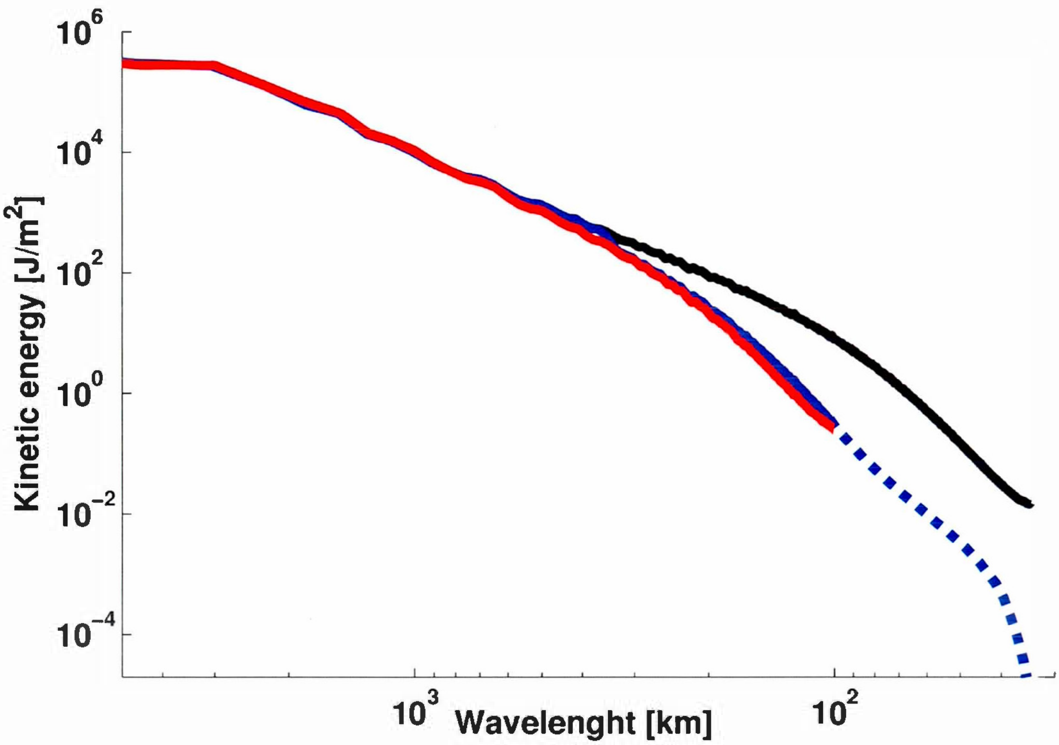

Figure 1.12 Kinetic energy spectrum for the 700-200 hPa atmospheric layer, averaged for 1997, 1998, 1999 and 2000, for the various simulations. The red line corresponds to 0.45°-mesh simulation driven by BB.45_F1.8 (noted LB.45 in Fig.1.9), the black line to the 0.15°-mesh simulation with optimal SN parameters driven by BB.15_F1.8 (noted SB.15 in the Fig.1.9), and the blue line the optimally filtered version of the latter (noted SB.45 in the Fig.1.9).

CHAPITRE II

SPATIAL SPIN-UP OF FINE SCALES IN A REGIONAL CLIMATE MODEL SIMULATION DRIVEN BY LOW-RESOLUTION BOUNDARY CONDITIONS

This chapter is presented in the format of a scientific article published in the journal *Climate Dynamics*. The detailed reference is:

Matte, D.; Laprise, R.; Thériault, J. M. & Lucas-Picher, P., 2016: Spatial spin-up of fine scales in a regional climate model simulation driven by low-resolution boundary conditions. https://doi.org/10.1007/s00382-016-3358-2, Clim. Dyn., 1-12, doi: 10.1007/s00382-016-3358-2

Abstract

In regional climate modelling, it is well known that domains should be neither too large to avoid a large departure from the driving data, nor too small to provide a sufficient distance from the lateral inflow boundary to allow the full development of the small-scale (SS) features permitted by the finer resolution. Although most practitioners of dynamical downscaling are well aware that the jump of resolution between the lateral boundary condition (LBC) driving data and the nested regional climate model affects the simulated climate, this issue has not been fully investigated. In principle, as the jump of resolution becomes larger, the region of interest in the limited-area domain should be located further away from the lateral inflow boundary to allow the full development of the small-scale features. A careless choice of domain might result in a suboptimal use of the full finer resolution potential to develop fine-scale features. To address this issue, regional climate model (RCM) simulations using various resolution driving data are compared following the perfect-prognostic Big-Brother protocol. Several experiments were carried out to evaluate the width of the spin-up region (i.e. the distance between the lateral inflow boundary and the domain of interest required for the full development of small-scale transient eddies) as a function of the RCM and LBC resolutions, as well as the resolution jump. The spin-up distance turns out to be a function of the LBC resolution only, independent of the RCM resolution. When varying the RCM resolution for a given resolution jump, it is found that the spin-up distance corresponds to a fixed number of RCM grid points that is a function of resolution jump only. These findings can serve a useful purpose to guide the choice of domain and RCM configuration for an optimal development of the small scales allowed by the increased resolution of the nested model.

Key words: Regional climate modelling, Nested model, Jump of resolution, Spatial spin-up, Big-Brother experiment.

2.1 Introduction

Climate models are useful tools to understand past, present and future climate conditions. Coupled global climate models (CGCM) are designed to represent the atmosphere, ocean, cryosphere and land surfaces and their interactions. To simulate the climate in a reasonable time, a large number of simplifying assumptions are made, and several processes are simply parameterised to reduce the computational cost. Nevertheless, achieving resolutions required by several impact studies would drastically increase the computational cost, which would exceed the limits of available computing infrastructure. To overcome this issue, the use of Regional Climate Models (RCM) has become a pragmatic avenue to achieve high-resolution climate simulations at an affordable computational cost. RCM are limited-area models, one-way nested at their lateral boundaries by low-resolution CGCM-simulated or reanalyses data.

CGCM spatial resolution has changed little over the last decade. The average grid mesh of CGCM participating in century-long IPCC AR5 climate projections was about 321 km (equivalent to $\approx$T62 using the linear transform grid spacing for spectral models). Whereas RCM grid meshes remained mainly unchanged at 45-60 km for the initial two decades, they have been refined to 10-15 km in the last decade (e.g. EURO-CORDEX, Vautard et al. 2013; Jacob et al. 2014) and have recently reached convection-permitting values of 2.5-4 km (e.g. Pan et al. 2011; Rasmussen et al. 2014; Fosser et al. 2014; Ban et al. 2015). The disparity of resolution between increasingly high-resolution RCM and lateral boundary conditions (LBC) provided by low-resolution CGCM raises important issues, such as the dynamical equilibrium between the inner solution calculated by the RCM and the outer solution provided by LBC, the different formulations and/or prognostic variables in LBC and RCM, and the spatial spin-up. The latter issue is the focus of this paper.

Spatial spin-up is the phenomenon by which small-scale (SS) features that are absent in the driving LBC develop as permitted by the higher spatial resolution of the nested model. Previous studies (Leduc and Laprise 2009; Leduc et al. 2011) have shown that a minimum domain size is required for the SS to develop and reach their full potential. These studies showed that for a jump of resolution between the LBC and the nested model of 12 (roughly equivalent to a T30 spectral model driving a 45 km RCM), a domain size of 144 x 144 grid points was barely sufficient for the SS to fully develop in the low levels in summer, and even larger domain sizes were required to reach a full development aloft and in winter due to stronger flow through the domain. Denis et al.

(2003) had shown that reducing the jump of resolution from 12 to 6 and the nesting interval improve the simulation. With a resolution jump of six, Colin et al. (2010) and Køltzow et al. (2011) noted that precipitation was underestimated near the western (inflow) boundary of their domain, a likely manifestation of spatial spin-up. Brisson et al. (2015) noted some deficiencies in their convection-permitting climate simulations when using single nesting, likely as a result of a large resolution jump combined with large nesting time intervals. Matte et al. (2016a) have shown that the use of multiple nesting reduces the resolution jump, with a positive impact on the SS development.

The focus of this study is on characterizing the impact of the resolution jump on SS spin-up in RCM simulations, by analysing the spatial development of SS from the lateral boundaries through the RCM domain, rather than the effect of domain size as in previous studies. The sought outcome of this study is the determination of the "trustworthy" region within an RCM domain, trustworthy in the sense that SS permitted by the high resolution have reached their asymptotic amplitude. The idealised Big-Brother experimental protocol will be used to address this issue. This paper is organized as follows. A brief description of the regional model followed by a description of the experimental design are presented in Section 2. The results are detailed in Section 3. Finally, Section 4 summarises the findings and concludes.

2.2 Experimental design

The experiments have been performed with the fifth-generation Canadian RCM (CRCM5; see Hernández-Díaz et al. 2013 for a detailed description). The physical parameterization of the CRCM5 is mostly based on the 33-km meso-global GEM model (Bélair et al. 2005, 2009) employed for numerical weather prediction by the Canadian Meteorological Centre (CMC). The model configuration uses Kain-Fritsch deep convection parameterization (Kain and Fritsch, 1990), Kuo-transient shallow convection (Kuo 1965; Bélair et al. 2005), Sundqvist resolved-scale condensation (Sundqvist et al. 1989), correlated-K terrestrial and solar radiation schemes (Li and Barker, 2005), subgrid-scale orographic effects are parameterized following the McFarlane mountain gravity-wave drag (McFarlane, 1987) and the low-level orographic blocking scheme of Zadra et al. (2003), and turbulent kinetic energy closure planetary boundary layer and vertical diffusion (Benoit et al. 1989; Delage and Girard 1992; Delage 1997). Unlike the NWP version of GEM however, CRCM5 uses the most recent version of the Canadian Land Surface Scheme (CLASS 3.5; Verseghy 2000, 2008) that allows a detailed representation of vegetation, land-surface types, organic soil and a flexible number of layers, and lakes are represented by the 1-D FLake model (Martynov et al. 2012). In the vertical, 56 levels are used.

To investigate the impact of the driving data resolution upon the development of SS features in a high-resolution RCM, the Big-Brother Experiment (BBE) protocol, originally designed by Denis et al. (2002b) is used. This experiment employs a perfect prognosis approach that isolates the nesting errors from other modelling errors, thus emphasizing the influence of nesting on the RCM solution. In the BBE, a first simulation named the Big Brother (BB) is realized on the largest possible domain. The BB simulation serves two purposes: (1) it is used as a reference to evaluate the test simulations nicknamed the Little-Brother (LB) simulations, and (2) it provides, after filtering, initial and driving lateral boundary conditions for LB simulations that are performed using the same model formulation and resolution as the BB. The BB data are processed by a low-pass filter to mimic the low-resolution GCM driving data. The resulting filtered BB datasets will be noted BB_Fr, with r the equivalent mesh size resolution. These BB_Fr fields are, in some sense, perfect as far as the large scales are concerned, because they do not suffer from simulation errors that would have occurred in coarse-mesh model simulations. However, the BB_Fr fields are devoid of SS as coarse-mesh GCM simulations would be. The LB-simulated SS can be compared with those of the verifying BB to assess the dynamical downscaling skill of various configurations of LBs and resolution jump by varying BB_Fr. Shown in Fig.2.1, the CRCM5 simulation on a 0.15° mesh (roughly 17 km) covering a 760 x 760 grid-point free domain centred on Montréal, Québec, Canada, served as BB. The BB simulation is driven by the ERA-Interim reanalysis for eight two-month long periods, starting on June 1st for summer and November 1st for winter, of the years 1997, 1998, 1999 and 2000. For these simulations the time step is 5 minutes. The BB simulation is driven by ERA-Interim data available at 6-hourly intervals.

Low-resolution LBC were generated by applying a low-pass filter based on the discrete cosine transform (DCT: Denis et al. 2002a), with a gradual response function that attempts to mimic the spectrum of equivalent grid-mesh simulations. The lower and upper limits were chosen to correspond, respectively, to the Nyquist length scale 2 Δx and to the smallest adequately resolved scales 7 Δx, as shown by Skamarock (2004) and Cholette et al. (2015), with a cosine-squared function transition between these two values. LBC corresponding to three resolution jumps (J) were generated. For J=24, corresponding to a mesh of 3.6° (noted as BB_F3.6), the lower and upper wavelength limits were chosen to be 792 km and 2772 km; for J=12, corresponding to a mesh of 1.8° (noted as BB_F1.8), the limits were 396 km and 1386 km; and for J=3, corresponding to a mesh of 0.45° (noted as BB_F0.45), the limits were 100 km and 346 km. The LB simulations were performed for 1.5-month periods starting on November 15 for winter and on June 15 for summer (thus leaving out the initial 15 days as spin-up of the BB simulation), for the years 1997 to 2000, using the BB_Fr dataset as IC and LBC (geopotential height, temperature, zonal and meridional winds, specific humidity and water content) at 1-hourly intervals. The LB simulations were performed on a free domain of 260 x 260 grid points (noted as D1 in Fig.2.1), surrounding by the Davies zone of 10 grid points which is weighted by a cosine-squared function. Unlike previous studies dealing with spatial spin-up with different domain sizes, here we used a rather large LB domain to ensure that SS amplitudes could develop to their asymptotic value within the domain. The climate statistics of the LB simulations will be compared to those of the BB for the four months of December and July, thus leaving out the initial 15 days as temporal spin-up of the LB simulations. Four sets of LB simulations will be performed; three of them will be nested with datasets BB_F3.6, BB_F1.8 and BB_F0.45, noted as LB_J24, LB_J12 and LB_J3, corresponding to resolution jumps of 24, 12 and 3, respectively, and a fourth one driven directly by BB, noted LB_J1, corresponding to a resolution jump of 1.

2.3 Results

In the analysis, fine-scale transient eddies in LB simulations driven by various BB_Fr will be compared with those of the reference BB. The departure of the time-mean components (also called transient-eddy component) will be analyzed. Any variable $\Psi(\vec{x}, t)$, function of space $\vec{x}$ and time t, will be decomposed as follows

$$\Psi(\vec{x}, t) = \overline{\Psi}(\vec{x}) + \Psi'(\vec{x}, t) \tag{2.1}$$

where $\overline{\bullet}$ is the temporal mean and ' the time deviation. The transient-eddy standard deviation is obtained as

$$\sigma'(\vec{x}) = \sqrt{\overline{\Psi'^2}}(\vec{x}) \tag{2.2}$$

A DCT filter is employed to isolate the SS from the total field. The DCT filter was configured to eliminate wavelengths larger than 400 km and retain those smaller than 300 km, with a gradual cosine-squared function transition in between. As defined, the SS that are analyzed in LB_J24 and LB_J12 were completely absent of the driving LBC and developed within the LB simulations. However, for LB_J3, the limits of the DCT filter used to produce LB_J3 and the SS field slightly overlap. Thus, a small part of the SS (those with wavelengths in the range 300 to 346 km) are present in the driving data for this case; nevertheless, the SS spin-up process can still be observed in LB_J3.

Figure 2.2 illustrates the SS spatial spin-up for different jumps of resolution for the 700-hPa relative vorticity in December; this variable is chosen for its abundant SS features. Figure 2.2a presents maps of the standard deviation of the SS transient-eddy component for the BB and the four LB_Ji simulations, called σ'_{BB} and σ'_{Ji}, respectively, on the free LB domain (see D1 domain in Fig.2.1). In the BB, large values are noted on the East Coast, corresponding to the North Atlantic storm track at this period of the year. Some spotty large values are also seen over the Appalachians and the Charlevoix Montains (Quebec) due to orographic effects. On the flat continent, relatively smooth small values are noted almost everywhere. In the LB_Ji simulations, weaker values can be seen at the western and southern edges of the domain, more pronounced for larger resolution jumps; these smaller values reflect the underdeveloped SS features downstream of the inflow boundaries, with the dominant westerly flow in winter. Spatial spin-up becomes even clearer by looking at the σ'_{Ji} normalized by the reference value σ'_{BB} as shown in Fig.2.2b. The red colour corresponds to values near unity, hence confirming the development of the SS features to their asymptotic amplitude. The underestimation of the SS transient-eddy amplitude near the boundary inflow of the domain is clearly visible, especially for the largest resolution jumps. Clearly, results in the spin-up zone should be taken cautiously because the fast atmospheric flow has not yet developed the SS permitted by the fine mesh. Figure 2.3 shows the corresponding results in July. Overall, the results in summer are similar than in winter, except that the spin-up zones at the western and southern edges of the domain are narrower due to the weaker general atmospheric circulation in summer than in winter, as noted before by Leduc et al. (2011).

Fig.2.4 and 2.5 show the value of the ratio $\left(\frac{\sigma'_{Ji}}{\sigma'_{BB}}\right)$ along a West-to-East cut, across the domain, for different jump of resolution J, for the 700-hPa relative vorticity SS transient-eddy standard deviation averaged over the middle third of the domain (indicated at the bottom right of Fig 2.4a), for December and July, respectively. This West to East section of the domain is used as it corresponds to the mean atmospheric flow for this region. The lower abscissa corresponds to the distance from the western boundary expressed in number of grid points (n) and the upper abscissa correspond to the distance expressed in km. Figures 2.4a and 2.5a show the gradual increase of the ratio towards unity with increasing distance from the western boundary. It can be noted that the distance required to approaching the full development of the SS increases with the resolution jump. Hence, when large jump of resolutions are considered, large domains are required to achieve the full development of the SS features permitted by the resolution of the driven model, as noted before by Leduc and Laprise (2009) and Leduc et al. (2011). Figures 2.4b and 2.5b show the ratio $\left(\frac{\sigma'_{Ji}}{\sigma'_{BB}}\right)$ for the relative vorticity at different levels for the J12 case. It can be seen that the SS spin-up distance increases in the vertical, likely related to faster wind speed in the upper levels.

Figure 2.6 shows the result obtained in a similar experiment configured as previously for December, but with a grid mesh of 0.45° rather than 0.15° for J8 and J12. By comparing this J12 result with the corresponding J12 case with 0.15° shown in Fig.2.4, it becomes clear that the spin-up distance varies in proportion to the RCM grid mesh in such a way that it covers the same number of grid points. This indicates that when varying the RCM resolution for a given resolution jump (hence varying the LBC resolution in proportion to the RCM resolution), the spin-up distance is best measured in terms of number of grid points rather than physical distance. On the other hand, when comparing the results obtained for J8 with a grid mesh of 0.45° shown in Fig.2.6 with those obtained for J24 with a grid mesh of 0.15° shown in Fig.2.4 (note that the LBC resolutions are the same in these two cases), the physical distance of spin-up are the same.

The experimental results shown in Fig.2.4 to 2.6 suggests a parametric curve for the spatial variation of SS transient eddies of the form

$$\frac{\sigma'_{Ji}}{\sigma'_{BB}}(\vec{x}) = 1 - k\exp(\frac{-x}{L}) \tag{2.3}$$

where x is the distance from the lateral sponge zone (when expressed in terms of grid points, x=nΔx_{RCM}, where n is the number of grid points whithin the RCM domain), L is the e-folding distance on which the asymptotic value is reached (in terms of grid points, L=NΔx_R, where N is a e-folding distance in grid points), and $0 \geq k \leq 1$ a parameter to account for possible overlap between the definition of the SS in the driving data and the RCM (k=1 for no overlap and k=0 for full overlap). Such form makes some intuitive sense: SS eddies that are absent in the LBC develop on the RCM high-resolution grid, as a result of various forcings (local physiographic, diabatic, non-linear interactions, hydrodynamic instabilities, etc.), gradually increasing in amplitude towards their asymptotic value within the domain. The results presented in Fig.2.4 and

2.5 covered several variations of RCM grid meshes (Δx_{RCM}), LBC resolution (Δx_{LBC}) and resolution jump (J=$\frac{\Delta x_{LBC}}{\Delta x_{RCM}}$). The following dependencies can be deducted from these results:

- L increases with height in the troposphere; closer analysis revealed that L varies with the average wind speed V through the domain at the level of the variable that is analysed: L$\propto$V.
- L varies with the shortest scale resolved by the LBC data: L$\propto 2\Delta x_{LBC}$

This suggests writing

$$L = \frac{2\Delta x_{LBC} V}{C}. \tag{2.4}$$

When Δx_{RCM} is held fixed and recalling the definition previously mentionned of L, Eq.(2.4) can be written as

$$N = \frac{2JV}{C}. \tag{2.5}$$

where C is a constant with units of speed for dimensional consistency. The optimum fit with the experimental results led to the value C=9 m s^{-1}, which happens to correspond roughly to the typical displacement speed of synoptic-scale weather systems and to the ratio of their length and time scales (Orlanski, 1975).

So, using Eq.(2.4), Eq.(2.3) becomes

$$\frac{\sigma'_{Ji}}{\sigma'_{BB}}(x) = 1 - k\exp(\frac{-xC}{2\Delta x_{LBC} V}), \tag{2.6}$$

while using Eq.(2.5), Eq.(2.3) then becomes

$$\frac{\sigma'_{Ji}}{\sigma'_{BB}}(x = n\Delta x_{RCM}) = 1 - k\exp(\frac{-nC}{2JV}). \tag{2.7}$$

The optimum fit was obtained by setting the empirical constant k to 1 for J24 and J12, to 0.7 for J3 and to 0 for J1, to reflect the overlap in the definition of SS in the experiments as carried out. Eq.(2.6) and Eq.(2.7) indicate that the adjustment distance is measured in terms of grid point numbers rather than physical distance when Δx_{RCM} is held fixed and Δx_{LBC} varies, while the adjustment distance is measured in terms of physical distance when Δx_{LBC} is held fixed and Δx_{RCM} varies. Those two equations are indicated by the dashed lines in Fig.2.4 to 2.6. Figure 2.7 illustrates the equations and can serve as an abacus to evaluate the domain required to obtain the full development of the SS for a given set of available LBC and RCM resolution. The figure shows the values of the distance 3 L (right hand y-axis) and 3 N (solid black lines) required to attain 95% of the asymptotic amplitude of SS. The left hand y-axis is the grid mesh of the LBC and the abscissa is the grid mesh of the RCM. Practitioners have to look at the intersection of the grid mesh of the LBC and the RCM of the wanted simulation to know the distance (in number of grid point or in physical distance, depending on the point of view) to correctly develop the small-scale features.

2.4 Conclusion

This study investigated the spatial spin-up distance as a function of the jump of resolution using the idealised Big-Brother protocol. A Big-Brother (BB) simulation was first performed with the CRCM5 on a 0.15° mesh over a very large domain over eastern North America, for two winter and two summer months of four years, driven by ERA-Interim reanalysis data. Then, this simulation was filtered to produce fields with a resolution equivalent to 3.6°, 1.8° and 0.45° meshes. The resulting dataset were used to drive a series of Little-Brother (LB) simulations, with a resolution jump of 24, 12 and 3, respectively, between the driving lateral boundary conditions and the LB mesh. An additional experiment with a jump of resolution of 1 was also made. Some limited experiments were also carried out with CRCM5 simulations on a 0.45° mesh.

Throughout this paper, the behaviour of small-scale transient eddies was studied using the relative vorticity field because this variable is typical of atmospheric variables that exhibit substantial small-scale amplitude, similar to vertical velocity or specific humidity, but unlike variables such as geopotential height whose spectrum is dominated by larger scales. It is worth noting that other variables have also been analysed but were not shown (such as meridional and zonal wind components, relative humidity), and conclusions remain the same. The 700-hPa level was chosen because it is close to the steering level of mid-latitude weather systems, near the level of non-divergence and maximum vertical velocity, and hence where precipitation is generated. In principle, this analysis could be extended to any variable and height of specific interest for some application of RCM simulations.

It has been shown that small-scale features take a large distance to develop within the simulated domain for large jump of resolution, particularly in winter and in the upper levels where the average flow through the domain is faster. It was found that the results could be summarized with a parametric equation describing the variation of the SS transient-eddy amplitude from the inflow boundary, and hence the spin-up distance.

Our initial preconception was that the spin-up distance would increase with the resolution jump between the LBC and the RCM resolutions. The results obtained with the idealised BBE have shown however that the spin-up "distance" that scales with the resolution jump is not the physical distance but rather the distance as measured in terms of RCM grid point numbers (see Eq.2.7). For a given set of LBC, its resolution alone determines the spin-up physical distance, independently of the RCM resolution; hence when varying the RCM resolution for a given set of LBC, the number of RCM grid points over which SS approach their asymptotic value increases linearly with the resolution jump (see Eq.2.6).

This parametric equation may be useful to RCM practitioners to determine an optimal domain to ensure the full development of the SS permitted by the resolution of the RCM used. The potentially trustworthy region of the RCM domain must exclude the spin-up region where fine scales have not yet reached their mature amplitude, thus shedding doubt on the simulated results in this region. Furthermore, RCM practitioners of the multiple nesting approach should also be aware of the location of the trustworthy region of each of their intermediate spatial-resolution simulation for an optimal used of this approach.

The fact that those results were provided from a 1-h nesting interval simulation might rise some questions about spatial spin-up at a more relaxed nesting interval. In fact, it can be demonstrated that the nesting time interval should be related to the resolution jump. For more detailed description, we referred the reader to the Appendix. A related point to also consider is the sensitivity to the width of the boundary relaxation zone. It is worth noting that this point has been assessed in another study, not reported in this paper. In essence the results have shown that the width of the blending zone has little effect upon the fine scales, its effect being felt mainly in the large scales that are better reproduced when expanding the blending zone.

Hence, in the interpretation of RCM simulations, it is important to take into account the small-scale spin-up region and exclude it from the analysis. In the last decade, several efforts have been made to foster high-resolution climate-change information through coordinated experiments such as CORDEX in which a strict simulation framework is imposed, including domain size and location. The results in this study suggest that the spatial spin-up should be taken into account in the design of the simulation framework and the ensuing analysis to avoid that spatial spin-up might contaminate results over the region of interest. Finally, further studies are needed for different domains location to validate the main conclusion of this study. However, the wind dependency of the empirical law suggests a strong relation between the weather regime and the small-scale development, which might give a good insight of how small scales are developed for other domains where the general weather regime is well known.

Acknowledgements: This research was supported by the Natural Sciences and Engineering Research Council (NSERC) of Canada. Computations were made on the supercomputer guillimin, managed by *Calcul Québec* and Compute Canada. The operation of this supercomputer is funded by the Canada Foundation for Innovation (CFI), the *Fonds de recherche du Québec - Nature et technologies* (FRQNT), NanoQuébec, and the *Réseau de médecine génétique appliquée* (RMGA). D.M. thanks the FRQNT for a graduate fellowship. The authors are greatly indebted to Dr. Ramón de Elía for his constructive comments, to Dr. Bernard Dugas and Ms. Katja Winger for their essential help with the use of CRCM5, and to Mr. Georges Huard and Ms. Nadjet Labassi for maintaining user-friendly local computing facilities.

2.5 Appendix: Spatial spin-up and nesting interval

Figure 2.8 shows the same results as Fig.2.4a, except that the nesting interval is extended to 6-hourly instead of hourly. To compare with the previous case, Eq.(2.5) or (2.7) has also been used to draw the parametric curves computed in Fig.2.8 for each Ji, showing clear differences with results when the nesting interval was set to 1 h. For the two larger jumps of resolution (i.e. J24 and J12), no difference is noted with respect to Fig.2.4a. However, J3 and J1 struggle more to fulfill the $\left(\frac{\sigma'_{Ji}}{\sigma'_{BB}}\right)$ deficit due to the excessively long nesting interval. This means that even when all scales are provided by the driving data, a excessively long nesting interval degrades the development of small-scale features, which has also been noted in previous studies (Denis et al. 2003; McDonald 2005, 2006; Termonia et al. 2009; Omrani et al. 2012). It will be demonstrated below that the nesting time interval should be related to the resolution jump. Consider a weather disturbance in the nesting data used to provide the LBC to drive an RCM. For simplicity we will assume a sinusoidal shape in one dimension, with wavenumber

$\kappa = \frac{2\pi}{\lambda}$, wavelength λ, moving at phase speed C:

$$\Psi(x, t_n) = Asin\kappa(x - Ct_n) \tag{2.8}$$

In practice, the nesting data is only available at discrete time intervals t_n, with n an integer, and hence it needs to be interpolated in time between nesting intervals $\tau = t_{n+1} - t_n$ to drive the RCM at each time step. For most RCM applications, linear interpolation is used between nesting intervals to obtain values at intermediate times. Consider the interpolated value at the middle time between two nesting intervals:

$$\Psi(x, t_{n+1/2}) \approx \frac{\Psi(x, t_n) + \Psi(x, t_{n+1})}{2} \tag{2.9}$$

Trigonometric identities give the result

$$\begin{aligned} \Psi(x, t_{n+1/2}) &\approx \frac{A}{2}\left(sin\kappa(x - Ct_n) + sin\kappa(x - C(t_n + \tau))\right) \\ &= Asin\kappa(x - C(t_n + \tau/2))cos\kappa C\tau/2 \end{aligned} \tag{2.10}$$

Recognising the exact solution as $Asin\kappa(x - C(t_n + \tau/2))$, the factor $r = cos\kappa C\tau/2$ appears as the numerical response of the linear interpolation. This factor may be written as $r = cos\pi\delta/\lambda$ where $\delta = C\tau$ is the displacement distance of the disturbance in between two nesting time intervals. The interpolation provides an excellent approximation when $\delta \ll \lambda$ (i.e. $\tau \to 0$) because factor $r \to 1$ as expected; but the results degrade for larger displacement and in fact r=0 for $\delta/\lambda = 1/2$. To obtain acceptable results, one should hence aim for values of $f \equiv \delta/\lambda$ definitely smaller than a half. The shortest length scales for λ are limited by resolution of the nesting data. Considering that LBC are provided by a driving model with grid mesh Δx_{LBC}, then $\lambda \geq N\Delta x_{LBC}$ where $2 \leq N \leq 7$; N=2 corresponds to the Nyquist cut-off and corresponds approximately to the shortest well resolved scales (e.g. Skamarock 2004). Consider a resolution jump J=$\frac{\Delta x_{LBC}}{\Delta x_{RCM}}$ between the resolution of the driving data and the RCM, we can then write

$$f = \frac{\delta}{\lambda} = \frac{C\tau}{N\Delta x_{LBC}} = \frac{C\tau}{NJ\Delta x_{RCM}} \tag{2.11}$$

or

$$\tau = fNJ\Delta x_{RCM}C \tag{2.12}$$

for the largest acceptable nesting time interval. Using parameter values f=1/5, N=7, C=30 km h^{-1} and $\Delta x_{RCM} = 20$ km, we get $\tau \approx Jh$. This empirical equation confirms the results shown in Fig.2.8 showing that, for an RCM with $\Delta x_{RCM} = 20$ km, a nesting interval of 6 h is adequate for J equal to 12 and 24, but not for J equal to 1 and 3, in which case $\tau = 1h$ is adequate.

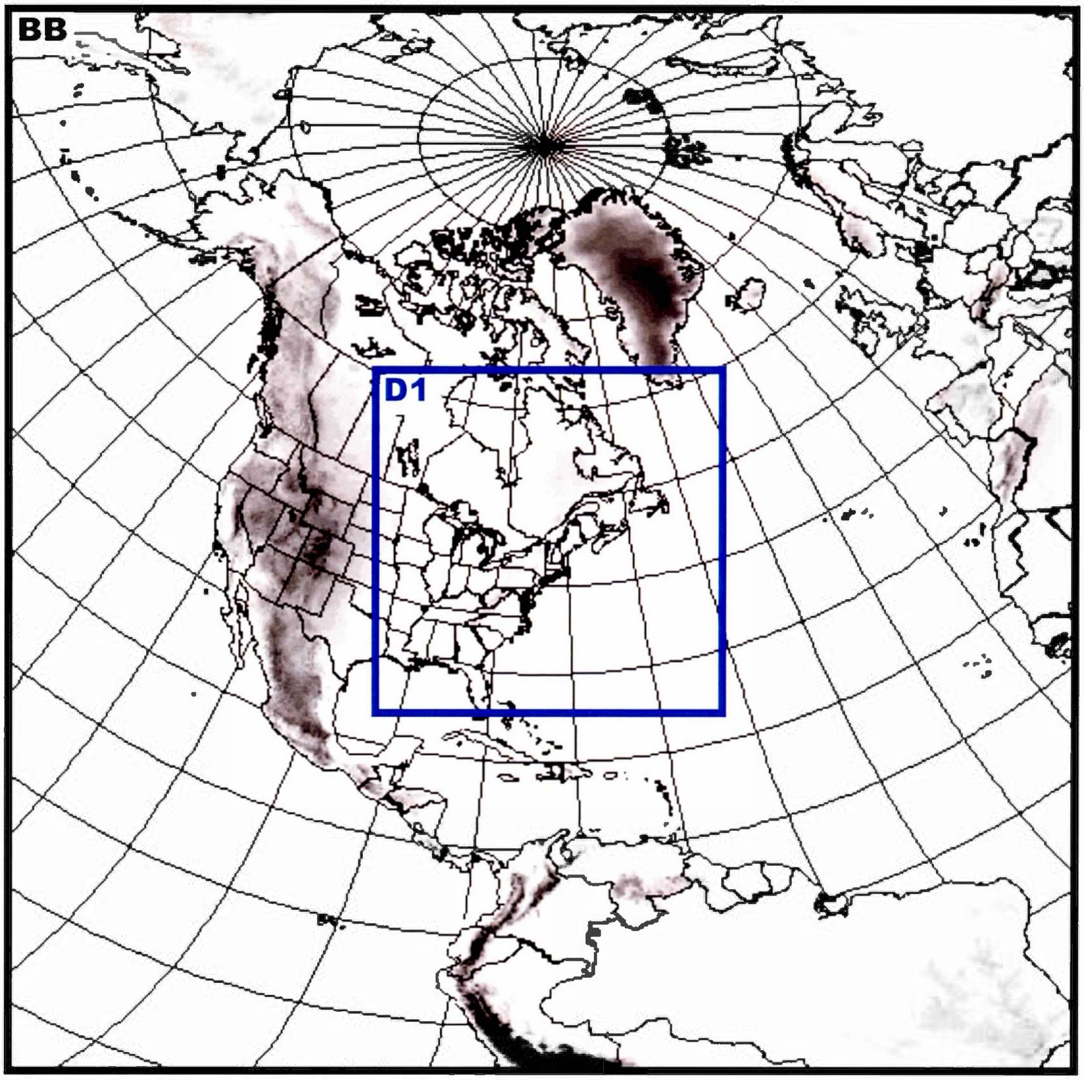

Figure 2.1 The domain of the Big-Brother simulation (BB)(free domain of 760 x 760 grid points). All the Little-Brother simulations have a free domain of 260 x 260 grid points centred on Montréal (D1)

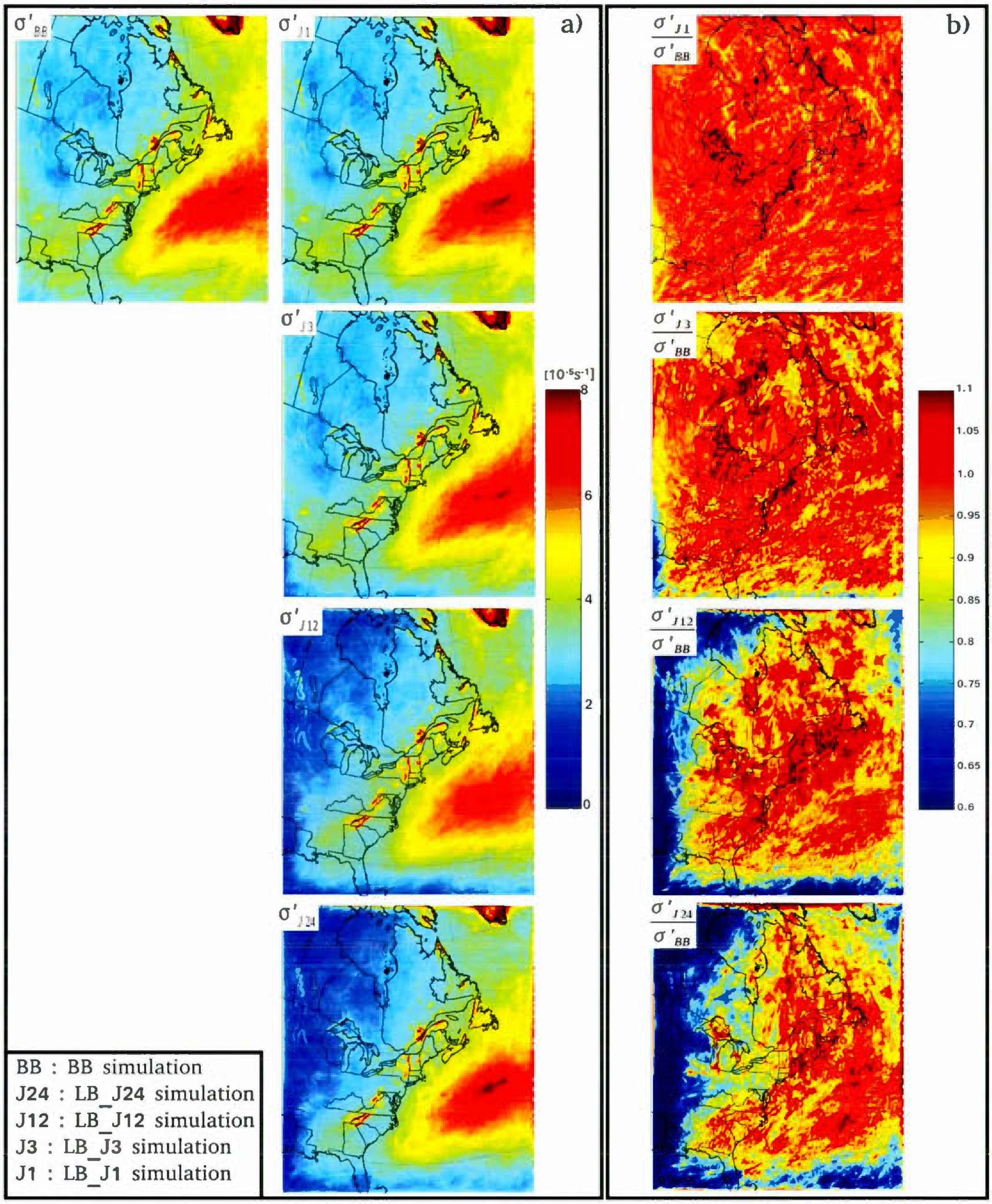

Figure 2.2 Small-scale transient-eddy standard deviation of the 700-hPa relative vorticity for the four December simulations. b) Ratios of the LB simulations standard deviation with that of the reference BB simulation $\left(\frac{\sigma'_{Ji}}{\sigma'_{BB}}\right)$

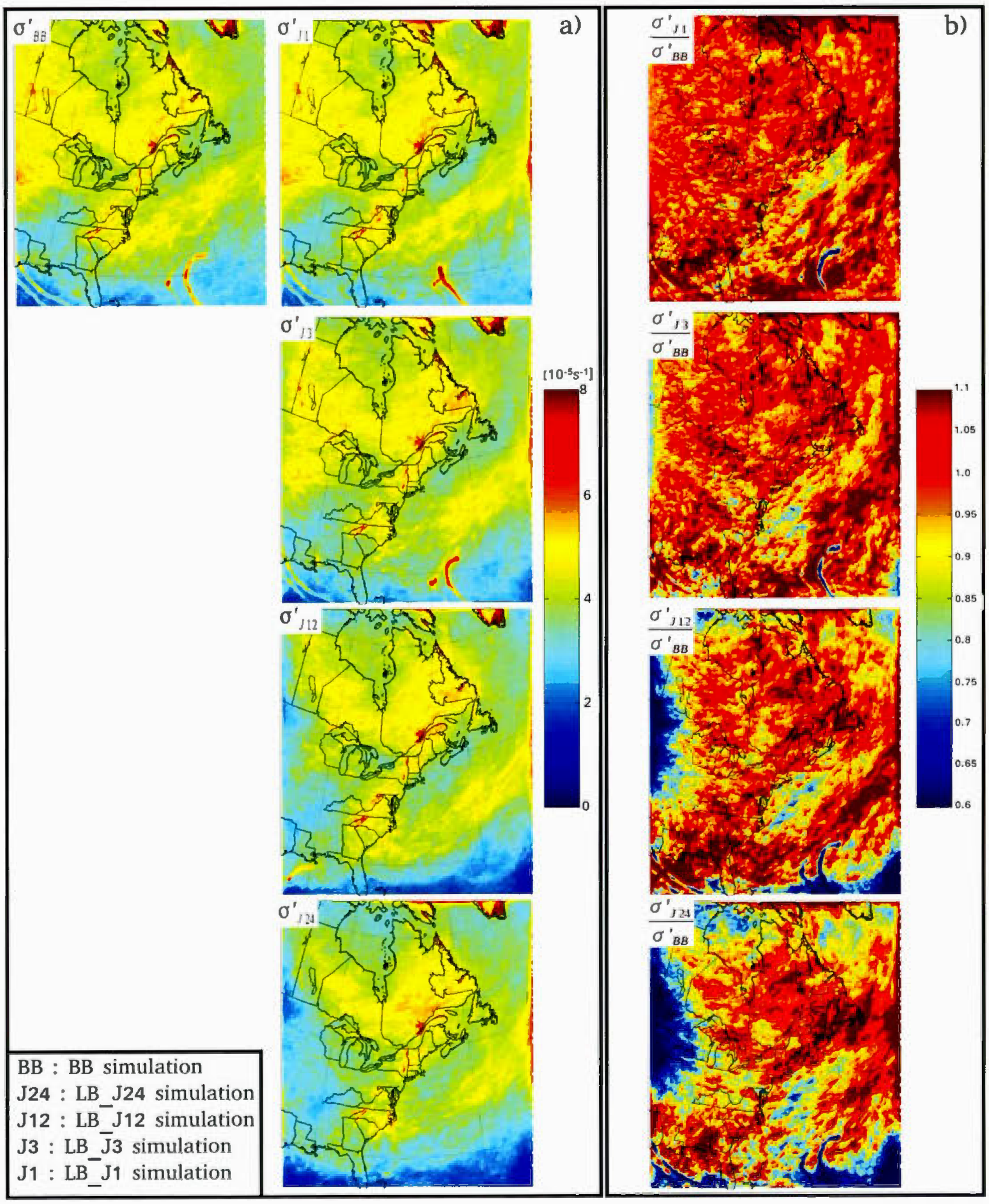

Figure 2.3 Same as Fig.2.2, but for the four July months.

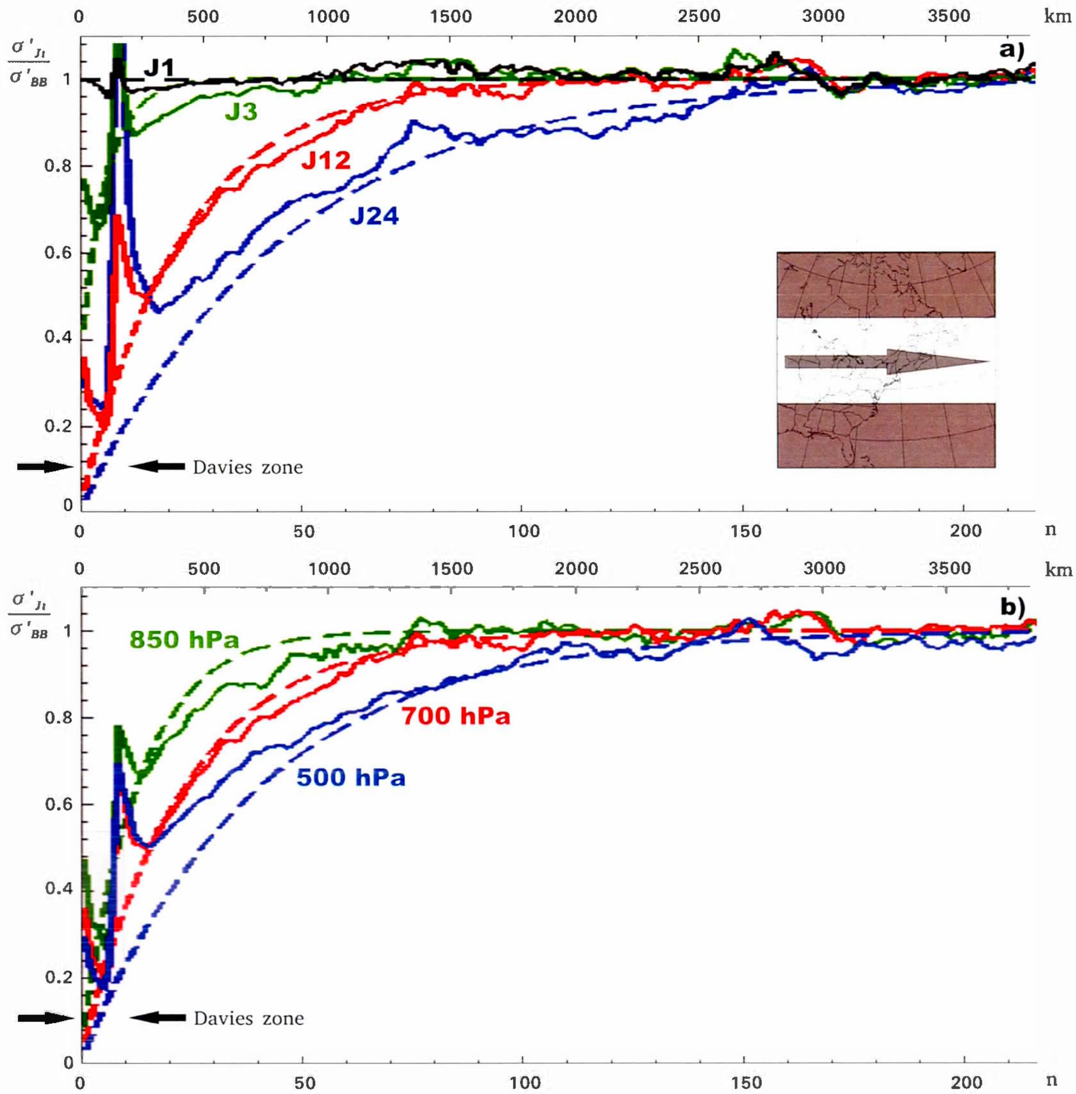

Figure 2.4 a): West to East cut, across the domain, (as shown at the bottom right of panel a) of the small-scale transient-eddy standard deviation for the relative vorticity at 700 hPa of LB_Ji normalized by the reference simulation BB, as a function of the distance from the western boundary (in km and number of grid points (n) in the upper and lower abscissa respectively in both panel), for the four months of December. The different jumps of resolution J24, J12, J3 and J1 are shown by the blue, red, green and black lines, respectively. b) Same as a) but only for J12 at three different levels: 850 hPa (green), 700 hPa (red) and 500 hPa (blue).The empirical equations (2.6) and (2.7) are indicated by the dashed lines

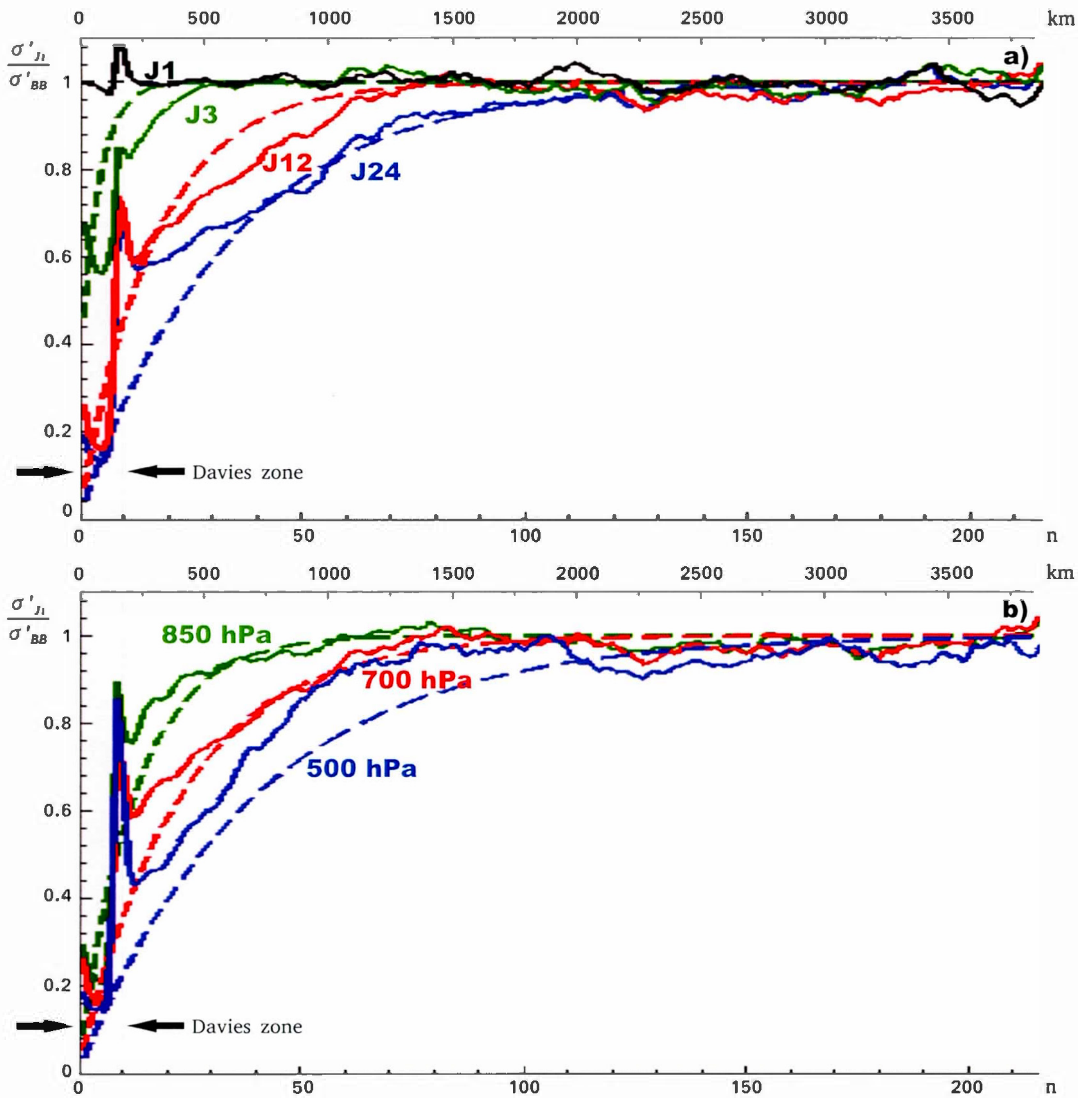

Figure 2.5 Same as Fig.2.4 but the four July months.

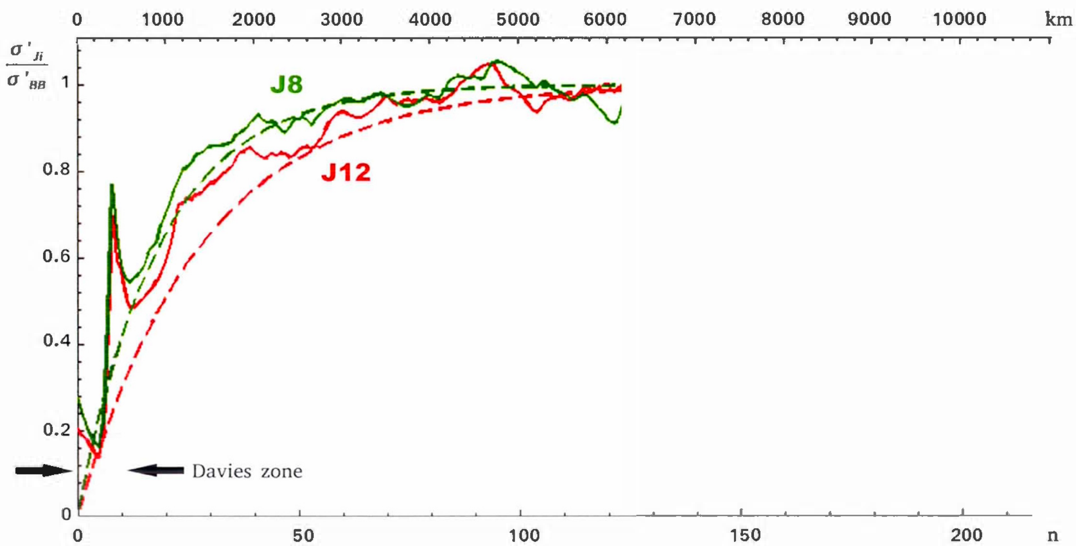

Figure 2.6 Equivalent to Fig. 4a, but for similar experiment realized with an RCM on a 0.45° mesh rather than 0.15° mesh.

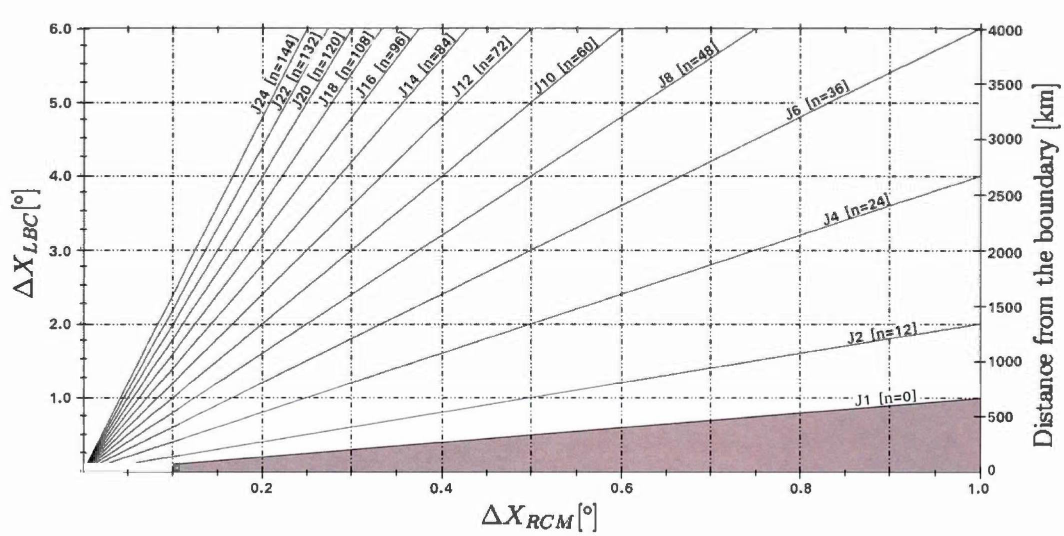

Figure 2.7 An abacus developed from Eq.(2.6) and Eq.(2.7) showing the distance 3 L (right hand y-axis) and 3 N (solid black lines) required to attain 95% of the asymptotic amplitude of the small-scale transient eddies, as a function of the grid mesh of the LBC (ordinate) and RCM (abscissa), respectively, for an average wind speed V equal to the typical speed of synoptic-scale weather systems C (V≈C).

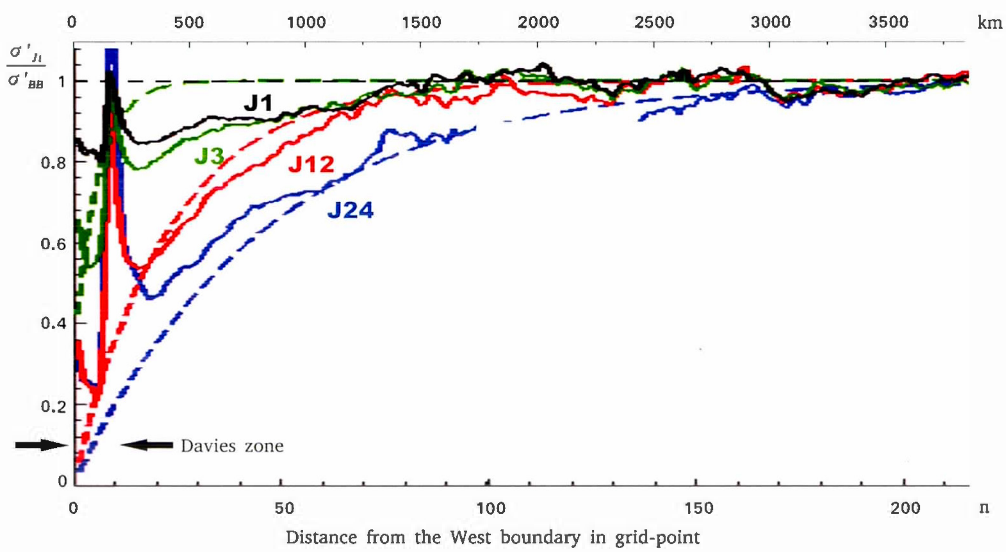

Figure 2.8 Same as Fig.2.4a but with a nesting time interval of 6 h.

CHAPITRE III

CLIMATE CHANGE STUDY OF MIXED PRECIPITATION OVER SOUTHERN QUÉBEC USING A REGIONAL CLIMATE MODEL

This chapter is presented in the format of a scientific article submitted to the journal *Climate Dynamics*. The detailed reference is:

Matte, D., Thériault, J. M. & Laprise, R., 2017: Climate change study of mixed precipitation over southern Québec using a Regional Climate Model. Submitted to Climate Dynamics

Abstract

Freezing and frozen precipitation events can have major impacts on the society by causing power outages and disruptions to the transportation networks. Despite the catastrophic consequences associated with these precipitation types, very few studies have investigated how the occurrences could evolve under climate change. This study aims to investigate the changes of mixed precipitation over southern Québec using regional climate modeling at high resolution. It uses the fifth-generation Canadian Regional Climate Model with climate scenario RCP 8.5 at 0.11° grid mesh. The precipitation types such as freezing rain, ice pellets or their combination are diagnosed using 5 methods (Cantin and Bachand, Bourgouin, Ramer, Czys and Baldwin). The statistics of the diagnosed precipitation for the recent past (1980-2009) are found to be comparable to that of observations. The projections for future scenario (2070-2099) suggest a general decrease in the occurrences of mixed precipitation over southern Québec from October to April. This is mainly due to a decrease in long-duration events ($\geq$6h). Overall, this study contributes to better understand how the distribution of winter precipitation types might change in the future using high-resolution regional climate model

Key words: Climate change, High-resolution climate simulation, Multiple nesting, Freezing Rain, Ice pellet, Precipitation-type algorithm

3.1 Introduction

Freezing and frozen precipitations are commonly formed in mid-latitude regions (Cortinas, 2000; Cortinas Jr et al., 2004; Groisman et al., 2016) during the passage of warm fronts in winter (Cortinas, 2000). This can lead to the typical vertical temperature structure composed of a warm air layer (T>0°C) overlaying a cold-air layer (T<0°C) near the surface. Some regions are particularly prone to such precipitation types, such as near St. Johns, Newfoundland, as well as mountainous areas of northeastern North America. The US Appalachian region (Rackley and Knox, 2016) is often influenced by the phenomena of cold air damming that could lead to freezing precipitation. Furthermore, the St. Lawrence River Valley (SLRV) is also prone to freezing precipitation because of wind channeling effects (Carrera et al., 2009).

Cortinas (2000) conducted a freezing rain climatology in the Great Lakes region in North America. He stated that storm track, the proximity of the Atlantic Ocean, the lakes and the topography create a large spatial and temporal variability of freezing rain in that region. Cortinas Jr et al. (2004) extended this study on the occurrence of freezing precipitation, freezing drizzle and ice pellets between 1976 and 1990 to the continental United State and Canada. They showed that the highest frequency of freezing rain and ice pellets occurs in St. Johns area as well as in the SLRV, as confirmed by the studies of Stuart and Isaac (1999) and Groisman et al. (2016). The maximum reported in the SLRV is due to a combination of factors such as the relative location of the extratròpical storm track, water source proximity and topographical features (Bernstein, 2000; Roebber and Gyakum, 2003; Cortinas Jr et al., 2004). Although topography is not considered a sufficient condition for freezing precipitation formation, many studies have mentioned its importance on producing the favorable near-surface conditions (Stuart and Isaac, 1999; Cortinas, 2000; Cortinas Jr et al., 2004; Henson et al., 2011). For example, the high frequency of freezing precipitation in the SLRV is related to wind channeling of cold air near the surface (Whiteman and Doran, 1993; Roebber and Gyakum, 2003).

The measurement and simulation of freezing rain and ice pellets is challenging because they are often composed of both liquid and solid, and they mainly occur at temperatures near 0°C. Two main approaches can be used to determine the precipitation types in atmospheric models. The first approach is diagnostic, which involves using the current state of the atmosphere for variables such as temperature and relative humidity on different pressure levels (Reeves et al., 2014; Bourgouin, 2000; Baldwin and

Contorno, 1993; Cantin and Bachand, 1993; Czys et al., 1996; Ramer, 1993). The second approach uses microphysics equations to predict the mass mixing ratio and number concentration of the different types of precipitation (Milbrandt and Yau, 2005a,b; Morrison and Grabowski, 2008; Morrison and Milbrandt, 2015). Although this approach is more physically based, it is computationally expensive. It is thus more affordable to use diagnostic methods to conduct climate studies.

Few studies have been focusing on freezing and frozen precipitation in a context of climate change (Cheng et al., 2007, 2011; Lambert and Hansen, 2011; Klima and Morgan, 2015). Cheng et al. (2011) studied freezing rain occurrences over eastern Canada by statistically downscaling several general circulation models at the location of observing stations. They found a projected increase of freezing rain during the coldest months and a decrease during the transition seasons (fall and spring). Lambert and Hansen (2011) used a different approach. They post-processed the third-generation Canadian Coupled Climate Model to diagnose the future freezing rain occurrences. Their study suggested a poleward shift of the freezing precipitation, which is explained by the poleward shift of the 0°C isotherm. Nevertheless, they also mentioned that their coarse spatial and temporal resolutions were probably not sufficient to highlight key factors producing freezing rain. Finally, Klima and Morgan (2015) performed an idealized experiment using historical vertical temperature profiles on which they applied several warming scenarios to explore how freezing rain may change under these conditions. They also found a poleward shift of the freezing precipitation as well as an increase of freezing rain in winter rather than in the transition seasons.

High-resolution climate simulations are required for an adequate representation of local topography and key processes leading to mixed precipitation formation. These would be, however, very expensive to run with Global Circulation models (GCMs). The use of nested limited-area Regional Climate Models (RCMs) to dynamically downscale GCM simulations allows drastically reducing the computational cost while benefiting from the value added by increased resolution. At very high spatial resolution, the computational cost of RCM can be further reduced using multiple dynamical downscaling (e.g., Cholette et al., 2015; Matte et al., 2016a). The study of Cholette et al. (2015) has shown that the wind channeling in the St. Lawrence River Valley is fairly well represented with a grid spacing of $\leq$ 9 km. Matte et al. (2016a) have shown that multiple nesting was not only technically feasible but also appropriate, to some extent, to conduct high-resolution climate modeling.

The main purpose of this study is to realize high-resolution regional climate simulations to study the evolution of mixed precipitation associated with climate change. The study focuses over the Québec Province during past (1980-2009) and projected future climate (2070-2099) under a Representative Concentration Pathway (RCP) 8.5 future scenario (Meinshausen et al., 2011).

The performance of the model with be evaluated by using reanalysis as driving data (named hindcast simulation) and compare its solution with observations. Then, to study the climate change signal, the historical and projected future climate simulation will be done using a GCM as driving data.

This paper is organized as follows. The experimental design, a description of the regional climate model, its configurations and a brief description of the algorithms used to diagnose the precipitation types are presented in the next Section. The past and future simulated climates are discussed in Section 3. Finally, the main results are summarized and discussed in Section 4.

3.2 Experimental design

3.2.1 CRCM5 configuration

The simulations have been performed with the fifth-generation Canadian Regional Climate model (CRCM5; see Hernández-Díaz et al., 2013, for a detailed description). The physical parameterization of the CRCM5 is mostly based on the 33-km meso-global GEM model (Bélair et al., 2005, 2009) employed for numerical weather prediction by the Canadian Meteorological Centre: Kain-Fritsch deep convection parameterization (Kain and Fritsch, 1990), Kuo-transient shallow convection (Kuo, 1965; Bélair et al., 2005), Sundqvist resolved-scale condensation (Sundqvist et al., 1989), correlated-K terrestrial and solar radiation schemes (Li and Barker, 2005), subgrid-scale orographic effects following the mountain gravity-wave drag of McFarlane (1987) and low-level orographic blocking scheme of Zadra et al. (2003) for the turbulent kinetic energy closure planetary boundary layer and vertical diffusion (Benoit et al., 1989; Delage and Girard, 1992; Delage, 1997). On the other hand CRCM5 uses the most recent version of the Canadian Land Surface Scheme (CLASS 3.5; Verseghy, 2000, 2008) that allows a detailed representation of vegetation, land-surface types, organic soil and a flexible number of ground layers, and lakes are represented by the 1-D FLake model (Martynov et al., 2012).

3.2.2 Hindcast simulation setup

The domain for the hindcast simulation is shown by the green square in Fig.3.1a. The grid mesh is 0.11° and the domain contains 160 x 160 grid points (including the Davies sponge zone). The integration is performed with a time step of 300 s and 56 terrain-following levels in the vertical. The hindcast simulation (noted CRCM5/ERA) was driven by ERA40 reanalysis data from 1975 to 1978 and continued with ERA-Interim reanalysis data (ERA-I) for the period 1979 to 2009, on a 0.75° grid, at a 6-hourly interval. The study starts in 1980 to ensure enough time for spin up. The jump of resolution between the lateral boundary conditions and the RCM mesh is about 7; as suggested by the study of Matte et al. (2016b), a lateral spin-up region should be taken into consideration to make sure that the fine-scale features can fully develop (Fig.3.1, green region). The analysis region centered on Montréal, Québec, Canada, encompasses 80 x 90 grid points (Fig.3.1a and b).

3.2.3 Historical and projected climate simulations setup

The Max-Planck Institute for Meteorology Earth System Model (MPI-ESM-LR) with a linear transform grid of a 2.8°, is used as boundary conditions to drive the CRCM5. For computational cost considerations (Matte et al., 2016a), the GCM-driven simulations have been realized using a two-stage dynamical downscaling approach. In the first stage a 0.45° grid mesh CRCM5 simulation is driven by MPI-ESM-LR, resulting in a jump of resolution of about 6, over a domain covering a 110 x 110 grid-point area (blue square in Fig.3.1a) with a time step of 20 min; this simulation is denoted as RCM45. In the second stage, the RCM45 data is used to provide the lateral boundary conditions at hourly intervals to the CRCM5 on a 0.11° mesh, resulting in a jump of resolution of about 4, covering a 130 x 130 grid-point domain (black square in Fig.3.1a), with a time step of 300 s; this simulation is denoted RCM11 The analysis domain is the same as that for the hindcast simulation; the CRCM5 domains for the two stages have been chosen to follow the optimal configuration suggested by the study of Matte et al. (2016b), and the lateral spin-up regions are shown by the colored bands in Fig.3.1a. The quoted domain sizes include the Davies sponge zones.

Time slices are used to reduce the CRCM5 computing cost. The first stage periods are 1970-2009 and 2060-2099, and the second stage periods are 1975-2009 and 2065-2099, for the historical and projected climate simulations, respectively; this leaves 5 years between each stage to ensure that the simulations had time to adjust correctly.

The simulations after 2006 followed the RCP 8.5 scenario (Meinshausen et al., 2011).

3.2.4 Diagnostic of precipitation types

Five precipitation-type algorithms have been used to provide a range of estimates in the distribution of mixed precipitation at the surface. The study focuses on mixed precipitation, rather than freezing rain and ice pellets separately, to overcome issues about their distinction in both the algorithms and the observations (Reeves et al., 2014). Most calculations have been computed on model levels, except for the partial thickness method of Cantin and Bachand (1993). Short descriptions of the five algorithms are provided below.

The Bourgouin (2000) algorithm is based on calculating, in an aerological diagram, the positive and negative area (in J kg^{-1}). By comparing those two areas and using defined thresholds, precipitation types can be snow, ice pellets, freezing rain and rain. The thresholds have been defined by Bourgouin (2000) using a database of collocated surface precipitation observations and upper air sounding for two cold seasons (1989-90 and 1990-91) over North America. Mixed precipitation is defined when freezing rain or/and ice pellet are diagnosed. This scheme is already implemented in GEM for weather forecast, and it has been tested in CRCM5 on past climatology over the province of Québec and demonstrated good comparison with observations (Bresson et al., 2017).

The Czys approach (Czys et al., 1996) is a physically-based algorithm using a non-dimensional parameter to distinguish freezing rain and ice pellets. The residence time of a 400-μm frozen hydrometeor falling in a warm layer is compared to its melting time. The onset melting temperature derives from the theory of Drake and Mason (1966), which is based on the rate of energy supplied by the environment to the particle and the rate of energy required to melt the frozen particle. The mixed precipitation is defined when freezing rain or ice pellets occurs.

The Ramer (1993) scheme is based on a calculation of an ice fraction using basic parameters such as the temperature, wet-bulb temperature and relative humidity. It differentiates among snow, ice pellets, mix of snow and rain, mix of freezing rain and ice pellets, snow, freezing rain and rain. The mixed precipitation diagnosed with this method is defined when ice pellet, mix of freezing rain and ice pellets or freezing rain occurs.

The partial thickness method developed by Cantin and Bachand (1993) scheme

(CB) compares the thickness of the 1000-850 hPa and the 850-700 hPa layers. Mixed precipitation is diagnosed when the precipitation falls within a 850-700 hPa layer with a thickness greater than 154 dam, followed by a 1000-850 hPa layer with a thickness less than 131 dam. An additional criterion, requiring that the 2-meter temperature is below freezing temperature has been added. This 2-meter temperature criterion is a necessary but not sufficient condition for mixed precipitation.

The method of Baldwin and Contorno (1993) diagnoses the precipitation level and then calculates diagnosed ice crystals if the temperature is below 269 K. Those ice crystals, then, evolve through different phases changes according to the wet-bulb temperature and the near-surface temperature. In this study, we have followed the modifications suggested by Cortinas et al. (2002), which use a similar decision tree but have modified the thresholds. Mixed precipitation diagnosed with this method includes both ice pellets and freezing rain.

3.2.5 Available Observations

To evaluate the precipitation type diagnostic, observation data from the Environment and Climate Change Canada surface stations (MANOBS for Manual Observations) were used. The database provides hourly occurrences of the precipitation types. The observations were carefully quality-controlled. Only the stations with hourly observations were used. Also, the stations associated with missing data for more than a month over the study period were rejected, as well as other data that were not validated by the National Climate Archive. The stations retained in this study are shown in Fig.3.1b.

3.2.6 Methodology

As suggested by Lambert and Hansen (2011), a minimal threshold of 1 mm/day is applied in order to consider a precipitation event. An event is defined when mixed precipitation was diagnosed at the surface, as defined for each of the 5 algorithms in section 3.2.4. If less than 6 h separate two mixed precipitation episodes, they are counted as a single event. For observations, mixed precipitation is defined when freezing rain or/and ice pellets were reported. The closest grid point associated with a similar topographic height is used to compare model results with a specific stations.

3.3 Past climatology of mixed precipitation

3.3.1 Occurrence of mixed precipitation

The mean annual number of hours of mixed precipitation at the stations (disks) and using the 5 algorithms in the CRCM5 hindcast simulation are shown in Fig.3.2. All algorithms captured the main mixed-precipitation occurrence pattern, such as the maximum values over the Appalachian Mountains, the Charlevoix mountains, the Laurentian mountains, the Saguenay River, as well as a relative maximum near the SLRV area. Relatively higher number of hours of mixed precipitation is found at higher elevations where the surface temperature is often below 0°C during winter. The average of all five algorithms is shown in panel 3.2f. Unfortunately, it is difficult to confirm the numerical results as few observations are available in the area. Panel 3.2g displays the annual standard deviation calculated around the average value, showing a wider range of occurrences in complex terrain, confirming that the occurrence of mixed precipitation is sensitive to the topography.

Figure 3.3 shows the mean annual hourly occurrence of mixed precipitation at 4 observation stations. There are some differences and similarities among the results of the 5 diagnostic algorithms. The Bourgouin, Czys, Ramer and Baldwin algorithms reproduce modestly well the observations at Mirabel (YMX), Montréal (YUL) and Québec City (YQB), although the Ramer and the Baldwin captured correctly the maximum number of hours of mixed precipitation at YMX. Substantial differences can be noted between the Czys an CB algorithms. The former produced an underestimation of mixed precipitation over the SLRV (see Fig.3.2b), which could be due temperature at which melting of hydrometeor starts. The latter also underestimates mixed precipitation occurrences for all four stations (Fig.3.3).

The frequency distribution of events duration at Dorval, Québec (YUL) is shown in Fig. 3.4. The standard deviation of the nine nearest grid points of the MANOBS station is also indicated by the black lines for each algorithm. Panel 3.4a shows the distribution for events with duration between 1 and 10 h. In general, the observation and most of the algorithms reveal that the shortest duration events are the most frequent and the number of events decreases monotonically as their duration increases. The Ramer and the Czys schemes overestimate the occurrence of 1-h events by around 12 and 20 events, respectively. But the large standard deviation of the nearest grid point suggests a sensibility in the chosen grid point for such short duration. The CB scheme, however, shows a distinct flat distribution for the shortest duration events, and it underestimates the events that last less than 6h; for example, for the events lasting 1 to 5 h, the occurrences are underestimated by 78, 68, 54, 58 and 63%, respectively. This underestimation correlates with the mean annual number of hours diagnosed by that method (Fig.3.2c and 3.3); since CB compares two fairly large atmospheric layers, when the melting occurs within the 1000-850 hPa layer, this scheme does not capture it, and hence no mixed precipitation is diagnosed (see Sect.3.6). This explains partly the underestimation of mixed precipitation for the CB show in Fig.3.2c and Fig.3.4a.

The number of events with a duration from 11 to 30 h and from 31h to 60 h is shown in Fig.3.4b and c, respectively. Those long-duration events are less frequent; for example, less than five events for duration between 11 and 30 h, and 1 event of duration between 31 and 60 h, although they vary among algorithms. This is due to the difficulty of the model to diagnose the duration of the events. For example, the observation may report an 11-h duration event when the model did not capture it because of no precipitation or/and no production of a melting/refreezing layer. Observational errors are also possible. Furthermore, the algorithms can diagnose different duration events. That being said, all algorithms diagnosed long-duration event meaning that the model correctly reproduces the long-duration atmospheric conditions associated with those events, which are discussed in the next subsection.

In summary, similar statements can be made for the other stations. In general, the large standard deviation of the nine nearest grid point shows that the distribution is quite sensitive to the chosen grid point.

3.3.2 Atmospheric conditions associated with long- and short-duration events

To study the atmospheric conditions in which the mixed precipitation events occur, these have been divided into short (<6h) and long (≥6 h) duration events. Long-duration events are important because of the potential for severe conditions resulting from large accumulations despite the fact that freezing rain events are usually associated with light precipitation (Ressler et al., 2012).

The synoptic scale pattern of the mean sea level pressure (MSLP) has been compiled for both short- and long-duration events (Fig.3.5a,b,c and d). Figure 3.5a-b show composites of the ERA-Interim MSLP at the nearest time associated with the beginning of events observed at YUL. The composite MSLP patterns are similar for short- and long-duration events, with a low pressure centered over Lake Huron and a ridge of high pressure over the Gaspé Peninsula; the pressure gradient over the SLRV, however, is much higher during the long-duration events. Figures 3.5c-d show composites of the monthly 2-m temperature anomalies, 2-meter 0°C isotherm, MSLP and 10-meter winds simulated by CRCM5 at the beginning of the mixed precipitation events diagnosed at a grid point at YUL with the Bourgouin method. For both types of event there is a tongue of cold air extending from the northeast to the southwest and a gradient of MSLP in the SLRV, which is much stronger for the long-duration events. These particular patterns suggest warm air advection aloft (Cortinas Jr et al., 2004).

Figure 3.5e and f show maps of the frequency (%) of occurrence of mixed precipitation over the domain of interest at the beginning of events diagnosed at YUL. The patterns indicate the very localized nature of the phenomenon, with the region of high frequency extending barely more than 50-100 km away from YUL station for both duration of events. For the long-duration events, however, an elongated north-west to south-east region of modest frequency is visible, suggestive of warm frontal passages (Cortinas, 2000). Warm air advection is confirmed by the veering wind profile during both types of events (Fig.3.5g-h), although much stronger for the long-duration events. Finally, a northeasterly 10-m wind (Fig.3.5i-j) is dominant during the beginning of the long-duration events, which supports the surface-based cold layer needed to produce freezing precipitation. No predominant wind direction is noted at the beginning of the short-duration events.

In summary, the MSLP and temperature anomaly patterns are similar for both durations of events with a stronger signal associated with the long-duration ones. Northeasterly winds are predominant and stronger for the long-duration events; these provide favorable conditions to maintain the cold layer near the surface that is necessary for freezing rain.

3.3.3 Seasonal variation

Figure 3.6 shows the monthly number of hours and number of short- and long-duration events at 4 locations (YUL, YMX, YQB and YBG) indicated on Fig.3.1b. There are two maxima, a main one in December and a smaller maximum in March. The number of hours of mixed precipitation associated with long-duration events is larger than for short-duration events, but the number of short-duration events is larger.

3.4 Projected climate change of mixed precipitation

In this section, the climate changes (i.e. future - past) of mixed precipitation projected by CRCM5 driven by MPI-ESM-LR under the RCP8.5 scenario is analyzed. A supplementary analysis (see Sect. 3.7) has shown that the historical simulation overall produces well the results from the hindcast simulation. Figure 3.7 shows the mean of the 5 algorithms for the past, future and climate change (future - past) for the mean annual number of hours and the number of occurrences of short-duration events. The pattern of the future number of hours (Fig.3.7c) resembles that in the past (Fig.3.7a), but the number is reduced in the south and slightly increased to the north. Such south to north migration of the number of annual hours of mixed precipitation follows the migration of the 0°C-isotherm (not shown). The climate change (Fig.3.7e) indicates a small decrease of mixed precipitation in the SLRV near YUL, YMS and YQB. Figure 3.7f shows that the change in number of events follows a similar pattern as the change in the number of hours. In the SLRV the change is correlated to the topography (not shown) while it is much less correlated in the rest of the domain.

Figure 3.8 shows the corresponding results for the long-duration events. Overall there is a projected reduction of the mean number of hours and the number of events, but no clear northward migration of mixed precipitation in the future. There is a projected slight increase in the number of hours for the Charlevoix area (south of the YBG).

The climate change projected in the number of hours and the number of short- and long-duration events per month at YUL, YMX, YQB and YBG is shown in Fig.3.9. The change of the number of hours (Fig.3.9a-c-e-g) is very different for short- and long-duration events. Small changes are projected for short-duration events (generally less than 4 h), whereas the long-duration events are projected to decrease by up to 12 h, with the maximum change occurring between December and April depending on the location and the diagnostic algorithm. The average of all algorithms suggests that the maximum reduction would occur in the month with maximum occurrence of mixed precipitation in the historical simulation (not shown). As noted before, the CB algorithm projects changes that are the most different from the others.

The projected changes in the number of long-duration events (Fig.3.9b-d-f-h) are small at most locations, with the largest decrease occurring in January at YUL and YMX. The number of short-duration events is generally projected to increase in December but decrease in fall (October, November) and at the end of the winter and early spring (February, March and April) at all locations except YUL where all algorithms project a decrease. The general changes for short-duration event is probably due to the warmer temperatures that produce more favorable conditions in winter, but less favourable conditions during the transition seasons.

3.5 Conclusions

This study focused on the occurrences of mixed precipitation (i.e. freezing rain and/or ice pellets) and its changes in the future over for southern Québec. The fifth-generation Canadian Regional Climate Model has been used to downscale the Era-Interim reanalysis for hindcast and a simulation of the Max-Planck Institute for Meteorology Earth System Model for the historical 1980-2009 and future 2070-2099 periods. Mixed precipitation has been diagnosed by post-processing the CRCM5 simulation using five algorithms. Events of short (<6h) and long (≥6h) duration have been analyzed separately to characterize the atmospheric conditions. For comparison with the observations, the closest grid point associated with a similar topographic height has been used when the occurrence of precipitation is compared at specific stations. But there is a great variability amongst the nearest grid point which is discussed in 3.8. First, to evaluate the model performance, the observations have been compared with the hindcast simulation. Second, an analysis of the historical and the projected future climate have been compared to study the associate climate change signal.

3.5.1 The hindcast simulation

The climatology of the hindcast simulation has been studied using five diagnostic algorithms and the results were found to agree reasonably well with the observations. The algorithms captured the main pattern of mixed-precipitation occurrences, with some differences in the annual number of hours. The Bourgouin, Czys, Ramer and Baldwin algorithms captured the relative maximum in the SLRV whereas partial thickness method of CB did not capture it. This is probably because this method compares the mean temperature of a layer, which cannot capture the shallow sub-freezing layer adequately near the surface during the short-duration events (<6h).

The combination of the surface pressure gradient and the temperature advection suggests that mixed precipitation generally occurs during a passage of a warm front. The high occurrence of northeasterly wind in the SLRV suggests that the long-duration events are maintained by the low-level cold air advection as suggested by Roebber and Gyakum (2003). It has also been shown that there are two maxima of occurrences, a main one in December and a second one in March, for both duration. Although that the long-duration events occur less often, they are responsible for the largest number of hours of mixed precipitation.

3.5.2 The historical and projected future climate.

Finally, the projected climate changes indicate a poleward migration of the mixed precipitation occurrences, and a general reduction of long-duration events, both in their number of hours and in their number of occurrences.

Despite the benefits of using high-resolution climate simulations to realize a climate-change study of mixed precipitation, there remain numerous sources of modeling errors, such as the use of empirical diagnostic algorithms to discriminate precipitation types, the parameterization of subgrid-scale physical effects, internal structure of the model, imperfections in boundary conditions that drive the regional model, and the nesting technique. The low spatial density of observational datasets and the limited information about the precipitation types and intensity makes difficult the objective evaluation of simulated results. If diagnostic precipitation-type algorithms were to continue being used, they should at least be tuned to optimize their performance for the region where they are applied. Eventually the diagnostic approach should be replaced by a physically-based representation using detailed cloud and precipitation microphysical algorithm when computing resources allow it. An actionable assessment of projected changes of mixed precipitation would require using an ensemble of models and simulations to estimate the associated uncertainty.

This study takes place in an international endeavor to better understand a warmer climate using high-resolution climate simulations. To our knowledge, no study has investigated future mixed precipitation occurrence using such high spatial resolution. Although that our study brings a more detailed spatial and temporal description of this type of precipitation, further effort is needed to improve physically-based representation of such precipitation types into climate models.

Acknowledgements: This research was supported by 2 Discovery Grants of the Natural Sciences and Engineering Research Council (NSERC) of Canada. Computations were made on the supercomputer guillimin, managed by Calcul Québec and Compute

Canada. The operation of this supercomputer is funded by the Canada Foundation for Innovation (CFI), the Fonds de recherche du Québec - Nature et technologies (FRQNT), NanoQuébec, and the Réseau de médecine génétique appliquée (RMGA). D.M. thanks the FRQNT for a graduate fellowship. The authors are greatly indebted to Dr. Émilie Bresson for her processing of the MANOBS and Eva Mekis to have provided them, to Dr. Bernard Dugas and Ms. Katja Winger for their essential help with the use of CRCM5, and to Mr. Georges Huard and Ms. Nadjet Labassi for maintaining user-friendly local computing facilities.

3.6 Appendix: Vertical profiles

Figure 3.10 show the vertical temperature profiles at t=0h for YUL for SE and LE diagnosed by Bourgouin (Fig.3.10a-b), Czys (Fig.3.10c-d), Ramer (Fig.3.10e-f), C&B (Fig.3.10g-h) and Baldwin (Fig.3.10i-j). The main goal to analyze those profiles is to better understand their characteristics in order to explain their differences. Overall, they all show a similar temperature profile for the short and long event. The SE have a low-level temperature inversion a relatively sharp warm nose while for LE the surface inversion begins at higher altitude and the warm nose is more imposing. The C&B profiles for SE and LE are different from the other algorithms and they clearly show artefacts of its own structure. Looking the profiles for SE from the other algorithms, it is clear the SE are characterized by a low-level inversion. Since C&B diagnoses MP by using the thickness of two layers, if the inversion occurs within the low-level layer, MP will not be diagnosed. In other words, low atmospheric layer effects might not be correctly caught by the C&B algorithm. Which explained the underestimation of the MP for the C&B shows in Fig.3.2c, Fig.3.3 and Fig.3.4a.

3.7 Appendix: Historical Simulation

To analyze the impact of the boundary conditions errors on the CRCM5 simulation, this section compares the reanalysis-driven hindcast and the CGCM-driven historical simulations. Figure 3.11 shows the number of hours per year of occurrence of mixed precipitation for the average of the 5 algorithms, for the short- and long-duration events, in the hindcast and historical CRCM5 simulations, and their differences (CRCM5/MPI-CRCM5/ERA). Overall the differences in mixed precipitation are small, the main difference being a slight positive bias in the southern part the domain, more pronounced for the long-duration events, occurring mainly from December to February (not shown).

Figure 3.12 shows the corresponding results for the number of events. In this case the short-duration events shows a positive bias in the south of the domain, with a maximum bias of 3 events per year. This positive bias in the number of events does not however have a strong impact on the number of hours, as noted in Fig.3.11. On the other hand it is worth noting that the maximum occurrence of mixed precipitation happens in January in the historical simulation rather than in December as in the hindcast simulation (not shown); this shift in the maximum results from a warm bias of low atmospherics layers in the historical simulation driven by the CGCM.

Overall, the historical simulation is reproducing fairly the mixed precipitation climatology, which increases the confidant with the climate projection.

3.8 Appendix: Spatial variability

To compare the occurrence of mixed precipitation diagnosed in model simulations with observations, the closest grid point with similar topographic height has been used throughout this study. Several alternative options were also contemplated. A paramount finding was that there is a large variability amongst the adjacent model grid points for mixed precipitation. Figure 3.13 shows the simulated results and the observed values for short- and long-duration events. A color plume shows the lowest and highest values of the nine nearest grid points to the observation station, hence the width of the plume reflects the spatial variability of adjacent grid points. Because mixed precipitation is sensitive to the surface elevation and the vertical atmospheric profile, this indicates that it might be inappropriate for such variable to use a spatial mean of adjacent grid points to compare with stations. Comparing a simulation with observations is always challenging, and the task appears to particularly difficult for mixed precipitation. In Fig.3.13 it would be expected that observations are located within the model results plume.

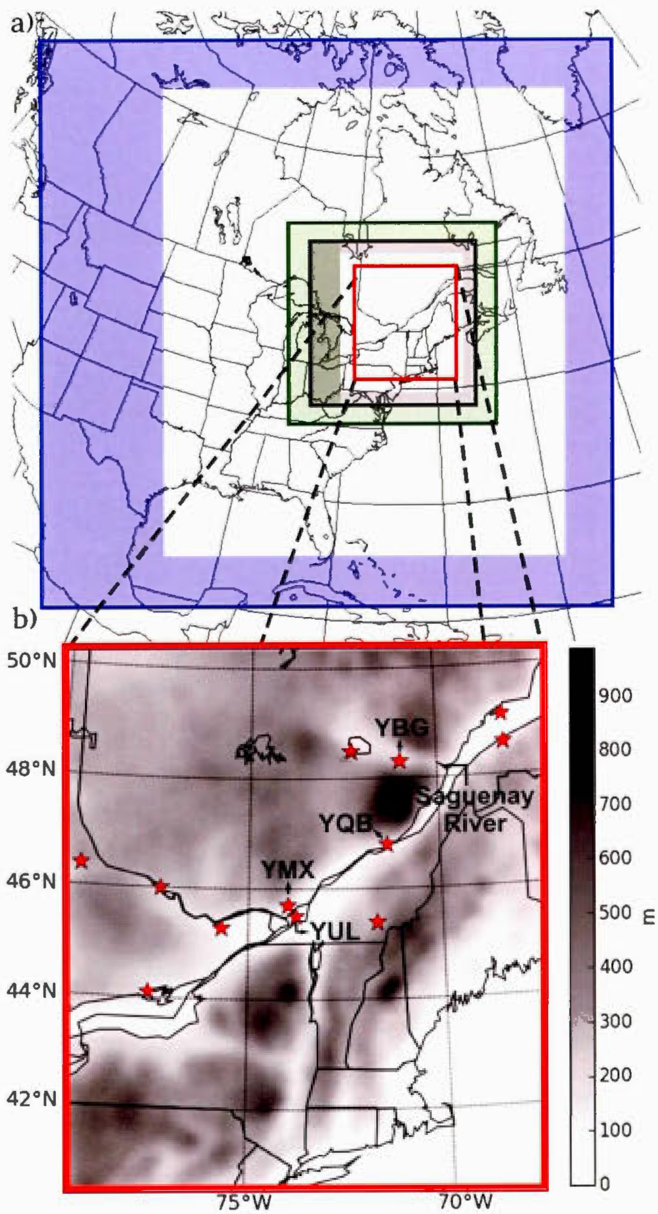

Figure 3.1 The domain location for the different experimental setups. Panel (a) shows the domain location of the intermediate-resolution simulation (in blue) and the high-resolution simulation (in black) used for the two-step dynamical downscaling of the historical and climate-change simulations. The green square is the domain location used for the hindcast simulation. The color shadings represent the spatial spin-up region for each case. The red square represents the "trustworthy" region of a size of 80 x 90 grid points. Panel (b) is the topography (grey shading) and the location of the MANOBS stations (red stars). The labeled ones are Pierre-Elliot Trudeau airport (YUL), Mirabel (YMX), Québec City (YQB) and Bagotville (QBG)

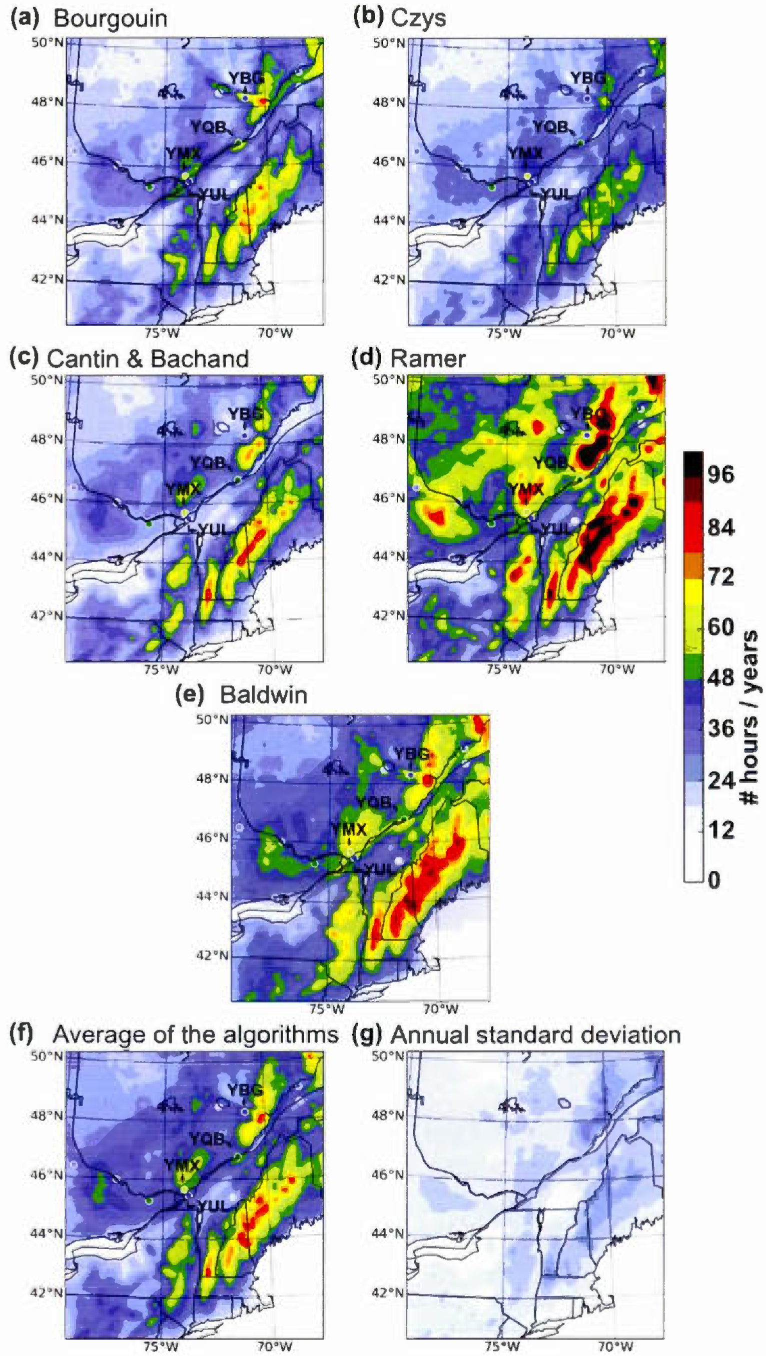

Figure 3.2 Mean annual hourly occurrence of mixed precipitation diagnosed by a) Bourgouin, b) Czys, c) Cantin and Bachand, d) Ramer, e) Baldwin, f) the average among the 5 algorithms and g) the standard deviation around their average. The stations are indicated by the white disks and the values are the same as the color bar.

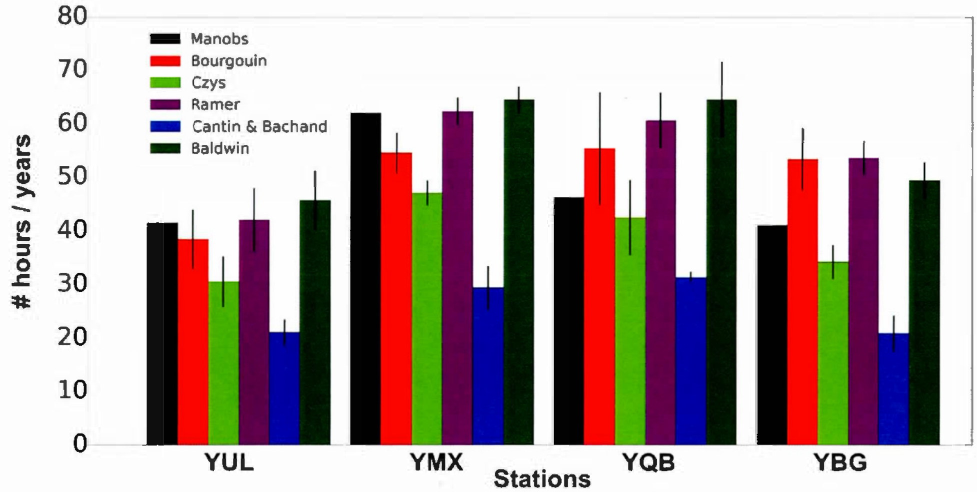

Figure 3.3 Mean annual hourly occurrence of mixed precipitation of the observation (black), and diagnosed by Bourgouin (red), Czys (green), Ramer (purple), CB (blue), and Baldwin (dark green), for the locations of YMX, YUL, YQB and YBG, respectively. The black lines represent the standard deviation of the nine grid points nearest to the corresponding MANOBS stations.

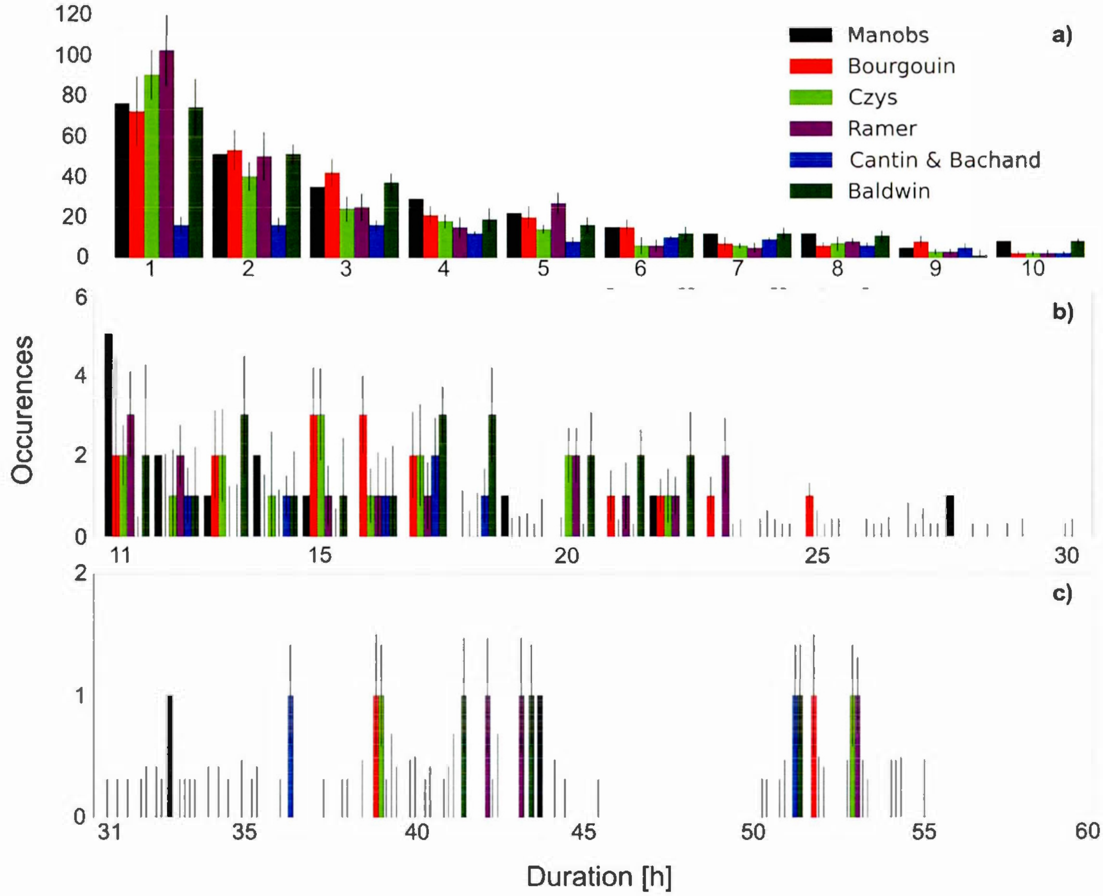

Figure 3.4 Histograms of the number of hours per mixed precipitation event in different time ranges; (a) from 1 to 10 hours; b) 11 to 30 hours and c) 31 to 60 hours, for Dorval (YUL, Figure 1) for the 5 algorithms: Bourgouin (red), Czys (lime green), Ramer (purple), CB (blue), and Baldwin (dark green). The black lines represent the standard deviation of the nine grid points nearest to the MANOBS station.

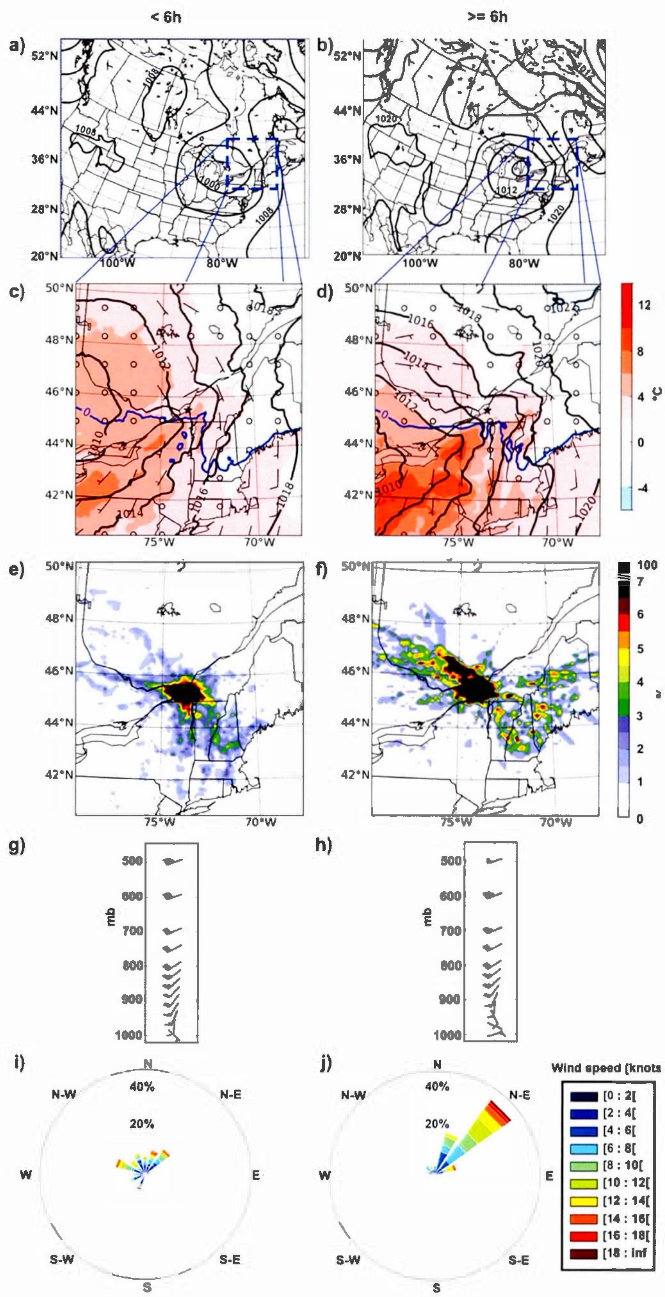

Figure 3.5 Composite analysis at the beginning of all short-duration (left column) and long-duration (right column) mixed precipitation events. Panels (a,b) show the mean sea level pressure (MSLP) in ERA-Interim, panels (c,d) show the simulated monthly 2-m temperature anomalies (color shading), the MSLP (black lines) and the 10-m wind speed and direction (barbs). The blue line is the 2-m 0°C isotherm. Panels (e,f) show the frequencies (%) of mixed precipitation when occurring at YUL, panels (g,h) show the vertical profile of horizontal wind speed and direction at YUL, and panels (i,j) show the 10-m wind roses, with the colors indicating wind speed. The black star indicates the location of Dorval, Québec (YUL).

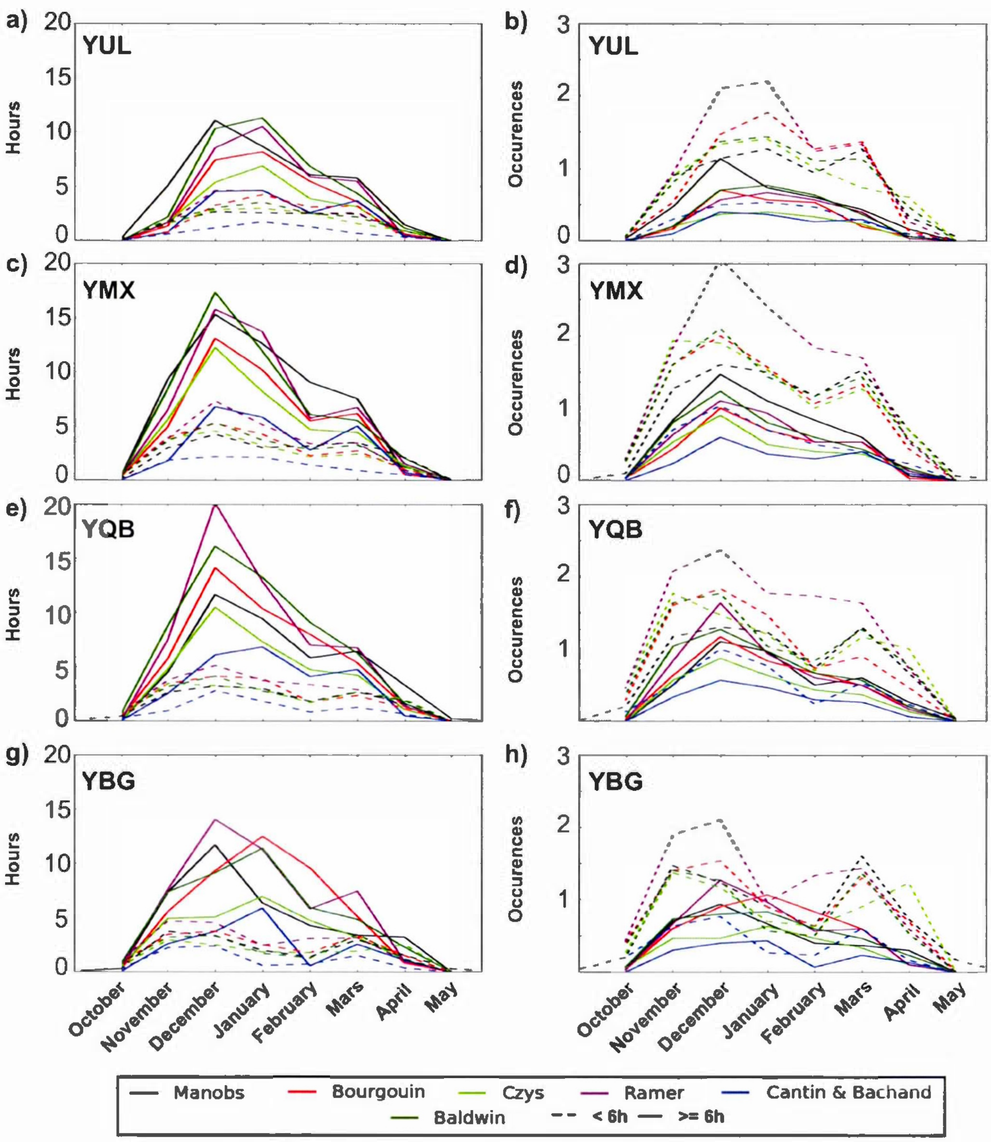

Figure 3.6 Monthly number of hours (left column) and the number of events (right column) for (a,b) YUL, (c,d) YMX, (e,f) YQB and (g,h) YBG. The black lines correspond to the observed values while the colored lines correspond to the mixed precipitation diagnosed by the various algorithms, Bourgouin (red), Czys (lime green), Ramer (purple), CB (blue) and Baldwin (dark green). The dashed lines and the plain lines are the short- and long-duration events, respectively.

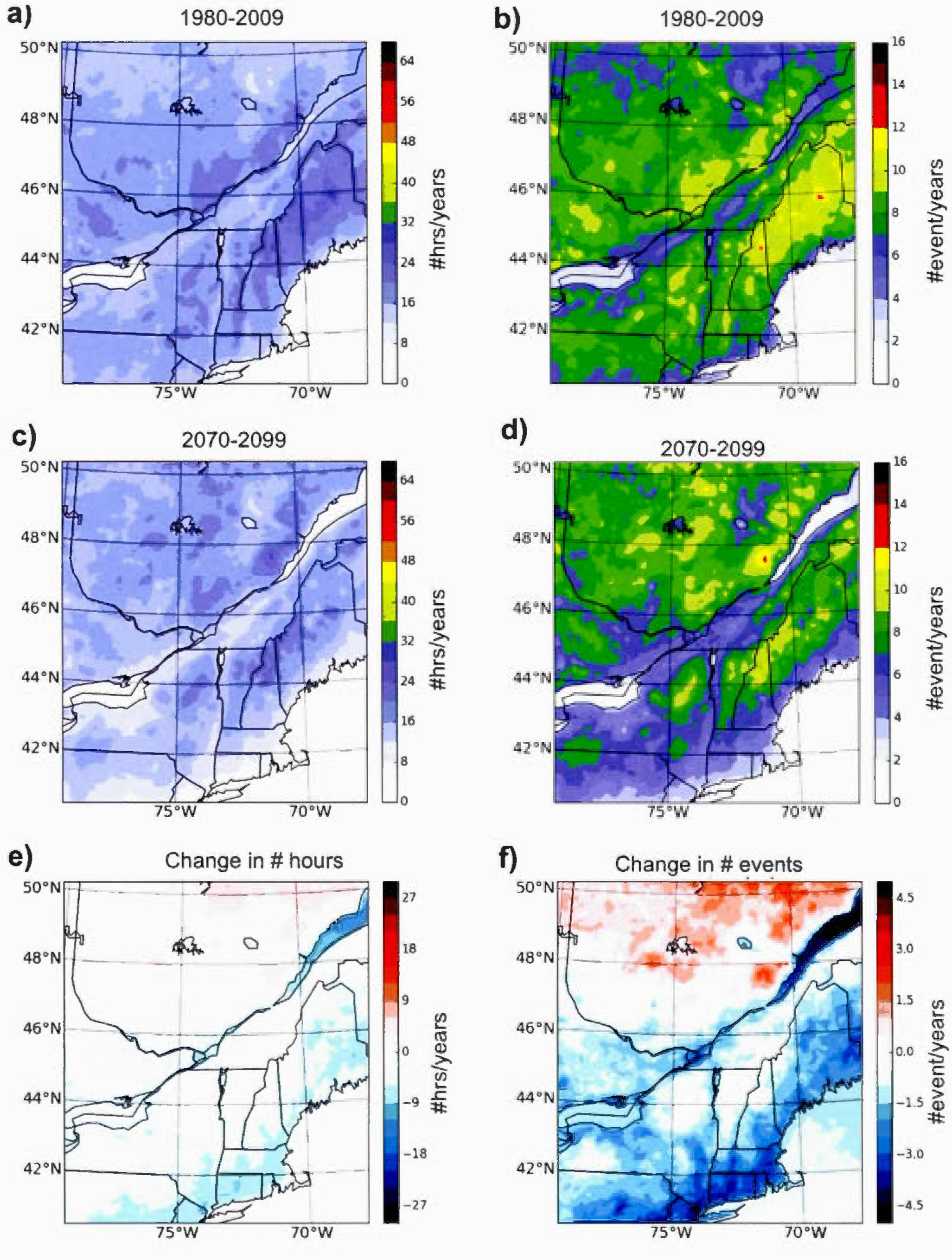

Figure 3.7 Annual number of hours (left column) and the number of events (right column) for the period of (a,b) 1980-2009, (c,d) the period of 2070-2099, and (e,f) the corresponding changes for short-duration events the average of the 5 algorithms.

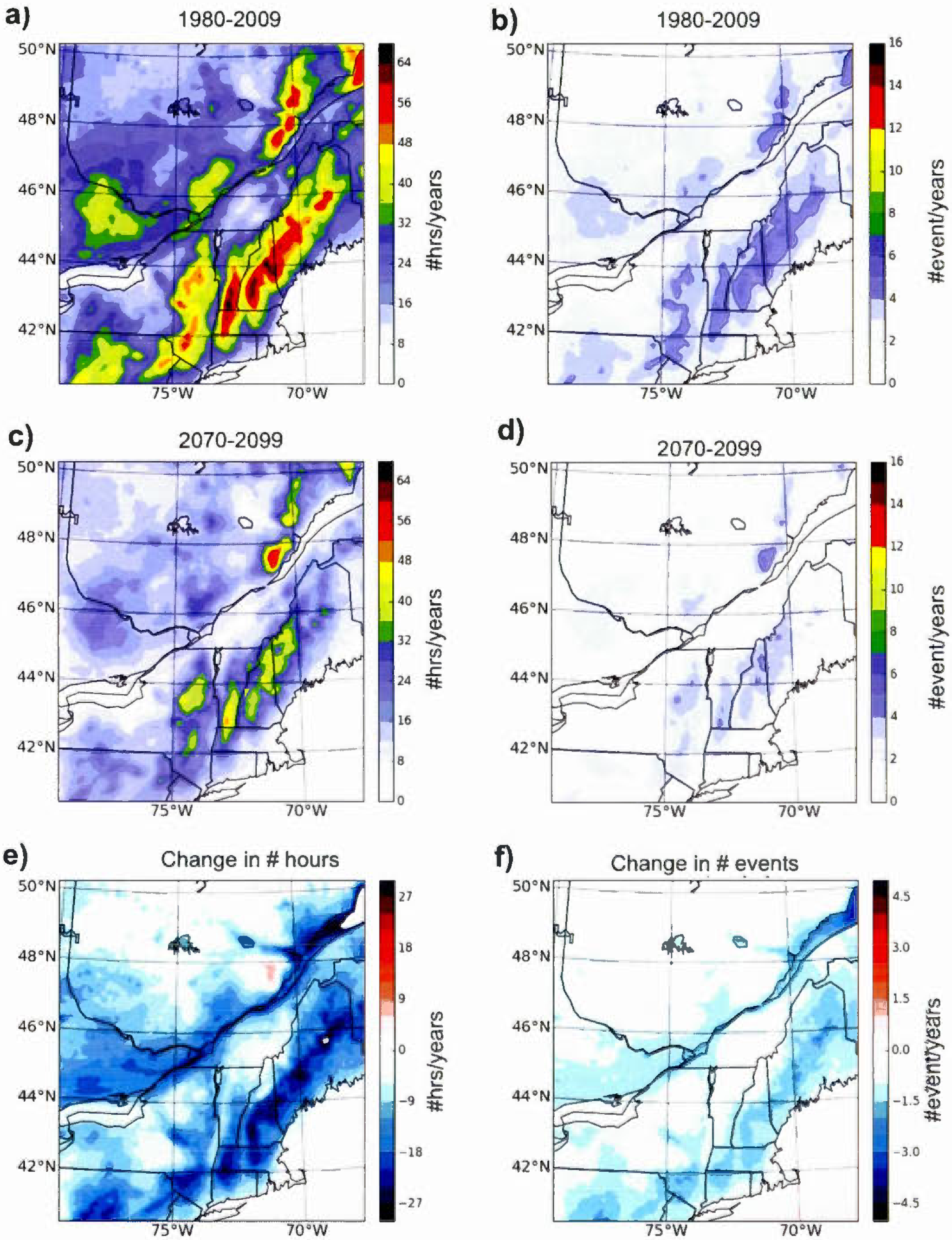

Figure 3.8 Same as Fig.3.7, but for long-duration events

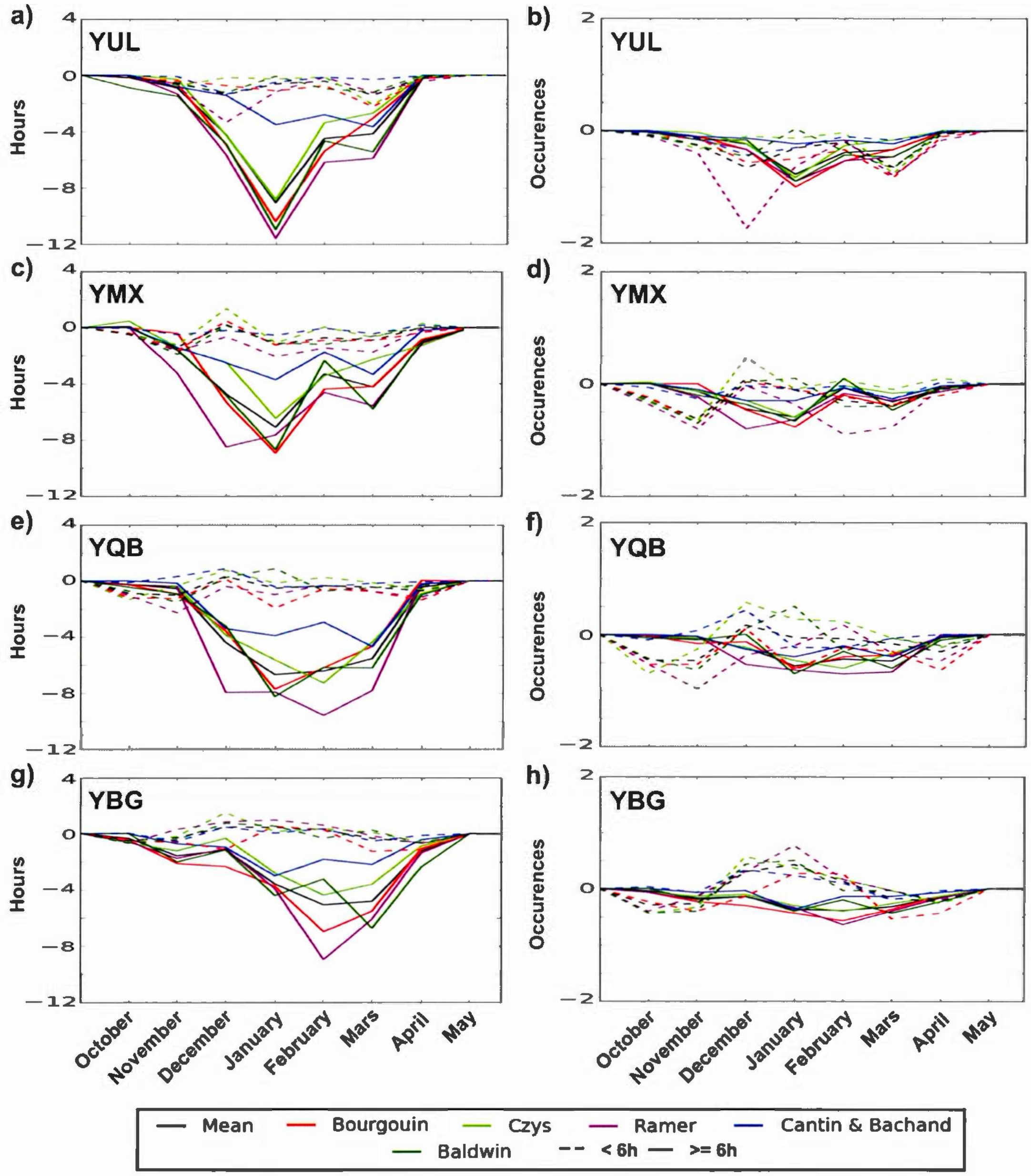

Figure 3.9 Climate change of monthly hours (left column) and number of events (right column) of mixed precipitation at (a,b) YUL, (c,d) YMX, (e,f) YQB and (g,h) YBG as diagnosed by Bourgouin (red), Czys (green), Ramer (purple), CB (blue), and the average of the 5 algorithms (black).

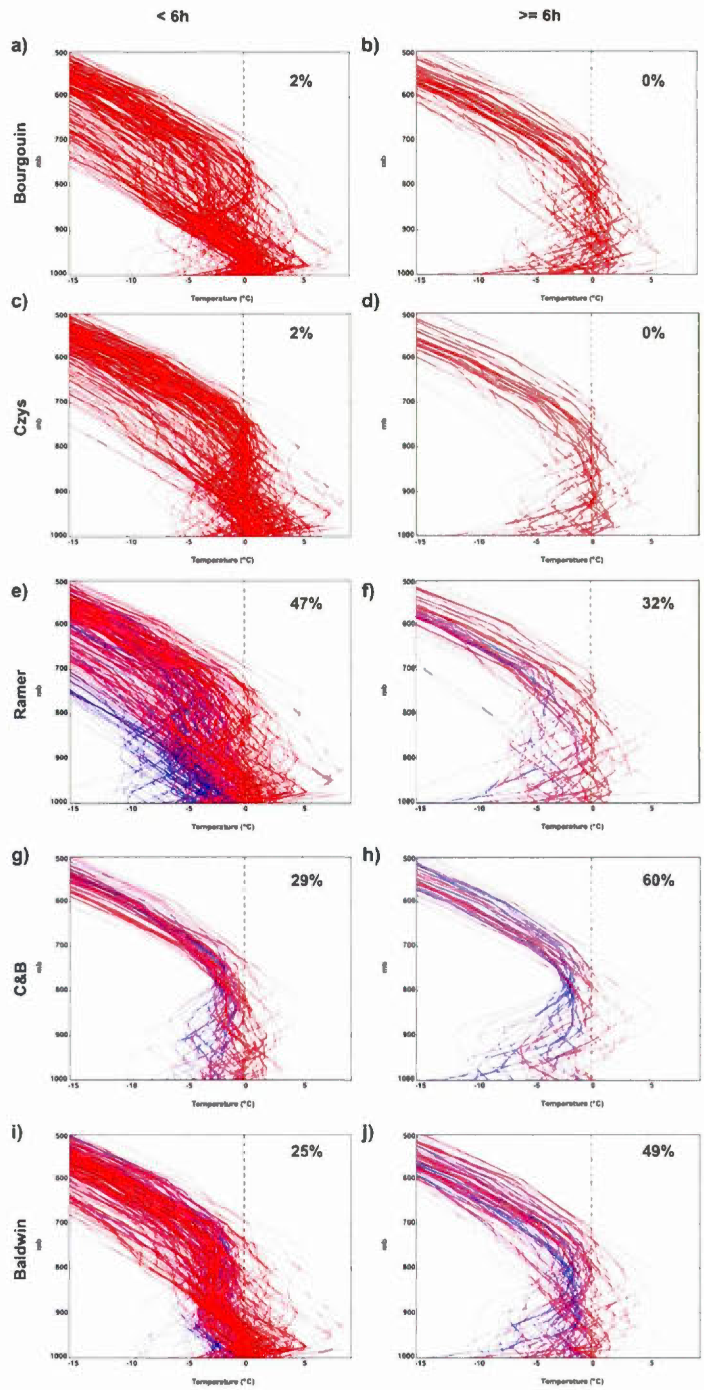

Figure 3.10 The vertical temperature profiles at t=0h for short and long event of MP when diagnosed by Bourgouin (a & b), Czys (c & d), Ramer (e & f), by Cantin & Bachand (g & h) and Baldwin (i & j). The blue and red lines represent the cold and warm profiles respectively. The upper-right number is the % of cold profiles.

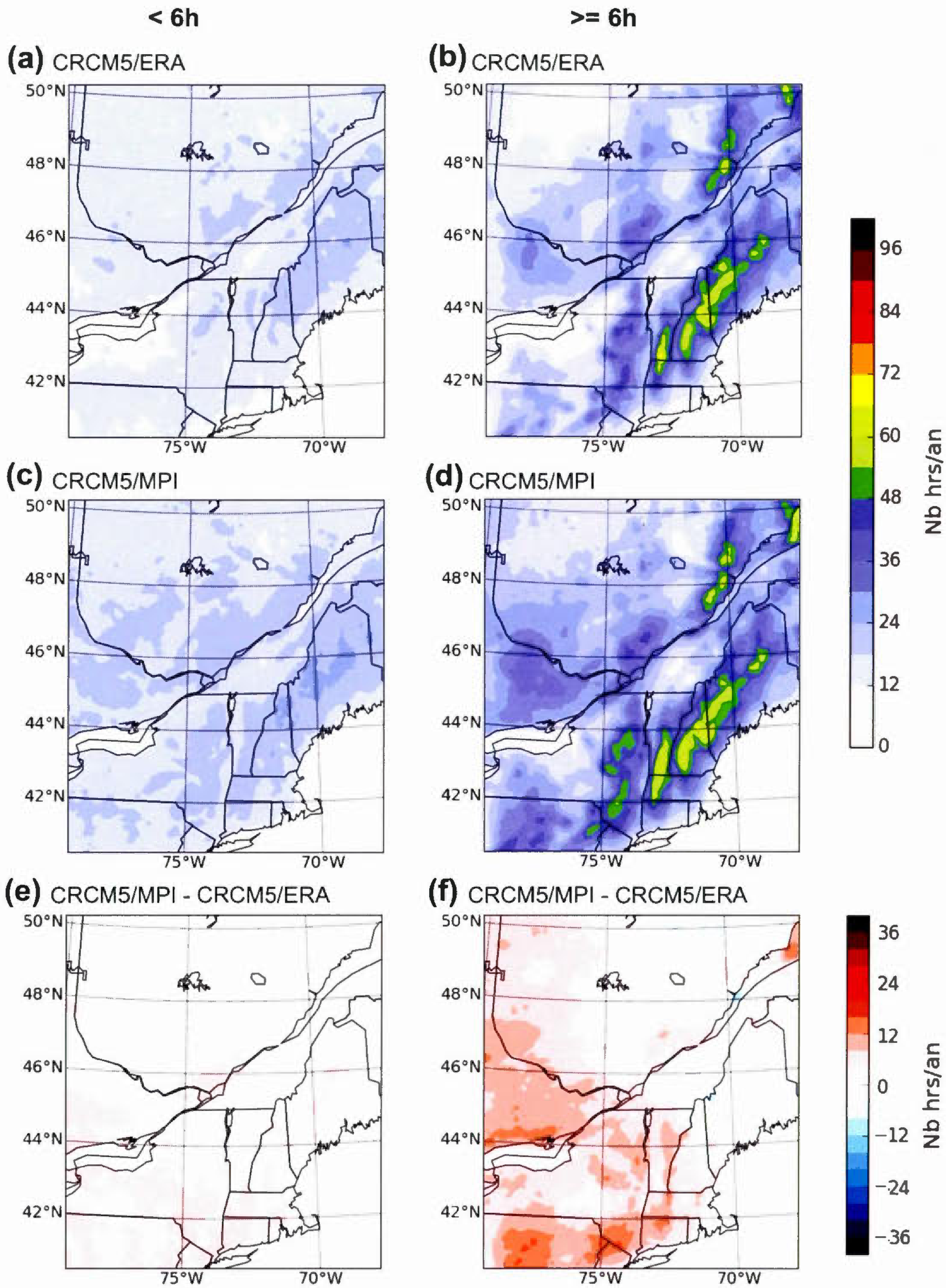

Figure 3.11 Number of hours per year for short-duration events (left column) and long-duration events (right column) the average of the 5 algorithms in the reanalysis-driven hindcast simulation (a,b) CRCM5/ERA, CGCM-driven historical simulation (c,d) CRCM5/MPI, and (e,f) their difference.

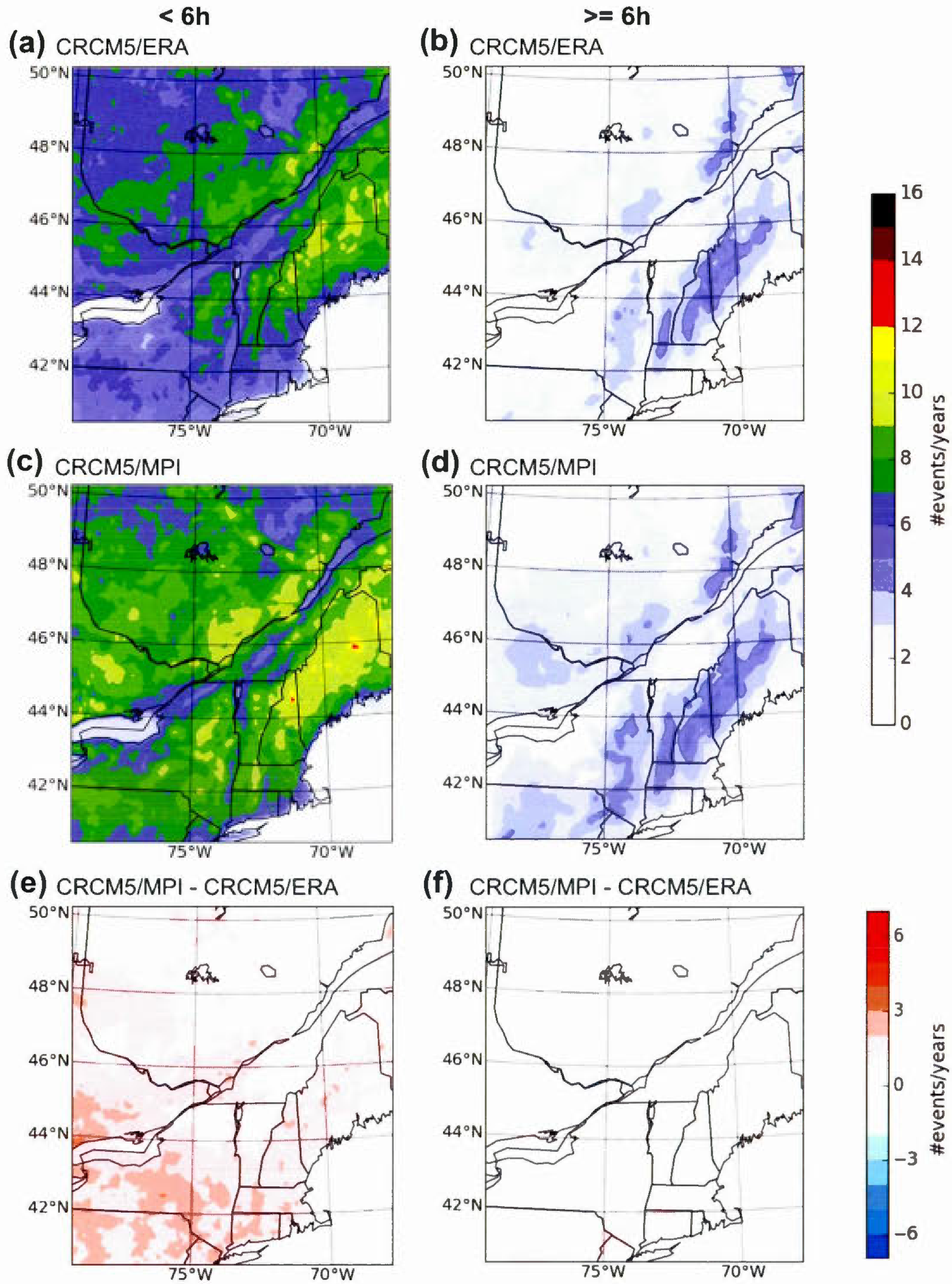

Figure 3.12 Number of events per year for short-duration events (left column) and long-duration events (right column) the average of the 5 algorithms. in the reanalysis-driven hindcast simulation (a,b) CRCM5/ERA, CGCM-driven historical simulation (c,d) CRCM5/MPI, and (e,f) their difference.

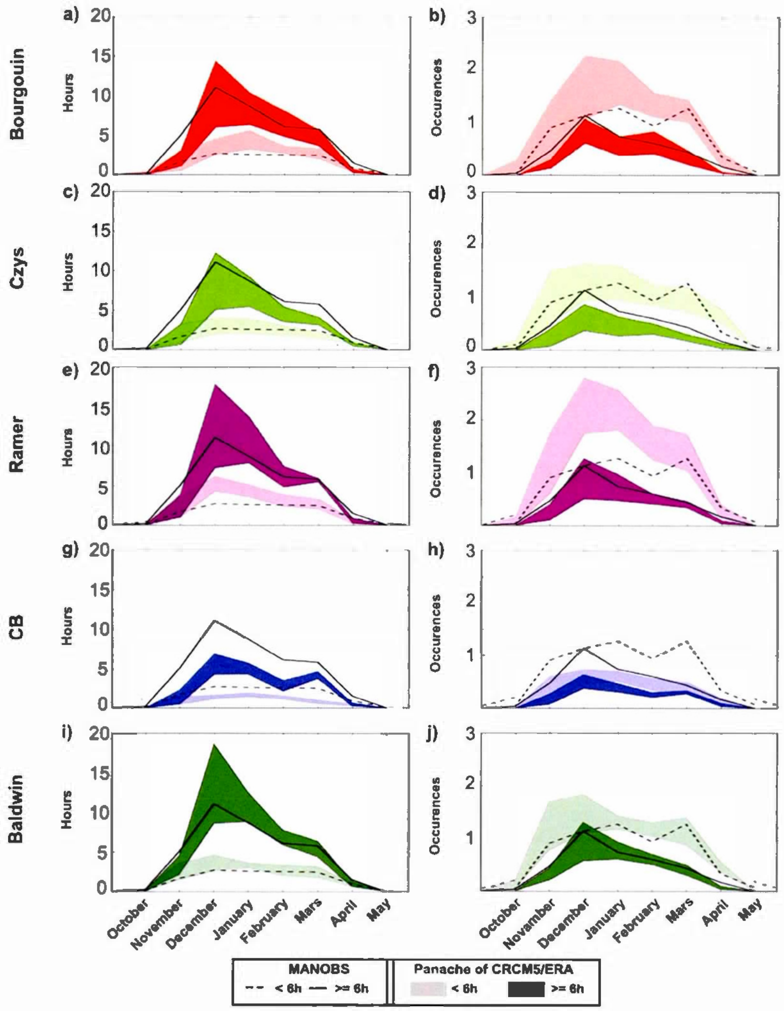

Figure 3.13 Monthly number of hours (left column) and the number of events (right column) for YUL as diagnosed by Bourgouin (a,b), Czys (c,d), Ramer (e,f), CB (g,h) and Baldwin (i,j) from the hindcast CRCM5/ERA solution. The plume indicates the lowest and the highest values at the nine grid points nearest to the YUL station. The black lines and the dark colors correspond to the observed value and the simulated results, respectively, for the long-duration events. The dashed lines and the pale colors are the observed value and the simulated results, respectively, for the short-duration events.

CONCLUSION

Certains phénomènes locaux simulés sont mieux représentés lorsque la résolution du modèle est plus fine. Par exemple, dans la vallée du Saint-Laurent une meilleure représentation de la topographie permet de mieux simuler la canalisation du vent, ce qui a un impact bénéfique sur la représentation de la précipitation verglaçante. Or, plus on augmente la résolution de la simulation, plus les ressources informatiques doivent être imposantes. Ceci est d'autant plus vrai lorsqu'on réalise des simulations avec des modèles de circulation générale (MCG) puisque ces derniers imposent de réaliser la simulation sur tout le globe. Conséquemment, les ressources informatiques exigées peuvent devenir une contrainte rédhibitoire. Une alternative est l'utilisation des modèles climatiques régionaux à aire limitée (MRC). Ces derniers permettent de réduire le coût de calcul puisque le domaine de calcul est limité sur une sous-région. La contrainte du coût de calcul devient alors un compromis entre la résolution de la simulation et la taille du domaine. Ceci étant dit, si l'expérience envisagée exige une très fine résolution, alors le coût de calcul lié à l'utilisation des MRC peut aussi devenir particulièrement contraignant. L'approche de la cascade peut être utilisée de façon avantageuse. Cette approche consiste à imbriquer plusieurs simulations d'un modèle régional du climat de résolution de plus en plus élevée tout en diminuant la taille du domaine. Avec une telle approche, on peut réaliser des simulations à haute résolution tout en gardant un coût de calcul raisonnable. L'intérêt essentiel de la thèse était ainsi de démontrer que cette approche est une alternative concevable et avantageuse pour réaliser une étude climatique de la précipitation verglaçante avec un coût de calcul raisonnable.

Premièrement, la méthodologie associée à la cascade adoptée pour simuler le climat a été analysée selon l'expérience du grand frère. Lors de cette première étude, la solution d'une simulation réalisée par réduction d'échelle simple fut comparée à la solution d'une simulation réalisée par réduction d'échelle double. En analysant la composante stationnaire, on remarque que lorsque le domaine augmente, il y a une diminution de la corrélation des champs de grande échelle, et ce pour les deux approches. En d'autres mots, le contrôle des conditions aux frontières (CF) diminue avec de grands domaines. Ce résultat concorde avec certaines études précédentes (Jones et al., 1995; Leduc and Laprise, 2009; Leduc et al., 2011). Toutefois, la corrélation des grandes échelles de la composante de la variabilité transitoire est systématiquement réduite pour l'approche de la réduction d'échelle double. Cette réduction provient de la performance de la simulation de résolution intermédiaire. Le pilotage spectral peut être avantageusement utilisé pour corriger cette situation. Ceci permet, au besoin, d'éviter un décrochage des grandes échelles qui pourrait occasionner des problèmes aux frontières du domaine. La plus grande différence entre les deux approches se trouve dans la composante de la variabilité transitoire des petites échelles. Pour l'approche de la réduction simple, on remarque que les petits domaines (c.-à-d. plus petits que 260 x 260 points de grille) ont un déficit important dans l'amplitude des petites échelles. Alors qu'avec l'approche de réduction d'échelle double, le déficit n'apparaît seulement qu'à partir d'une grandeur de domaine plus petit que 110 x 110 points de grille. Ces deux grandeurs de domaine représentent respectivement la grandeur minimale requise pour développer adéquatement les petites échelles pour l'une ou l'autre approche dans la région commune. L'amélioration dans le cas de la réduction d'échelle double est une conséquence de l'ajout de la simulation à résolution intermédiaire. Ceci s'explique par le fait qu'au lieu de faire un saut de résolution de 12 entre les CF et le MRC, on fait plutôt deux sauts consécutifs de 4 et de 3. Comme on l'a vu dans la deuxième section de cette thèse, la réduction du saut de résolution permet de réduire aussi le "spin-up" spatial, permettant ainsi de réduire la dimension minimale requise pour développer les petites échelles. Conséquemment, l'approche de la réduction d'échelle double représente une diminution du coût de calcul par un facteur de 5 comparativement à l'approche utilisant une réduction d'échelle simple.

Bien que cette réduction du coût de calcul soit une importante conclusion, certaines informations supplémentaires peuvent aussi être extraites de l'analyse de l'approche de la réduction d'échelle simple. Dans la configuration utilisée, il a été montré que: (1) pour un domaine plus grand que 160 x 160 points de grille, les grandes échelles se dégradaient et (2) un domaine plus petit que 260 x 260 points de grille ne suffisaient pas pour développer adéquatement les petites échelles. Pour un tel saut de résolution, il n'existe donc pas une grandeur de domaine qui puisse satisfaire à la fois le contrôle adéquat des CF sur la simulation et le développement adéquat des petites échelles. Le choix de la grandeur du domaine est donc un compromis entre ces deux contraintes. Puisque le "spin-up" spatial se dégrade avec le saut de résolution, le compromis peut devenir de plus en plus difficile à réaliser à mesure que le saut de résolution augmente. Il est ainsi devenu de plus en plus clair au cours de cette première étude que le "spin-up" spatial devait être caractérisé non pas en termes de la taille du domaine, mais plutôt en termes de distance à la frontière en amont du domaine. Il était alors important, pour la cascade, de faire un choix judicieux sur la localisation des sous-domaines pour s'assurer d'une utilisation optimale de la solution simulée. Pour ce faire, une caractérisation plus approfondie du "spin-up" spatial était nécessaire.

Deuxièmement, le "spin-up" spatial a été analysé en fonction du saut de résolution selon l'expérience du grand frère a été utilisée. Cette fois, différents filtres ont été appliqués pour produire des conditions aux frontières de différentes résolutions. Les filtres appliqués ont produit l'équivalent de solutions qu'auraient eu des simulations avec des maillages de 3.6°, 1.8° et 0.45° et celles-ci sont utilisées pour piloter les simulations ayant un maillage de 0.15° avec une grandeur de domaine libre de 260 x 260 points de grille. Les sauts de résolution sont donc de 24, 12 et 3 respectivement. Une expérience additionnelle où aucun filtre n'a été appliqué aux CF (donc un saut de résolution de 1) a aussi été réalisée. Pour étudier le "spin-up" spatial, les petites échelles de la composante de la variabilité transitoire ont été exclusivement analysées. Il a été montré que les caractéristiques propres aux fines échelles prennent une plus grande distance à se développer pour un grand saut de résolution, particulièrement en hiver et en altitude, situations dans lesquelles l'écoulement moyen à travers le domaine est plus fort. Les résultats ont montré que la résolution des conditions aux frontières définit la distance physique du "spin-up" spatial, peu importe la résolution du MRC piloté. Cette distance physique correspond à un nombre de points de grille qui varie évidemment selon la résolution du MRC. Ce qui implique que plus la résolution du MRC est fine, plus le nombre de points de grille nécessaires pour le "spin-up" spatial est grand. Il est alors aussi possible de décrire le "spin-up" spatial selon le saut de résolution entre les CF et le MRC. Le saut de résolution permet d'estimer la distance du "spin-up" par rapport aux frontières. Ainsi, une zone de confiance externe à la zone de "spin-up" peut alors être définie, servant soit à l'analyse des sorties de simulation, soit pour définir les frontières d'une prochaine étape de la cascade.

Troisièmement, une méthode optimale pour réaliser une simulation climatique en utilisant l'approche de la cascade a été utilisée pour mener une projection climatique de la précipitation mixte dans le sud du Québec. Le maillage choisi pour réaliser cette étude devait être suffisant fin pour correctement représenter les effets topographiques de la vallée du Saint-Laurent. Les résultats de Cholette et al. (2015) ont montré qu'avec un maillage de 0.09°, la canalisation des vents dans la vallée était bien capturée par la simulation. À des fins de conformité avec les expériences CORDEX, le maillage a cependant été fixé à 0.11°. Le domaine d'intérêt fût le sud du Québec, centré sur

Montréal. La taille du domaine d'intérêt a été choisie pour respecter et à la fois la disponibilité des ressources informatiques et les objectifs scientifiques. La simulation climatique du passé récent a été réalisée en utilisant les réanalyses Era-Interim (ERA-I) à 0.75° comme CF, ce qui correspond à un saut de résolution d'environ 7 ($\approx$40 points de grille en amont). Pour compenser cette région de spin-up, la localisation du domaine a été légèrement décentrée vers l'ouest et la taille du domaine augmentée pour s'assurer que la région d'intérêt reste à l'extérieur de la zone de "spin-up". Le même cadre expérimental a été appliqué pour réaliser les simulations historiques et futures, pilotées par le modèle du système terrestre de l'institut météorologie du Max Planck (MPI-ESM) à 2.8°. Conséquemment, le saut de résolution d'environ 25 se traduisait par une région de spin-up de plus de 150 points de grille. Évidemment, une telle zone de spin-up représente une part non négligeable de la taille du domaine de simulation. Dans ce cas, la cascade permettait alors de considérablement réduire le saut de résolution et donc le coût de calcul associé. La première étape fut donc de réaliser une simulation à une résolution intermédiaire de 0.45° qui fut utilisée comme CF pour réaliser la simulation de 0.11°, convertissant donc le saut de résolution original en deux sauts consécutifs de 6 et de 4 respectivement. Leurs zones de "spin-up" respectives sont alors de 36 et 24 points de grille, réduisant considérablement le "spin-up" et conséquemment le coût de calcul. Les deux domaines de la cascade ont été décentrés vers l'ouest pour compenser ces zones de "spin-up". Bien que la somme de la zone de "spin-up" est moindre dans la cas de l'approche double, il est important de mentionner que le coût de calcul relié à la simulation de résolution intermédiaire est négligeable comparativement à la simulation de plus haute résolution.

Les types de précipitation ont été diagnostiqués sur le domaine d'intérêt commun se trouvant hors des zones de spin-up de la cascade. Pour diagnostiquer les types de précipitation, cinq algorithmes ont été utilisés (Baldwin and Contorno, 1993; Cantin and Bachand, 1993; Ramer, 1993; Czys et al., 1996; Bourgouin, 2000), et les résultats comparés avec des données d'observations d'occurrences horaires de précipitation verglaçante (c.-à-d. une occurrence de pluie verglaçante ou/et de grésil). Les événements de courte durée ($<$6h) et les événements de longue durée ($\geq$6h) ont été étudiés séparément. En étudiant les deux types d'événements séparément, il fut alors possible de mieux comprendre certaines différences dans les résultats diagnostiqués par les différents algorithmes. Par exemple, dans la vallée du Saint-Laurent, l'algorithme de Cantin and Bachand (1993) peine à correctement diagnostiquer la précipitation verglaçante de courte durée puisque ceux-ci sont produits par des inversions de température près de la surface qui ne sont pas bien capturées par l'algorithme. Pour l'étude de projection climatique des types de précipitation, la moyenne des cinq algorithmes fut utilisée. Nos résultats indiquent une migration vers le nord de la précipitation verglaçante des événements de courte durée, ainsi qu'une diminution générale du nombre d'heures d'événements de longues durées. Une migration du maximum des occurrences de précipitation dans la saison froide est aussi projetée.

En conclusion, l'approche de la cascade a été étudiée pour permettre de réaliser une étude climatique de la précipitation verglaçante. Il a été mentionné que pour adéquatement représenter ce type de précipitation, les modèles doivent avoir une résolution horizontale et verticale suffisante qui impose coût de calcul qui peut devenir une contrainte importante. Il a été aussi démontré qu'une utilisation optimale de l'approche de la réduction d'échelle double permet d'atteindre une résolution nécessaire tout en gardant le coût de calcul raisonnable, ce qui est un avantage majeur. Il est important de mentionner que les avantages reliés à l'approche suggérée sont les mêmes que ceux de la configuration traditionnelle. Ici l'avantage est de pouvoir réaliser adéquatement une telle étude avec des ressources informatiques raisonnables.

Bien que ces résultats nous apporte une certaine lumière sur le cadre expérimental utilisér pour réaliser des simulations à haute résolution, il y a beaucoup à faire pour atteindre des résolutions encore plus fines. Pour certains centres de recherche possédant des ressources informatiques plus modestes, un choix cornélien s'impose entre le coût en temps de calcul et la capacité du modèle à correctement simuler ces phénomènes de fine échelle. Or, pour s'assurer que les modèles produisent une information adéquate à de telles résolutions, ils auront besoin de ressources informatiques non négligeables. D'autant plus qu'à des résolutions plus fines, des schémas microphysiques complexes doivent être activés, ce qui augmente encore plus le coût de calcul.

L'approche de la cascade peut alors devenir une alternative intéressante pour réaliser des études climatiques à haute résolution à un faible coût de calcul et ainsi s'affranchir du dilemme précédemment mentionné. Au cours des dernières années, une nouvelle stratégie semble émerger dans la communauté. Celle-ci implique une approche phénoménologique de la cascade. L'idée derrière cette approche est de préalablement diagnostiquer le phénomène à l'étude à partir de simulation à basse résolution et d'appliquer la cascade seulement sur la période requise pour simuler un évènement à haute résolution. Une telle démarche permettrait de réaliser des études climatiques à hautes résolutions pour certains phénomènes. Un avantage majeur serait d'étudier des phénomènes à une résolution où la convection n'a plus besoin d'être paramétrée et les nuages/précipitation mieux représentés à un coût de calcul raisonnable. Ceci étant dit, une telle approche appliquée à ces résolutions soulève aussi certaines contraintes méthodologiques telles que le "spin-up" et la grandeur du domaine. Il semble légitime de se demander si ces contraintes seront similaires à de telles résolutions et si le saut de résolution jouera toujours un rôle dominant. Il sera prémordiale d'évaluer l'impact de l'activation d'un schéma de microphysique par exemple. De plus, le spectre de résolution appelé la zone grise (c'est-à-dire le spectre de résolution où il n'est pas clair si la convection doit être paramétrée ou explicitement modélisée, à peu près entre un $\Delta x > 4$km et $\Delta x < 10$km; voir Prein et al. (2015) pour une revue de la littérature) est aussi une contrainte importante à une telle utilisation de la cascade.

REFERENCES

Antic, S., Laprise, R., Denis, B., and de Elía, R. (2004). Testing the downscaling ability of a one-way nested regional climate model in regions of complex topography. *Clim. Dyn.*, 23(5):473–493.

Baldwin, E. and Contorno, S. (1993). Development of a weather-type prediction system for NMC's mesoscale ETA model. In *Preprints, 13th Conf. on Weather Analysis and Forecasting, Vienna, VA*, pages 86–87. Amer. Meteor. Soc.

Ban, N., Schmidli, J., and Schär, C. (2015). Heavy precipitation in a changing climate: Does short-term summer precipitation increase faster? *Geophys. Res. Lett.*, 42(4):1165–1172.

Bélair, S., Mailhot, J., Girard, C., and Vaillancourt, P. (2005). Boundary layer and shallow cumulus clouds in a medium-range forecast of a large-scale weather system. *Mon. Weather Rev.*, 133(7):1938–1960.

Bélair, S., Roch, M., Leduc, A.-M., Vaillancourt, P. A., Laroche, S., and Mailhot, J. (2009). Medium-range quantitative precipitation forecasts from Canada's new 33-km deterministic global operational system. *Weather Forecast.*, 24(3):690–708.

Benoit, R., Côté, J., and Mailhot, J. (1989). Inclusion of a TKE boundary layer parameterization in the Canadian regional finite-element model. *Mon. Weather Rev.*, 117(8):1726–1750.

Bernstein, B. C. (2000). Regional and local influences on freezing drizzle, freezing rain, and ice pellet events. *Weather Forecast.*, 15(5):485–508.

Bourgouin, P. (2000). A method to determine precipitation types. *Weather Forecast.*, 15(5):583–592.

Bresson, E., Laprise, R., Paquin, D., Thériault, J., and de Elía, R. (2017). Evaluating the ability of CRCM5 to simulate mixed precipitation. *Atmos.-Ocean*, 55(2):79–93.

Brisson, E., Demuzere, M., and van Lipzig, N. P. (2015). Modelling strategies for performing convection-permitting climate simulations. *Meteor. Z.*

Cantin, A. and Bachand, D. (1993). Synoptic pattern recognition and partial thickness techniques as a tool for precipitation types forecastng associated with a winter storm. Technical report, Environnement Canada, 9 p.

Carrera, M. L., Gyakum, J. R., and Lin, C. A. (2009). Observational study of wind channeling within the St. Lawrence river valley. *J. Appl. Meteorol. Clim.*, 48(11):2341–2361. doi: 10.1175/2009JAMC2061.1.

Chan, S., Kendon, E., Fowler, H., Blenkinsop, S., Ferro, C. T., and Stephenson, D. (2012). Does increasing the spatial resolution of a regional climate model improve the simulated daily precipitation? *Clim. Dyn.*, pages 1–21.

Changnon, S. A. and Karl, T. R. (2003). Temporal and spatial variations of freezing rain in the contiguous united states: 1948-2000. *J. Appl. Meteorol.*, 42(9):1302–1315.

Cheng, C., Auld, H., Li, G., Klaassen, J., and Li, Q. (2007). Possible impacts of climate change on freezing rain in south-central Canada using downscaled future climate scenarios. *Nat. Hazard Earth Sys.*, 7(1):71–87.

Cheng, C. S., Li, G., and Auld, H. (2011). Possible impacts of climate change on freezing rain using downscaled future climate scenarios: updated for eastern Canada. *Atmos.-Ocean*, 49(1):8–21.

Cholette, M., Laprise, and Thériault, J. M. (2015). Perspectives for very high-resolution climate simulations with nested models: Illustration of potential in simulating St. Lawrence River valley channelling winds with the fifth-generation Canadian Regional Climate Model. *Climate*, 3(2):283–307.

Colin, J., Déqué, M., Radu, R., and Somot, S. (2010). Sensitivity study of heavy precipitation in Limited Area Model climate simulations: influence of the size of the domain and the use of the spectral nudging technique. *Tellus A*, 62(5):591–604.

Cortinas, J. (2000). A climatology of freezing rain in the great lakes region of North America. *Mon. Weather Rev.*, 128(10):3574–3588.

Cortinas, J., Brill, K., and Baldwin, M. (2002). Probabilistic forecasts of precipitation type. In *Preprints, 16th Conf. on Probability and Statistics in the Atmospheric Sciences, Orlando, FL, Amer. Meteor. Soc*, volume 3.

Cortinas Jr, J. V., Bernstein, B. C., Robbins, C. C., and Walter Strapp, J. (2004). An analysis of freezing rain, freezing drizzle, and ice pellets across the United States and Canada: 1976-90. *Weather Forecast.*, 19(2):377–390. doi: 10.1175/1520-0434(2004)019¡0377:AAOFRF¿2.0.CO;2.

Côté, J., Desmarais, J.-G., Gravel, S., Méthot, A., Patoine, A., Roch, M., and Staniforth, A. (1998a). The operational CMC-MRB global environmental multiscale (GEM) model. Part II: Results. *Mon. Weather Rev.*, 126(6):1397–1418.

Côté, J., Gravel, S., Méthot, A., Patoine, A., Roch, M., and Staniforth, A. (1998b). The operational CMC-MRB global environmental multiscale (GEM) model. Part I: Design considerations and formulation. *Mon. Weather Rev.*, 126(6):1373–1395.

Czys, R. R., Scott, R. W., Tang, K., Przybylinski, R. W., and Sabones, M. E. (1996). A physically based, nondimensional parameter for discriminating between locations of freezing rain and ice pellets. *Weather Forecast.*, 11(4):591–598.

Davies, H. (1976). A lateral boundary formulation for multilevel prediction models. *Q. J. Roy. Meteor. Soc.*, 102(432):405–418.

Delage, Y. and Girard, C. (1992). Stability functions correct at the free convection limit and consistent for both the surface and Ekman layers. *Bound. Layer Meteor.*, 58(1-2):19–31.

Delage, Y. A. A. (1997). Parameterising sub-grid scale vertical transport in atmospheric models under statically stable conditions. *Bound. Layer Meteor.*, 82(1):23–48.

Denis, B., Côté, J., and Laprise, R. (2002a). Spectral decomposition of two-dimensional atmospheric fields on limited-area domains using the discrete cosine transform (DCT). *Mon. Weather Rev.*, 130(7):1812–1829.

Denis, B., Laprise, R., and Caya, D. (2003). Sensitivity of a regional climate model to the resolution of the lateral boundary conditions. *Clim. Dyn.*, 20(2-3):107–126.

Denis, B., Laprise, R., Caya, D., and Côté, J. (2002b). Downscaling ability of one-way nested regional climate models: the Big-Brother Experiment. *Clim. Dyn.*, 18(8):627–646.

Di Luca, A., de Elía, R., and Laprise, R. (2015). Challenges in the quest for added value of regional climate dynamical downscaling. *Current Climate Change Reports*, 1(1):10–21.

Diaconescu, E. P., Laprise, R., and Sushama, L. (2007). The impact of lateral boundary data errors on the simulated climate of a nested regional climate model. *Clim. Dyn.*, 28(4):333–350.

Drake, J. and Mason, B. (1966). The melting of small ice spheres and cones. *Q. J. Roy. Meteor. Soc.*, 92(394):500–509.

Field, C. B., Barros, V., Stocker, T. F., Dahe, Q., Dokken, D. J., Ebi, K. L., Mastrandrea, M. D., Mach, K. J., Plattner, G.-K., and Allen, S. K. (2013). *Managing the risks of extreme events and disasters to advance climate change adaptation: Special report of the Intergovernmental Panel on Climate Change.*

Fosser, G., Khodayar, S., and Berg, P. (2014). Benefit of convection permitting climate model simulations in the representation of convective precipitation. *Clim. Dyn.*, 44(1-2):45–60.

Groisman, P. Y., Bulygina, O. N., Yin, X., Vose, R. S., Gulev, S. K., Hanssen-Bauer, I., and Førland, E. (2016). Recent changes in the frequency of freezing precipitation in North America and Northern Eurasia. *Environ. Res. Lett.*, 11(4):045007–.

Henson, W., Stewart, R., Kochtubajda, B., and Thériault, J. (2011). The 1998 ice storm: Local flow fields and linkages to precipitation. *Atmos. Res.*, 101(4):852–862.

Hernández-Díaz, L., Laprise, R., Sushama, L., Martynov, A., Winger, K., and Dugas, B. (2013). Climate simulation over CORDEX Africa domain using the fifth-generation Canadian Regional Climate Model (CRCM5). *Clim. Dyn.*, 40(5-6):1415–1433.

Hohenegger, C., Brockhaus, P., and Schaer, C. (2008). Towards climate simulations at cloud-resolving scales. *Meteorologische Zeitschrift*, 17(4):383–394.

Jacob, D., Petersen, J., Eggert, B., Alias, A., Christensen, O. B., Bouwer, L. M., Braun, A., Colette, A., Déqué, M., and Georgievski, G. (2014). EURO-CORDEX: new high-resolution climate change projections for european impact research. *Reg. Environ. Change*, 14(2):563–578.

Jones, R. G., Murphy, J. M., and Noguer, M. (1995). Simulation of climate change over Europe using a nested regional-climate model. I: Assessment of control climate, including sensitivity to location of lateral boundaries. *Q. J. Roy. Meteor. Soc.*, 121(526):1413–1449.

Kain, J. S. and Fritsch, J. M. (1990). A one-dimensional entraining/detraining plume model and its application in convective parameterization. *J. Atmos. Sci.*, 47(23):2784–2802.

Kendon, E. J., Roberts, N. M., Fowler, H. J., Roberts, M. J., Chan, S. C., and Senior, C. A. (2014). Heavier summer downpours with climate change revealed by weather forecast resolution model. *Nature Climate Change*.

Kendon, E. J., Roberts, N. M., Senior, C. A., and Roberts, M. J. (2012). Realism of rainfall in a very high-resolution regional climate model. *J. Climate*, 25(17):5791–5806.

Kjellström, E., Fowler, H. J., Kendon, E. J., Leung, R., and Truhetz, H. (2014). Taking the next step towards very-high-resolution regional climate modeling. *GEWEX News*, 24(3).

Klima, K. and Morgan, M. G. (2015). Ice storm frequencies in a warmer climate. *Climatic Change*, 133(2):209–222.

Køltzow, M. A., Iversen, T., and Haugen, J. E. (2011). The importance of lateral boundaries, surface forcing and choice of domain size for dynamical downscaling of global climate simulations. *Atmosphere*, 2(2):67–95.

Kuo, H.-L. (1965). On formation and intensification of tropical cyclones through latent heat release by cumulus convection. *J. Atmos. Sci.*, 22(1):40–63.

Laflamme, J. N. and Périard, G. (1998). The climate of freezing rain over the province of Québec in Canada: a preliminary analysis. *Atmos. Res.*, 46(1-2):99–111.

Lambert, S. J. and Hansen, B. K. (2011). Simulated changes in the freezing rain climatology of north america under global warming using a coupled climate model. *Atmos.-Ocean*, 49(3):289–295.

Laprise, R. (1992). The Euler equations of motion with hydrostatic pressure as an independent variable. *Mon. Weather Rev.*, 120(1):197–207.

Lauwaet, D., Viaene, P., Brisson, E., van Noije, T., Strunk, A., Van Looy, S., Maiheu, B., Veldeman, N., Blyth, L., and De Ridder, K. (2013). Impact of nesting resolution jump on dynamical downscaling ozone concentrations over Belgium. *Atmos. Environ.*, 67:46–52.

Leduc, M. and Laprise, R. (2009). Regional climate model sensitivity to domain size. *Clim. Dyn.*, 32(6):833–854.

Leduc, M., Laprise, R., Moretti-Poisson, M., and Morin, J.-P. (2011). Sensitivity to domain size of mid-latitude summer simulations with a regional climate model. *Clim. Dyn.*, 37(1-2):343–356.

Li, J. and Barker, H. W. (2005). A radiation algorithm with correlated-k distribution. Part I: local thermal equilibrium. *J. Atmos. Sci.*, 62(2):286–309.

Lucas-Picher, P., Laprise, R., and Winger, K. (2016). Evidence of added value in North American regional climate model hindcast simulations using ever-increasing horizontal resolutions. *Clim. Dyn.*, pages 1–23.

Martynov, A., Laprise, R., Sushama, L., Winger, K., Šeparović, L., and Dugas, B. (2013). Reanalysis-driven climate simulation over CORDEX North America domain using the Canadian Regional Climate Model, version 5: model performance evaluation. *Clim. Dyn.*

Martynov, A., Sushama, L., Laprise, R., Winger, K., and Dugas, B. (2012). Interactive lakes in the Canadian Regional Climate Model, version 5: the role of lakes in the regional climate of North America. *Tellus A*, 64.

Matte, D., Laprise, R., and Thériault, J. M. (2016a). Comparison between high-resolution climate simulations using single- and double-nesting approaches within the Big-Brother experimental protocol. *Clim. Dyn.*, 47(12):3613–3626.

Matte, D., Laprise, R., Thériault, J. M., and Lucas-Picher, P. (2016b). Spatial spin-up of fine scales in a regional climate model simulation driven by low-resolution boundary conditions. *Clim. Dyn.*, 49(1-2):563–574.

McDonald, A. (2005). Transparent lateral boundary conditions for baroclinic waves: a study of two elementary systems of equations. *Tellus A*, 57(2):171–182.

McDonald, A. (2006). Transparent lateral boundary conditions for baroclinic waves ii. introducing potential vorticity waves. *Tellus A*, 58(2):210–220.

McFarlane, N. A. (1987). The effect of orographically excited gravity wave drag on the general circulation of the lower stratosphere and troposphere. *J. Atmos. Sci.*, 44(14):1775–1800.

Meehl, G. A. and Tebaldi, C. (2004). More intense, more frequent, and longer lasting heat waves in the 21st century. *Science*, 305(5686):994–997.

Meinshausen, M., Smith, S. J., Calvin, K., Daniel, J. S., Kainuma, M., Lamarque, J., Matsumoto, K., Montzka, S., Raper, S., and Riahi, K. (2011). The RCP greenhouse gas concentrations and their extensions from 1765 to 2300. *Climatic change*, 109(1-2):213–241.

Milbrandt, J. A. and Yau, M. K. (2005a). A multimoment bulk microphysics parameterization. Part I: Analysis of the role of the spectral shape parameter. *J. Atmos. Sci.*, 62(9):3051–3064.

Milbrandt, J. A. and Yau, M. K. (2005b). A multimoment bulk microphysics parameterization. Part II: A proposed three-moment closure and scheme description. *J. Atmos. Sci.*, 62(9):3065–3081.

Morrison, H. and Grabowski, W. W. (2008). A novel approach for representing ice microphysics in models: Description and tests using a kinematic framework. *J. Atmos. Sci.*, 65(5):1528–1548.

Morrison, H. and Milbrandt, J. A. (2015). Parameterization of cloud microphysics based on the prediction of bulk ice particle properties. Part I: Scheme description and idealized tests. *J. Atmos. Sci.*, 72(1):287–311.

Omrani, H., Drobinski, P., and Dubos, T. (2012). Spectral nudging in regional climate modelling: how strongly should we nudge? *Q. J. Roy. Meteor. Soc.*, 138(668):1808–1813.

Orlanski, I. (1975). A rational subdivision of scales for atmospheric processes. *Bull. Amer. Meteor. Soc.*, 56:527–530.

Pan, L.-L., Chen, S.-H., Cayan, D., Lin, M.-Y., Hart, Q., Zhang, M.-H., Liu, Y., and Wang, J. (2011). Influences of climate change on California and Nevada regions revealed by a high-resolution dynamical downscaling study. *Clim. Dyn.*, 37(9-10):2005-2020.

Pavlik, D., Söhl, D., Pluntke, T., Mykhnovych, A., and Bernhofer, C. (2012). Dynamic downscaling of global climate projections for eastern Europe with a horizontal resolution of 7 km. *Environ. Earth Sci.*, 65(5):1475–1482.

Prein, A. F., Langhans, W., Fosser, G., Ferrone, A., Ban, N., Goergen, K., Keller, M., Tlle, M., Gutjahr, O., and Feser, F. (2015). A review on regional convectionpermitting climate modeling: demonstrations, prospects, and challenges. *Rev. Geophys.*, pages 323–361.

Rackley, J. A. and Knox, J. A. (2016). A climatology of southern appalachian cold-air damming. *Weather Forecast*, 31(2):419–432.

Ramer, J. (1993). An empirical technique for diagnosing precipitation type from model output. In *Amer. Meteor. Soc.*, pages 227–230. International conference on aviation Weather Systems, 5th, Vienna, VA.

Rasmussen, R., Ikeda, K., Liu, C., Gochis, D., Clark, M., Dai, A., Gutmann, E., Dudhia, J., Chen, F., and Barlage, M. (2014). Climate change impacts on the water balance of the Colorado Headwaters: High-resolution regional climate model simulations. *J. Hydrometeorol.*, 15(3):1091–1116.

Rasmussen, R., Liu, C., Ikeda, K., Gochis, D., Yates, D., Chen, F., Tewari, M., Barlage, M., Dudhia, J., and Yu, W. (2011). High-resolution coupled climate runoff simulations of seasonal snowfall over Colorado: a process study of current and warmer climate. *J. Climate*, 24(12):3015–3048.

Reeves, H. D., Elmore, K. L., Ryzhkov, A., Schuur, T., and Krause, J. (2014). Sources of uncertainty in precipitation-type forecasting. *Weather Forecast*, 29(4):936–953.

Ressler, G. M., Milrad, S. M., Atallah, E. H., and Gyakum, J. R. (2012). Synoptic-scale analysis of freezing rain events in Montreal, Quebec, Canada. *Weather Forecast.*, 27(2):362–378.

Roebber, P. J. and Gyakum, J. R. (2003). Orographic influences on the mesoscale structure of the 1998 ice storm. *Mon. Weather Rev.*, 131(1):27–50.

Šeparović, L., Alexandru, A., Laprise, R., Martynov, A., Sushama, L., Winger, K., Tete, K., and Valin, M. (2013). Present climate and climate change over North America as simulated by the fifth-generation Canadian regional climate model. *Clim. Dyn.*, 41(11-12):3167–3201.

Sillmann, J., Kharin, V., Zwiers, F., Zhang, X., and Bronaugh, D. (2013). Climate extremes indices in the CMIP5 multimodel ensemble: Part 2. Future climate projections. *J. Geophys. Res.: Atmospheres*, 118(6):2473–2493.

Skamarock, W. C. (2004). Evaluating mesoscale NWP models using kinetic energy spectra. *Mon. Weather Rev.*, 132(12):3019–3032. doi: 10.1175/MWR2830.1.

Stuart, R. A. and Isaac, G. A. (1999). Freezing precipitation in Canada. *Atmos.-Ocean*, 37(1):87–102.

Sundqvist, H., Berge, E., and Kristjánsson, J. E. (1989). Condensation and cloud parameterization studies with a mesoscale numerical weather prediction model. *Mon. Weather Rev.*, 117(8):1641–1657.

Taylor, K. E. (2001). Summarizing multiple aspects of model performance in a single diagram. *J. Geophys. Res. : Atmospheres (1984–2012)*, 106(D7):7183–7192.

Termonia, P., Deckmyn, A., and Hamdi, R. (2009). Study of the lateral boundary condition temporal resolution problem and a proposed solution by means of boundary error restarts. *Mon. Weather Rev.*, 137(10):3551–3566.

Trapp, R. J., Halvorson, B. A., and Diffenbaugh, N. S. (2007). Telescoping, multimodel approaches to evaluate extreme convective weather under future climates. *J. Geophys. Res.: Atmospheres (1984–2012)*, 112(D20).

Vautard, R., Gobiet, A., Jacob, D., Belda, M., Colette, A., Déqué, M., Fernández, J., García-Díez, M., Goergen, K., and Güttler, I. (2013). The simulation of European heat waves from an ensemble of regional climate models within the EURO-CORDEX project. *Clim. Dyn.*, 41(9-10):2555–2575.

Verseghy, D. L. (2000). The Canadian land surface scheme (CLASS): its history and future. *Atmos. Ocean*, 38(1):1–13.

Verseghy, L. (2008). The Canadian land surface scheme: technical documentation–version 3.4. *Climate Research Division, Science and Technology Branch, Environment Canada.*

von Storch, H., Langenberg, H., and Feser, F. (2000). A spectral nudging technique for dynamical downscaling purposes. *Mon. Weather Rev.*, 128(10):3664–3673.

Vries, H., Lenderink, G., and Meijgaard, E. (2014). Future snowfall in western and central europe projected with a highresolution regional climate model ensemble. *Geophys. Res. Lett.*, 41(12):4294–4299.

Wang, C., Jones, R., Perry, M., Johnson, C., and Clark, P. (2013). Using an ultrahigh-resolution regional climate model to predict local climatology. *Q. J. Roy. Meteor. Soc.*, 139(677):1964–1976.

Whiteman, C. D. and Doran, J. C. (1993). The relationship between overlying synoptic-scale flows and winds within a valley. *J. Appl. Meteorol.*, 32(11):1669–1682.

Xu, Q. (1990). A theoretical study of cold air damming. *J. Atmos. Sci.*, 47(24):2969–2985.

Yeh, K.-S., Côté, J., Gravel, S., Méthot, A., Patoine, A., Roch, M., and Staniforth, A. (2002). The CMC-MRB global environmental multiscale (GEM) model. Part III: Nonhydrostatic formulation. *Mon. Weather Rev.*, 130(2):339–356.

Zadra, A., Roch, M., Laroche, S., and Charron, M. (2003). The subgridscale orographic blocking parametrization of the GEM model. *Atmos.-Ocean*, 41(2):155–170.

Zappa, G., Shaffrey, L. C., Hodges, K. I., Sansom, P. G., and Stephenson, D. B. (2013). A multimodel assessment of future projections of North Atlantic and European extratropical cyclones in the CMIP5 climate models. *J. Climate*, 26(16):5846–5862.